EXPERIMENTAL AND NUMERICAL STUDIES FOR A NOVEL BED-BASED AIR SOURCE HEAT PUMP (B-ASHP) HEATING SYSTEM FOR IMPROVING INDOOR THERMAL ENVIRONMENTS IN WINTER

FANG GUANYU

PhD

The Hong Kong Polytechnic University

2021

The Hong Kong Polytechnic University

Department of Building Services Engineering

Experimental and Numerical Studies for a Novel Bed-based Air Source Heat Pump (B-ASHP) Heating System for Improving Indoor Thermal Environments in Winter

Fang Guanyu

A thesis submitted in partial fulfillment of the requirements for the degree of Doctor of Philosophy

February, 2021

Certificate of Originality

I hereby declare that this thesis is my own work and that, to the best of my knowledge and belief, it reproduces no material previously published or written, nor material that has been accepted for the award of any other degree or diploma, except where due acknowledgement has been made in the text.

_____(Signed)

Fang Guanyu (Name of student)

Abstract

Abstract of thesis entitled :		Experimental and Numerical Studies for a Novel Bed-based Air Source Heat Pump (B-ASHP) Heating System for Improving Indoor Thermal Environments in Winter
Submitted by	:	Fang Guanyu
For the degree of	:	Doctor of Philosophy

at The Hong Kong Polytechnic University in June, 2021

Air source heat pumps (ASHPs) have been increasingly used for space heating due to their high energy efficiency and installation flexibility. In China, with the implementation of the Chinese National strategy of clean-heating, as part of the national efforts of combating severe air pollution in winter, the use of air source heat pumps (ASHPs) has been strongly recommended to replace traditional fossil-fuel based space heating technology. However, when using a conventional ASHP system for space heating, its fan-powered convection-based indoor heating terminal is usually located at a higher level in a heated room. This results in an undesired vertical indoor air temperature gradient and thermally discomfort to occupants as a result of directly blowing warm air to their upper bodies including heads. On the other hand, in many rural areas in northern Chinese provinces, Kangs, a kind of traditional heating systems based on burning biofuels, are still being used for space heating in winter. A Kang-bed in a Chinese Kang-based heating system serves as not only a space heating terminal at

daytime for daytime activities but also a heated bed for sleeping at nighttime. However, employing such a Chinese Kang-based heating system can also lead to a number of environmental and operational problems such as local air pollution and safety. Therefore, a research project on developing, based on the pros and cons of both ASHPs and Kang-based heating systems, a novel bed-based ASHP (B-ASHP) system by combining the advantages from both an ASHP and a Kang-based heating system has been carried out and the project results are presented in this Thesis.

The Thesis begins with presenting an experimental study, as the first part of the research project, on the operational performances of an experimental B-ASHP system. The experimental B-ASHP system was designed and established in an experimental B-ASHP, and its bed-based heating terminal contained two sections: a horizontal section (H-Section) and a vertical section (V-Section). The dynamic and steady-state operating performances of the experimental B-ASHP system were examined in four test cases. The test results from the four test cases demonstrated that the experimental B-ASHP system can be used to achieve quicker increases in indoor air temperatures and bed-surface temperatures than Kang-based heating systems. The use of experimental B-ASHP system can lead to a more uniformed vertical indoor air temperature gradient, thus a better occupants' thermal comfort, than the use of a conventional convection-based ASHP system. Furthermore, compared to using a Kang-based heating system, a more uniformed bed surface temperature may be obtained when using a B-ASHP system. Nonetheless, although currently the experimental B-ASHP system can be satisfactorily operated, a number of issues related to the designs of a B-ASHP system such as choices of refrigerant, refrigerant tube layout optimizations, and the use of

variable speed compressors for capacity control, should be carefully considered to further improve its operational safety and energy efficiency.

In the experimental study, the operating characteristics of the experimental B-ASHP system were experimentally evaluated under a fix set of design/operating parameters for its bed-based heating terminal. Therefore, a fellow-up numerical study, as the second part of the research project, to evaluate the impacts of optimizing these design/operating parameters, including the location, dimension, surface temperature (t_{bed}) and surface emissivity (ε) of the bed-based heating terminal, on the indoor thermal environment and the operating efficiency of the B-ASHP system, is reported. A CFD method to be used in the numerical study was established and experimentally validated. The numerical study results suggested that the variation in these parameters did impact both indoor thermal environment and the operating efficiency of the B-ASHP system, in terms of the uniformity of indoor thermal environment, indoor air velocity distribution and the output heating capacity, as well as the installation space requirement and cost implication. Therefore, care must be exercised in properly balancing all influencing parameters. Also, to both provide full space heating and thus maintain an acceptable indoor thermal environment that can meet the Chinese National Standard, and achieve the best possible operating efficiency of the B-ASHP system, the t_{bed} of its bed-based heating terminal without a mattress on it may be set at around 35 ^{o}C. Furthermore, although the changes in ε did not significantly impact on indoor thermal environment, a higher ε should be preferred when a lower t_{bed} was used, so as to further improve potentially the operating efficiency of the B-ASHP system.

Furthermore, the bed-based terminal can virtually act as a bed, similar to a heated Kang-bed in a Chinese Kang-based heating system, to provide a sleeping person with a suitable micro-environment that was conducive to quality sleep. Therefore, as the third part of the research project, a further numerical study using a digital thermal manikin (DTM) on the impacts of the following four factors, i.e., operating mode of the bed-based heating terminal, t_{bed}, thermal resistance of mattress (R_{mat}), and thermal resistance of quilt (R_q) on the thermal comfort of a person sleeping on top of the bed-based heating terminal is reported. In this numerical study, the CFD method developed and used in the second part of the project was modified considering the presence of the DTM and its complex geometry, and the modified CFD method was further experimentally validated. The numerical study results using the modified CFD method firstly suggested that to maintain a suitable sleeping thermal environment, the use of H-Section only was adequate. However, using H+V-Section could minimize the temperature difference between the micro-climate inside a quilt and its outer environment, but at a higher energy consumption. Secondly, the t_{bed} value of the bed-based terminal should be carefully selected, and unlike that in the second part of the research project, a t_{bed} at 44 ^{o}C was recommended to both meet the requirement of sleeping thermal comfort at nighttime for localized heating and achieve the highest possible operating efficiency of the B-ASHP system. Thirdly, the use of a mattress with a higher R_{mat} value would not only reduce the output heating capacity and lower the operating efficiency of the B-ASHP system, but also lead to a cold sleeping environment. Fourthly, although using quilts of appropriate R_q value would help prevent the heat loss from a sleeping person, a higher-than-necessary R_q would rather decrease the thermal comfort of a sleeping person.

Publications Arising from the Thesis

Journal Papers

2020 **Fang, G.,** Chan, M., Yan, H., Chen, W., Deng, S., and Liu, X., 2020. An experimental study on the operating performances of a novel bed-based air source heat pump (B-ASHP) system, *Energy and Buildings*, 223, 110191. (Based on Chapter 4)

2021 **Fang, G.,** Chan, M., Yan, H., Chen, W., Deng, S., and Liu, X., 2021. A numerical study on evaluating the thermal environment in a space served by a bed-based air source heat pump (B-ASHP) system, *Energy and Buildings*, 234, 110693. (Based on Chapter 5)

2021 **Fang, G.,** Deng, S., and Liu, X., 2021. A numerical study on evaluating sleeping thermal comfort using a bed-based air source heat pump (B-ASHP) space heating system, *Energy and Buildings*, Accepted. (Based on Chapter 6)

Conference Papers

2018 **Fang, G.**, Du, J., Chan, M., and Deng, S., 2018. A Numerical Study On The Indoor Thermal Environment Served By A Novel Air Source Heat Pump Powered Bed-Based Space Heating (ASHP-BBSH) System. *International High Performance Buildings Conference*, Purdue University, USA, July 12-15, 2018

Acknowledgements

First of all, I must express my grateful thanks to my supervisor, Prof. Deng Shiming from the Department of Building Services Engineering of The Hong Kong Polytechnic University, for his tireless supports, valuable suggestions and continuous guidance during my PhD study. He has set a very good model for me in my future career by being modest, dedicated, earnest and passionate. I also must express my grateful thanks to my former supervisor, Dr. Chan Ming-yin for his readily available supervision, valuable suggestions, continuous helps and encouragements throughout my study. I would also like to express my gratitude to Prof. Liu Xuefeng from South China University of Technology for his care and encouragements.

Secondly, I would like to thank The Hong Kong Polytechnic University for providing me with a scholarship to support my PhD study.

Thirdly, I am indebted to all my colleagues and friends in Hong Kong, including Dr. Chen Wenjing, Dr. Du Jing, Dr. Mao Ning, Dr. Pan Dongmei, Dr. Pan Yan, Dr. Wang Caixia, Dr. Xia Yudong, Dr. Yan Huaxia, Dr. Zhang Long, Dr. Zhang Wanyi, Dr. Yang Da, Dr. Dai Yuwei, Mr. Yang Liu, Ms. Liu Shengnan and Mr. Bai Xiaoxia for their valuable helps and suggestions on my research. Their talents and diligence always inspire and encourage me. Thanks to all my friends who have supported me during the period of my PhD study.

Finally, I would like to dedicate this thesis to my family. This thesis would not have been completed without their love, supports and understandings.

Table of Contents

List of Figures

List of Tables

Nomenclature

ρ	Air density (kg/m^3)
t_a	Air temperature (^{o}C)
$\vec{v}$	Air velocity (m/s)
$\overline{v}$	Averaged air velocity, m/s
t_{op}	Averaged operative temperature (^{o}C)
COP	Coefficient of performance
P_{com}	Compressor input power (W)
Q_{conv}	Convective heat loss from a human body (W)
t_{core}	Core temperature (^{o}C)
$\overline{\overline{\tau}}_{eff}$	Deviatoric stress tensor (Pa)
k_{eff}	Effective conductivity, W/m·^{o}C
ε	Emissivity
h	Enthalpy (J)
u^*	Friction velocity (m/s)
$\vec{g}$	Gravitational acceleration (m/s^2)
Q_{cond}	Heat gain from the bed surface to a human body (W)
Q	Heating capacity (W)
y	Height of first mesh layer off the surface of the DTM (m)
v	Kinematic viscosity of air (kg/(m · s))
$\overline{t_r}$	Mean radiant temperature (^{o}C)

t_{op}	Operative temperature (^{o}C)
t_{out}	Outdoor temperature (^{o}C)
PTS	Partial thermal sensation
PTS_{CB}	Partial thermal sensation of body parts covered by quilt
PTS_{H}	Partial thermal sensation of body parts outside the quilt (i.e., head and neck)
PPD	Predicted percentage of dissatisfied
PMV	Predicted mean vote
Q_{rad}	Radiative heat loss from a human body (W)
h_{in}	Refrigerant enthalpy at the inlet of the bed-based heating terminal (kJ/kg)
h_{out}	Refrigerant enthalpy at the inlet of the bed-based heating terminal (kJ/kg)
M	Refrigerant mass flow rate (g/s)
P	Static pressure (Pa)
$\bar{\bar{\tau}}$	Stress tensor (Pa)
A	Surface area of a human body (m^2)
A_{back}	Surface area of the back of a human body (m^2)
t_{bed}	Surface temperature of the bed-based terminal (^{o}C)
t_{mat}	Surface temperature of the mattress (^{o}C)
R_{clo}	Thermal resistance of clothing ($m^2 \cdot {}^{o}C$ /W)
R_{mat}	Thermal resistance of mattress ($m^2 \cdot {}^{o}C$ /W)
R_{q}	Thermal resistance of quilt ($m^2 \cdot {}^{o}C$ /W)
R_{skin}	Thermal resistance of skin ($m^2 \cdot {}^{o}C$ /W)

t	Time (s)
E	Total energy (J)
Q_{total}	Total sensible heat loss from a human body (W)
R_t	Total thermal resistance of a bedding system ($m^2 \cdot {}^oC$ /W)
p_a	Water vapor pressure (kPa)
WPD	Whole predicted percentage of dissatisfaction (%)
y^+	Y-plus

List of Abbreviations

ASHP	Air source heat pump
B-ASHP	Bed-based air source heat pump
CFD	Computational fluid dynamics
DTM	Digital thermal manikin
DO	Discrete ordinates
EEV	Electronic expansion valve
H-Section	Horizontal section of the B-ASHP heating terminal
V-Section	Vertical section of the B-ASHP heating terminal
H+V-Section	Horizontal and vertical section of the B-ASHP heating terminal
HVAC	Heating, ventilation, and air conditioning
OZ	Occupied zone
S2S	Surface-to-surface
UZ	Unoccupied zone

Chapter 1 Introduction

Air source heat pumps (ASHPs) have been increasingly used for space heating because they are highly energy efficient, and flexible in installation. However, when using a conventional ASHP system for space heating, its fan-powered convection-based indoor heating terminal is usually located at a higher level in a heated room. This results in an undesired vertical indoor air temperature gradient and thermally discomfort to occupants as a result of directly blowing warm air to their upper bodies including heads.

On the other hand, in many rural areas in northern Chinese provinces, Kangs, a kind of traditional biofuel-burning heating systems, are still being widely used for space heating in winter. A Kang-bed in a Chinese Kang-based heating system serves as not only a space heating terminal at daytime for daytime activities but also a heated bed for sleeping at nighttime. However, employing such a Chinese Kang-based heating system can also lead to a number of environmental and operational problems such as local air pollution and safety.

Therefore, based on the pros and cons of both ASHPs and Kang-based heating systems, a novel bed-based ASHP (B-ASHP) system by combining the advantages from both an ASHP and a Kang-based heating system, has been proposed. A research project to evaluate the performances of an experimental B-ASHP system in terms of operating characteristics and indoor thermal environment and sleeping comfort has been therefore carried out and the project outcomes are presented in this Thesis.

To begin with, an extensive literature review is presented in Chapter 2. Firstly, a brief introduction to ASHP systems is included. This is followed by presenting a review on the Chinese Kang-based heating systems and their pros and cons. Thirdly, the fundamentals of sleep and the factors influencing sleep quality are reviewed. Fourthly, a review on the previous studies on thermal comfort in sleeping environment is presented. Fifthly, previous numerical studies on evaluating indoor thermal environment by using CFD methods are reviewed. Finally, identified research gaps where further research efforts should be directed to are summarized.

Chapter 3 presents the title, aims and objectives of the research project, and the research methodologies adopted in the research project.

Chapter 4 reports the first part of the research project: an experimental study on the operational performances of an experimental B-ASHP system. The experimental B-ASHP system was designed and established in an experimental indoor space, and its bed-based heating terminal contained two sections: a horizontal section (H-Section) and a vertical section (V-Section). The dynamic and steady-state operating performances of the experimental B-ASHP system were examined in four test cases.

Chapter 5 presents a numerical study on the impacts of optimizing these design/operating parameters, including the location, dimension, surface temperature (t_{bed}) and surface emissivity (ε) of the bed-based heating terminal, on the indoor thermal environment and the operating efficiency of the B-ASHP system. A CFD method to be used in the numerical study was established and experimentally validated. Numerical study cases were designated for different purposes. The numerical study results and a number of related discussions are presented.

In Chapter 6, as the third part of the research project, a further simulation study using a digital thermal manikin (DTM) on the impacts of the following four factors, i.e., operating mode of the bed-based heating terminal, t_{bed}, thermal resistance of mattress (R_{mat}), and thermal resistance of quilt (R_q), on the thermal comfort of a person sleeping on top of the bed-based heating terminal, is reported In this further numerical study, the CFD method developed and used in the second part of the project was modified considering the presence of the DTM and its complex geometry, and the modified CFD method was further experimentally validated. Study cases were designated and grouped for various study purposes.

In the final Chapter of the Thesis, the conclusions and the proposed future work are given.

Chapter 2 Literature review

2.1 Introduction

Air source heat pumps (ASHPs) have been widely applied worldwide due to their distinguished advantages of higher energy efficiency and installation flexibility (Dong et al. 2012). In the last 10 years, the European Union (Hewitt et al. 2011, Zhang et al. 2018b), China (Zhang et al. 2017) and the US (USDOE 2021) respectively classified the ASHP as a renewable energy source technology or an energy saver. However, conventionally, when using ASHPs for space heating in residential buidlings, convection-based fan-powered indoor terminals are commonly used (Lin et al. 2016, Yang et al. 2020). These terminals are usually located at a higher level in heated rooms, which is particularly true when the ASHPs are also used for space cooling in summer seasons. This would lead to a number of operating issues such as an undesired indoor air temperature gradient (Imanari et al. 1999), a lower indoor relative air humidity and therefore thermally discomfort to occupants as a result of directly blowing warm and dry air to their upper bodies including heads (Wang and Liu 2000).

On the other hand, in many rural areas of northern China, currently, a heated bed, or a Kang, which has a long history of more than 2000 years (Guo 2002) as a localized space heating system, is still being used in nearly 85 % of village houses (Zhuang et al. 2009b) to maintain a warmer indoor thermal environment in winter (Cao et al. 2011). A Kang-bed releases heat via radiation and natural convection, with the radiative heat transfer accounting for between 40 % and 60 % of the total (Zhuang et al. 2015). A Kang-bed not only provides a multifunctional living/sleeping area, but

also serves as a space heating terminal at both daytime and nighttime. However, employing such a traditional Kang-based heating system may also lead to a number of problems with respect to environment, operation and safety. Firstly, local air pollution cannot be avoided, as biofuels are burned and the burning products locally discharged without proper treatments (Zhuang et al. 2009b). Secondly, it is hard for a Kang heating system to continuously real-time meet the demand of space heating, as occupants would have to feed the stove with biofuels regularly to maintain the Kang at a suitable temperature (Wang et al. 2014). Thirdly, leakages of burning products, such as CO and CO_2 to a heated indoor space may potentially take place, putting occupants at risk (Zhang et al. 2000, Shan et al. 2015). Therefore, novel heating systems applied to a bedroom should be developed, based on the pros and cons from both ASHP and a Kang-based heating system.

Furthermore, a Kang-bed can also provide localized heating for a person(s) during sleep. As known, sleeping plays an important role in the daily life of a human being. In fact, about one-third of human life is spent in sleep, as reflected in a survey that the mean sleep duration is 6.9 hours per night on weekdays and 7.5 hours on weekends (Sleep in America poll 2014). Sleep is not merely a state of rest but has its own specific functions (Hobson 1995), such as helping people overcome tiredness and benefiting the performance of daytime activities (Engle-Friedman et al. 2003). It was commonly known that the quality of sleep was mainly affected by mental-physical factors of a sleeping person and environmental factors in a bedroom (Olesen et al. 1980). The environmental factors, such as the lighting and noise levels, and the air temperature and humidity inside a bedroom, can significantly affect the comfort level of a sleeping person inside a bedroom (Cuellar et al. 2006, Kemal Sayar et al. 2002).

In this Chapter, an extensive review on a number of important issues related to air source heat pump (ASHP) systems, Chinese Kang heating systems, sleep and sleeping thermal environment, and the CFD methods in evaluating indoor thermal environments in the existing literatures is reported. Firstly, a brief introduction to ASHP systems and Chinese Kang heating systems covering system characteristics, energy consumption, and existing operating issues is presented. Secondly, a review on the fundamentals of sleep, the environmental factors affecting sleeping quality, and the existing thermal comfort models for sleeping environments in a heated bedroom is included. Thirdly, a review on using the CFD methods to evaluate indoor thermal environments and energy performances in buildings is reported. Finally, the identified research gaps where future research should be directed to are summarized.

2.2 Air source heat pump (ASHP) systems

2.2.1 ASHP system descriptions and applications

Air source heat pumps (ASHPs) have been widely applied worldwide due to their distinguished advantages of higher energy efficiency and installation flexibility, environmental protection, safety and reliability (Dong et al. 2012, Xiao et al. 2020). Therefore, ASHP has been recognized as one of the promising renewable energy technologies. Conventionally, an ASHP system consists of 4 parts, i.e., a compressor, a condenser or indoor unit, an evaporator or outdoor unit, and an expansion device. A schematic diagram of a conventional ASHP system is shown in Fig. 2.1 (Chen 2018).

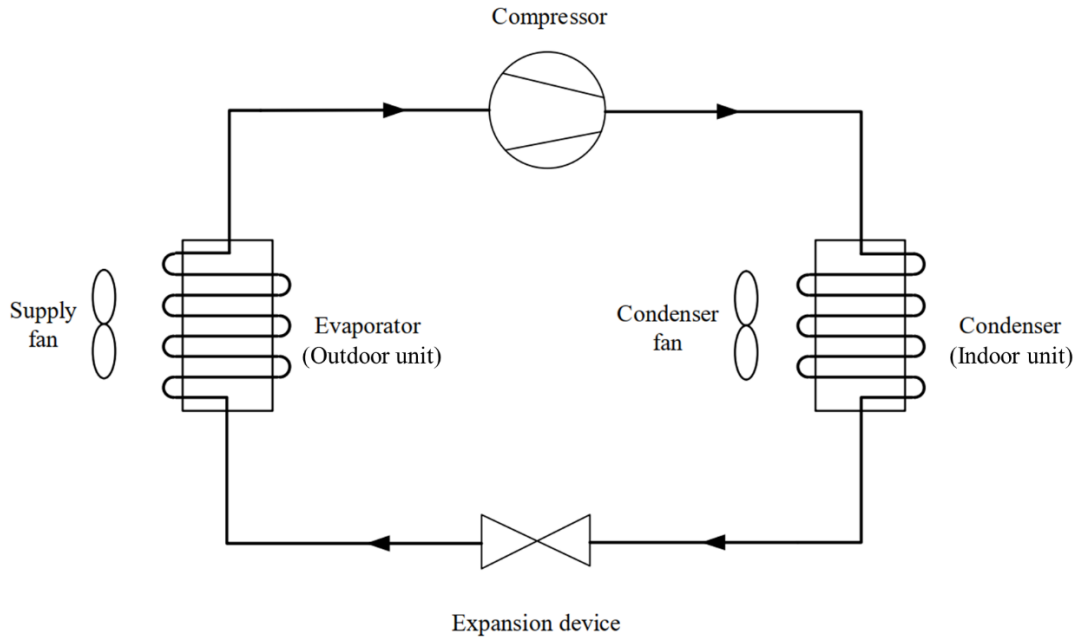

Fig. 2.1 Schematic diagram of a conventional ASHP system (Chen 2018)

A larger number of studies on improving the operating performances of ASHPs have been carried out. According to a recent review (Zhang et al. 2018a), the related studies mainly focused on the following aspects of ASHPs, the use of an ejector, new type of refrigerant and the use of oil injected compressor, respectively. Chen et al. (2011) developed an ASHP system with both an ejector and a sub-cooler, and the study results showed that the improvements in heating capacity and *COP* were 15.2 - 37.3 % and 1.6 - 6.9 %, respectively. Zhu and Yu (2015) improved a conventional ASHP system by using an ejector and a thermoelectric heat exchanger, and ~ 16.4 - 21.7 % improvements in both heating capacity and *COP* were obtained, as compared to the conventional ASHP system. On the other hand, to replace conventional hydro-chlorofluorocarbon refrigerant of R-22, different types of zeotropic mixture refrigerant such as R-417 and R-410A have been developed. By mixing R-32 with CO_2 with a volume ratio of 80:20, Hakkaki-Fard et al. (2014) developed a novel refrigerant, which can help improve the heating capacity of an ASHP by 30 %, as compared to R-410A.

Zhao et al. (2014) designed a novel ASHP system and compared 15 types of refrigerant to be used in the novel system, and the study results showed that using a mixture refrigerant of R-143A and R-600 with a volume ratio of 80:20 achieved the best operating performances of the novel ASHP system. Horton et al. (2014) built up an oil injected ASHP system and the experimental results showed that the novel system could improve both the heating capacity and *COP* by 2.0 % and 8.0 %, respectively, compared to a conventional ASHP system. Ramaraj et al. (2014) experimentally studied the performances of an ASHP system using an oil injected compressor, and the study results showed that the *COP* could be improved by 13.0 % at an ambient temperature of -10.0 ^{o}C, compared to a conventional ASHP system.

On the other hand, a large number of studies have been carried out on the practical applications of ASHPs. Liang et al. (2020) doubled the outdoor airflow rate and the surface area of outdoor coils in a conventional ASHP system and the study results showed that the frosting rate and frosting-defrosting loss efficiency of the ASHP system could be reduced by 37.2 - 39.6 %, and 31 - 34.2 %, respectively, leading to 5 % - 22 % improvements in operating performances. Yan et al. (2016) experimentally studied a variable speed (VS) ASHP system with a flash tank, and the study results showed that the VS-ASHP system had a better heating performance in cold regions. Qu et al. (2010) added a storage tank filled with phase change material to an ASHP unit for a better reverse-cycle defrosting performance. It was demonstrated that when using reverse-cycle defrosting, the time duration when occupants would feel cold was shortened by 23.1 %, suggesting a better indoor thermal comfort level. Hewitt (2011) developed a water heating boiler, and an ASHP was used for pre-heating. A higher energy efficiency was achieved.

2.2.2 Markets and national strategies for the applications of ASHPs

In European Union, based on the current framework for 80 - 95 % CO_2 emission reduction as laid down in the 2050 energy roadmap published by the European Union Commission in 2011 (European Parliament 2011), the European heat pump market grew at a rate of 12.2 % in 2015 (Nowak and Westring 2015). With this growth rate, it was expected the European heat pump market can be doubled by 2024 (EHPA 2018a). Currently, over 11.8 million heat pump units are being used across Europe, and more than 5.3 million out of the 11.8 million units are of ASHP type (EHPA 2018b). In China, with implementation of the Chinese National strategy of clean-heating through the "coal to electricity" conversion projects, there have been great efforts to mitigate the severe air pollution in northern China in winter, partly due to the use of coal-based space heating. This has enabled both the further development of ASHP technology and the fast growth of the Chinese ASHP market (Su et al. 2018, Song et al. 2018b, Shen et al. 2019). In 2017, more than 2.92 million ASHP units were sold in China, with a yearly growth rate of 43.7 %. It can be expected that in the next five years, the Chinese ASHP market will continue to grow at a rate of not less than 20 % (Li 2018). In the United States, the federal government did not offer incentives for the use of ASHPs at the national level (Kaufman et al. 2019). However, several state governments such as California (Stern 2017) and Connecticut (DEEP 2018) did offer incentives. The annual shipments of ASHPs expanded from 2.3 million units in 2015 to 3.1 million in 2019 (AHRI 2021), and the annual installation is expected to exceed 2.8 million units by 2026 (Ankit Gupta 2020).

2.2.3 The existing problems of using ASHPs with conventional convection-based heating terminals for space heating

Conventionally, when using ASHPs for space heating, convection-based fan-powered indoor terminals are used (Lin et al. 2016). These terminals are usually located at a higher level in heated rooms, which is particularly true when the ASHPs are also used for space cooling in summer seasons. This would lead to a number of operating problems such as an undesired vertical indoor air temperature gradient (Imanari et al. 1999) and thermally discomfort to occupants as a result of directly blowing warm air to their upper bodies including heads. Therefore, alternative heating terminals have been developed to address the above problems. For example, when using radiation-based heating terminals such as floor heating and ceiling heating (Li et al. 2015), the level of discomfort can be significantly reduced with a smaller temperature fluctuation and a more uniformed vertical indoor air temperature distribution (Olesen 2002). Karmann et al. (2017) provided a summary of the previous related studies on the differences in indoor thermal comfort level between using radiator heating and full-air heating, and pointed out that the use of radiator heating provided better thermal comfort than the use of full air heating. Furthermore, it should also be pointed out that when an ASHP unit was operated at an ambient temperature of between -15 ^{o}C and 6 ^{o}C, and at a relative humidity of greater than 45 %, frosting would occur on the surface of its outdoor coil (Song et al. 2018b), leading to a degradation of the operation performance of the ASHP.

2.3 Chinese Kang systems

2.3.1 Definition and history of traditional Chinese-Kang systems

In many rural areas of northern China, currently, Chinese Kangs or heated beds (Cao et al. 2011), which have a long history of more than 2000 years (Guo 2002), for providing localized space heating, are still being used in nearly 85 % of village houses to maintain a warmer indoor thermal environment in winter. A schematic diagram and a photo of a traditional Chinese Kang are shown in Fig. 2.2.

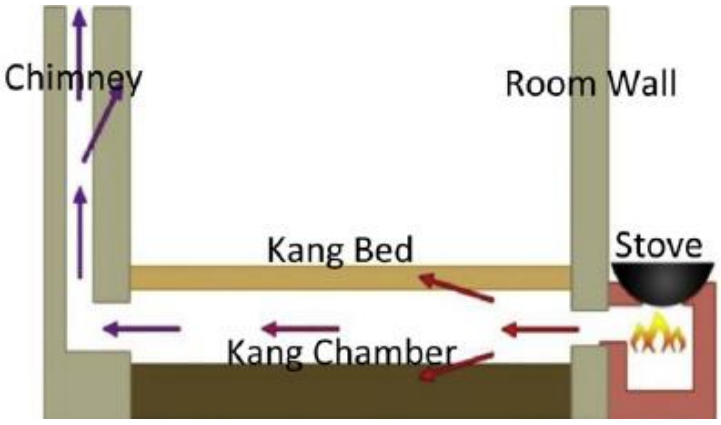

(a)

(b)

Fig. 2.2 Details of a traditional Chines Kang (a) a schematic diagram (Zhai et al. 2015) (b) the indoor section of a Chinese Kang (Kang-bed) in a village house (Yu et al. 2020)

Traditionally, a Kang-bed heating system is powered by burning biofuel such as stalk or firewood, or even coal in a cooking stove normally placed in a kitchen adjacent to a heated room. The waste heat from the cooking stove flows through the flue of the Kang Bed and thus releases the heat to its structure, as driven by buoyancy force and wind as shown in Fig. 2.2(a) (Zhai et al. 2015). Inside the heated room, the heated Kang Bed maintains a warm space where occupants could either sit or sleep on bed top. A Kang-bed structure can also store heat in its massive thermal mass (Yu et al. 2020). The Kang Bed releases heat via radiation and natural convection, with the former accounting for between 40 % and 60 % of the total (Zhuang et al. 2015). Hence, a heated Kang bed not only provides a multifunctional living area, but also serves as a space heating terminal at both daytime and nighttime.

2.3.2 The applications and the pros and cons of Chinese Kang systems

Chinese Kang systems, which are usually powered by burning coal or bio-fuels, have been widely used in the rural areas of northern China to provide a warm indoor environment in winter at both daytime and nighttime (Guo 2002). A heated Kang-bed can also be used for providing a thermally comfortable micro-environment for a sleeping person. Similar bed-based space heating technologies may also be found around the world, such as Korean Ondol (Kim and Kim 2005) and Rome Hypocaust (Bansal and Shail 1998). There are three key performance indicators for a Kang-based heating system, i.e., the temperature of Kang-plate, the thermal inertia of a Kang-body and the operating efficiency, respectively. The temperature of a Kang-plate is an important parameter as a Kang-plate is the place for both daytime and nighttime activities (Zhang and Chen 2016). A Chinese Kang usually works twice a day, i.e., during the morning at 8:30-9:30 am and afternoon around 3:30-5:00 pm. In addition, to maintain a suitable Kang-plate temperature and indoor air temperature, a high thermal inertia for the Kang-body is required. With a high thermal inertia, a Kang-body can prolong a heat-releasing stage and thus meet the need for indoor space heating (Zhai et al. 2015). At the same time, a higher thermal inertia also leads to a smaller fluctuation in indoor air temperature, which also contributes to improving indoor thermal comfort (Zhuang et al. 2009a). A traditional Chinese Kang has the advantages of low cost and easy construction. Therefore, rural residents can easily build a Kang by themselves (Li et al. 2016). Most of the materials for building a Kang are clay bricks, stone and adobe, which can be easily obtained locally. Fuels used for a Kang heating system include straw, stick or other biomass, which are abundant in rural areas (Yang and Jiang 2008). As a result, a Chinese Kang is the most suitable

space heating provision in the rural area of northern China. However, although a traditional Kang space heating system has various advantages, it still has many operational limitations. Firstly, the energy efficiency of a traditional Kang heating system is relatively low, due to the severe heat loss from exhausted flue gas (Li et al. 2009), usually with a comprehensive energy efficiency of between 40 % and 50 % (Zhai et al. 2015). The heat loss would include incomplete combustion loss, exhaust flue gas heat loss and heat transfer loss through conduction to walls or ground (Qiu et al. 2018). Secondly, a Kang heating system can only maintain and improve the local thermal environment nearby, rather than that of the whole room (Yeo et al. 2003). In most cases, a Kang space heating system is considered as a localized one and only provides localized thermal comfort (Feng et al. 2016). The operation of a Kang heating system may sometimes have a limited effect on the indoor air temperature of an entire room, due to the limited heat supply of fuels (He et al. 2013). Thirdly, the surface temperature of a Kang plate was not uniform. The surface temperature normally is higher at the head region (next to the stove) than that of the tail region (next to the chimney) using a Kang-based heating system, because a large temperature difference along flue gas flow direction (Wei et al. 2015). Finally, it is hard for a Kang heating system to continuously real-time meet the demand of space heating, as occupants would have to feed the stove with biofuels regularly to maintain a Kang-bed at a suitable temperature (Wang et al. 2014).

On the other hand, employing such a traditional Kang heating system may also lead to a number of safety and environmental problems. Firstly, local air pollution cannot be avoided, as biofuels are burned and the burning products locally discharged without proper treatments (Zhuang et al. 2009b). Secondly, leakages of combustion products,

such as CO and CO_2 to a heated indoor space may potentially take place, putting occupants at risk (Zhang et al. 2000, Shan et al. 2015).

2.3.3 Novel Kang-based heating systems

To address some of the operating problems when using tradional Chinese Kangs as mentioned in Section 2.3.2, a number of new Kang-based heating systems, where hot water was used as heating medium, were proposed. Hot water may be produced by solar energy (Zhao et al. 2019, He et al. 2013) or other heat sources (Zhao et al. 2017). Wang et al. (2017a) integrated an electrical hot water heating system into a bed and enhanced the heat transfer by a fan, to satisfy the requirement of thermal comfort in a bedroom. Futhermore, Wang et al. (2017b) further proposed an enhanced-convection overhead heating system by adding holes on top of the heating terminal surface, based on the intergrared electrucal hot water bed-based heating system. Both the experimental and numerical results showed that the surface temperature of the indoor heating terminal and indoor air temperature were more responsive to the changes in ambient air temperature. Li et al. (2018) developed an integrated heating system that could be operated with an electric water heater and a combined heating terminal having a floor section and a Kang section. The two sections may be operated either seperately for localized heating or jointly for full space heating. However, it would take up to 4 hours for the system to reach indoor air temperature set-point at an outdoor air temperature of 8.0 ^{o}C, almost the same as a traditional Kang (Gao et al. 2017). Nonetheless, for a hot water based Kang heating system, there were also a number of additonal issues of concerns, such as requiring an additional water circulatiuon pump

and its associated energy use, and uneven Kang surface temperature distribution as hot water flowed through it, etc.

2.4 Sleep and factors influencing sleeping quality

2.4.1 Definition and functions of sleep

To help better understand the impacts of various factors on sleeping quality, it is necessary to introduce the definition of sleep and the related methods for measuring sleep quality.

Sleep is usually defined as a variable but specific brain activity, which is a highly organized and complex behavior characterized by a relative disengagement from the outer world (Sterman 1974). Under normal conditions, sleep is associated with little muscular activity with stereotypic posture, and reduced response to environmental stimuli (Teofilo 2011). Sleep consists of two states, which are known as non-rapid eye movement (NREM) sleep, and rapid eye movement (REM) sleep. The former occupies 75 - 80 %, and the later the rest of a sleep duration, respectively. Based on the pattern of brainwaves as shown in Fig. 2.3, NREM sleep maybe further divided into four stages. In stage 1, the sleeping activity is transited from full wakefulness to sleep of a sleeping person, in which the reverse process could also take place. In stage 2, the sleeping activity is called the emergence of electroencephalography, which occupies around half of the total sleeping duration. In stage 3 and 4, the sleeping activity turns into deep sleep, also named as delta sleep, or slow wave sleep. Moreover, in stage 4, the body response of a sleeping person is characterized by intermixed cerebral activity together with striated muscle atonia and rapid eye movements

(Wolpert 1969). Therefore, the whole process of sleeping activity can be recorded by a hypnogram as shown in Fig. 2.3 (Brebbia and Altshuler 1965, Lavie 1998).

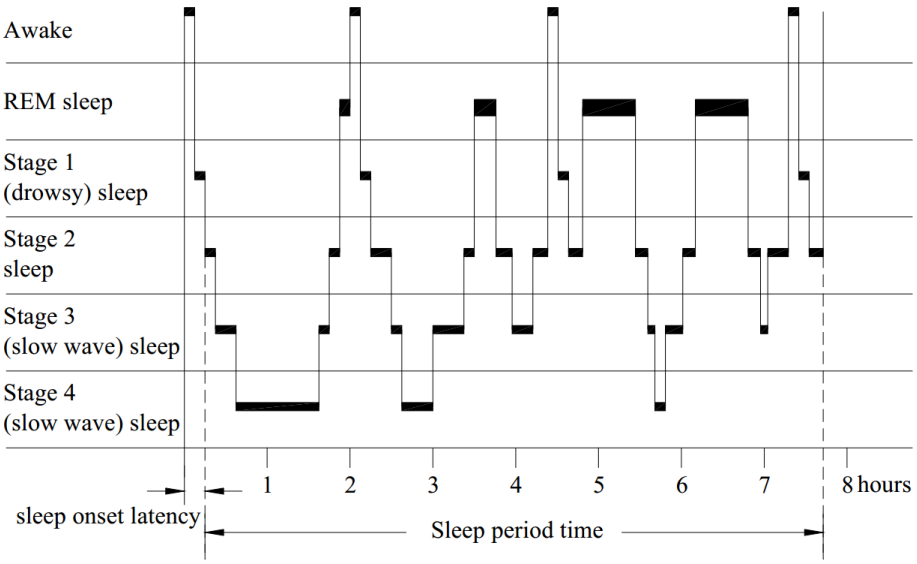

Fig. 2.3 The hypnogram of a sleeping person (Lavie 1998)

The function of sleep can be recognized by the positive effects on both human body and general health, respectively. According to a medical report on the effects of sleep (Åkerstedt and Nilsson 2003), mortality, morbidity and the endocrine and immune systems can be significantly affected by sleeping activity. Moreover, sleep also affects the mental behavior of a human being, such as the abilities of working, talking and learning (Benington and Frank 2003, Stickgold et al. 2001).

2.4.2 Factors influencing sleeping quality

It was widely acknowledged that mental-physical factors and environmental factors could significantly affect the sleeping quality of a sleeping person. The environmental factors included noise level, lighting level, thermal environment and indoor air quality.

Noise stimuli can be processed by the sensory functions of a sleeping person, despite a non-conscious perception of their presence (Muzet 2007, Basner et al. 2011). The World Health Organization (2009) recommended a guideline level of 30 dB for undisturbed sleep. Lighting level, as one of the most important environmental factors, can also affect the quality of sleep. Exposure to a brighter environment before sleeping could lead to a delay of the internal clock of a sleeping person and therefore make him/her to trend to a late sleep (Gooley et al. 2011).

In addition to noise level and lighting level, it has been widely recognized that the thermal parameters in a sleeping environment could strongly affect the quality of sleeping (Haskell et al. 1981). Kendel and Schmidt-Kessen (1973) demonstrated that the effect of high air temperature could shorten the duration of sleeping. Karacan et al. (1978) reported that an air temperature of 39 ^{o}C inside a heated blanket could lead to a decline of the sleeping duration of a sleeping person. Henane et al. (1977) suggested that the awakening periods were increased with air temperature at between 35 - 39 ^{o}C. On the other hand, an exposure to a cold environment could also lead to a poor sleeping quality. According to a survey carried out by Buguet et al. (1979) in an Arctic winter, the subjects who slept in tents suffered from a shortened sleeping duration and frequently interruption of awakenings and body movements. Haskell et al. (1981) studied the sleeping durations by comparing the effects of high (34 - 37 ^{o}C) and low (21 ^{o}C) air temperatures, and the study results showed that between a cold sleeping environment could lead to an increase in wakefulness of stage 1 sleep and a decrease in stage 2 sleep. Therefore, it was concluded that a cold sleeping environment had more negative effects on sleeping quality.

Moreover, other thermal environmental factors including indoor air velocity and humidity level may also affect sleeping quality. According to a survey carried out by Tsuzuki et al. (2008), an appropriate and moderate air velocity field inside a sleeping environment could reduce the wakefulness during sleeping by decreasing skin temperature, rectal temperatures, and body mass loss, respectively, in a warm and humid condition. Okamoto-Mizuno et al. (1999) demonstrated that exposed to a high humidity environment could increase the thermal load of a sleeping person, leading to therefore a poorer sleeping quality.

However, in winter, when a person slept with a covered quilt, the micro-environment inside the quilt would affect more sleep quality and sleep thermal comfort than that outside (Van Someren 2006, Bischof et al. 1993). Survey results indicated that most rural residents in north China and northwest China preferred to improve the micro-climate environment inside a quilt instead of increasing the whole room air temperature in winter (He et al. 2013, Liu et al. 2016). The reason for this attribute to achieving the purpose of energy and cost savings, but also to preventing the physiological response and health discomfort caused by a large indoor and outdoor air temperature difference (Xiong et al. 2017b, Xiong et al. 2016b, Xiong et al. 2017a).

After investigating the sleeping quality of twelve healthy volunteers using bed heating in Northwest China, Liu et al. (2016) found that the thermal environment near a bed was also an important aspect of a sleeping thermal environment and that bed heating influenced human thermal sensations of an indoor thermal environment. It was shown that bed heating not only increased the skin temperature of the covered body of a sleeping person, but also affected his/her face skin temperature. The overall thermal

satisfaction of a sleeping person resulted from the joint effect of the thermal conditions on both the face and the covered body of a sleeping person. Normally, a low ambient temperature was more disruptive to quality sleep.

2.5 Thermal comfort in sleeping environments

2.5.1 Characteristics parameters affecting sleeping thermal comfort

In general, indoor air temperature is the one of the most important thermal environmental parameters affecting the thermal comfort of people. In Section 2.4.2, a review of related studies on how indoor air temperature affected sleeping quality is presented. Apart from air temperature, other thermal environmental parameters such as mean radiant temperature ($\overline{t_r}$), indoor air velocity and humidity level would also impact the quality of sleep and thermal comfort of a sleeping person. Kim et al. (2010) investigated the relationship between the quality of sleep and mean radiant temperature, and used *%FL* (number of flow-limited breaths without snoring) as a measure of sleep quality. The study results showed that the best $\overline{t_r}$ range for good sleep quality would be different at different seasons and in winter, was at 19.8 - 27.08 ^{o}C, when space heating was provided.

2.5.2 Existing sleeping thermal comfort models

According to ASHRAE (ASHRAE Standard 55 2017), thermal comfort is defined as "The condition of mind that expresses satisfaction with a thermal environment". However, for a sleeping thermal environment, the term "thermal comfort" is difficult to define, since comfort is not only a state of condition, but also a state of mind.

Therefore, to understand the relationship between sleeping quality of a sleeping person and his/her sleeping thermal environment, it was suggested that a "sleeping thermal comfort zone" may be defined, within which the quantitative measures of sleep such as sleep stage latencies, time spent in each sleep stage, number and duration of awakening were only slightly modified (Lan et al. 2017).

A large number of studies have been carried out on thermal comfort of building occupants for the last few decades, including establishing comfort models (Fanger 1970) and indices (Gagge et al. 1986), carrying out experiments in climate chambers (Nakano et al. 2002), performing field surveys (Schiller 1990), establishing thermal comfort standards and evaluation methods (De Dear and Brager 2002), etc. However, only a limited number of studies have considered the thermal comfort of sleeping thermal environments.

2.5.2.1 Thermal comfort models applicable to air conditioned sleeping environment

Based on the thermal comfort model established by Fanger (1970), Lin and Deng (2008) developed a thermal comfort model for air conditioned sleeping environments.

The heat balance between a sleeping person and his/her sleeping thermal environment may be expressed as:

$$40 = \frac{34.6 - t_o}{R_t} + \frac{0.06 i_m L_R (p_{sk,s} - p_a)}{R_t} + 0.056(34 - t_a) + 0.6925(5.87 - p_a) \quad (2.1)$$

Where R_t is the total thermal resistance, which is affected by beddings, sleepwear, bed and mattress, percentage coverage of body surface area by beddings and bed, air velocity, the direction of airflow and sleeping posture, etc. (Lin and Deng 2008); p_a water vapor pressure in ambient air, kPa; t_a air temperature, °C; i_m the total vapor permeation efficiency; L_R the Lewis ration, K/kPa; $p_{sk,s}$ the water vapor pressure in saturated air at skin temperature, kPa.

By solving Equation (2.1), a comfort equation for air conditioned sleeping environments which contained both environmental and personal variables was derived:

$$40 = \frac{1}{R_t}\left[\left(34.6 - \frac{4.7\overline{t_r} + h_c t_a}{4.7 + h_c}\right) + 0.3762\left(5.52 - p_a\right)\right] + 0.056(34 - t_a) + 0.6925(5.87 - p_a) \quad (2.2)$$

where $\overline{t_r}$ is the mean radiant temperature, °C; h_r radiative heat transfer coefficient, W/m$^{2\cdot}$°C, which was determined at 4.7 W/m$^{2\cdot}$°C for most applications; h_c convective heat transfer coefficient, W/m$^{2\cdot}$°C, calculated by (ASHRAE Standard 55 2017):

$$\begin{aligned} h_c &= 2.7 + 8.7|\vec{v}|^{0.67} \ (0.15m/s < |\vec{v}| < 1.5m/s) \\ h_c &= 5.1 (0 < |\vec{v}| < 0.15m/s) \end{aligned} \quad (2.3)$$

By solving Equation (2.2) with different combinations of parameters, comfort lines were established. As shown in Fig. 2.4, the comfort lines combined the parameters of

operative temperature, wet bulb temperature and the total insulation value of beddings and bed, respectively, under which thermal neutrality for a sleeping person in an air conditioned sleeping environment can be achieved. The results showed that the effect of relative humidity on the thermal comfort of a sleeping person was insignificant.

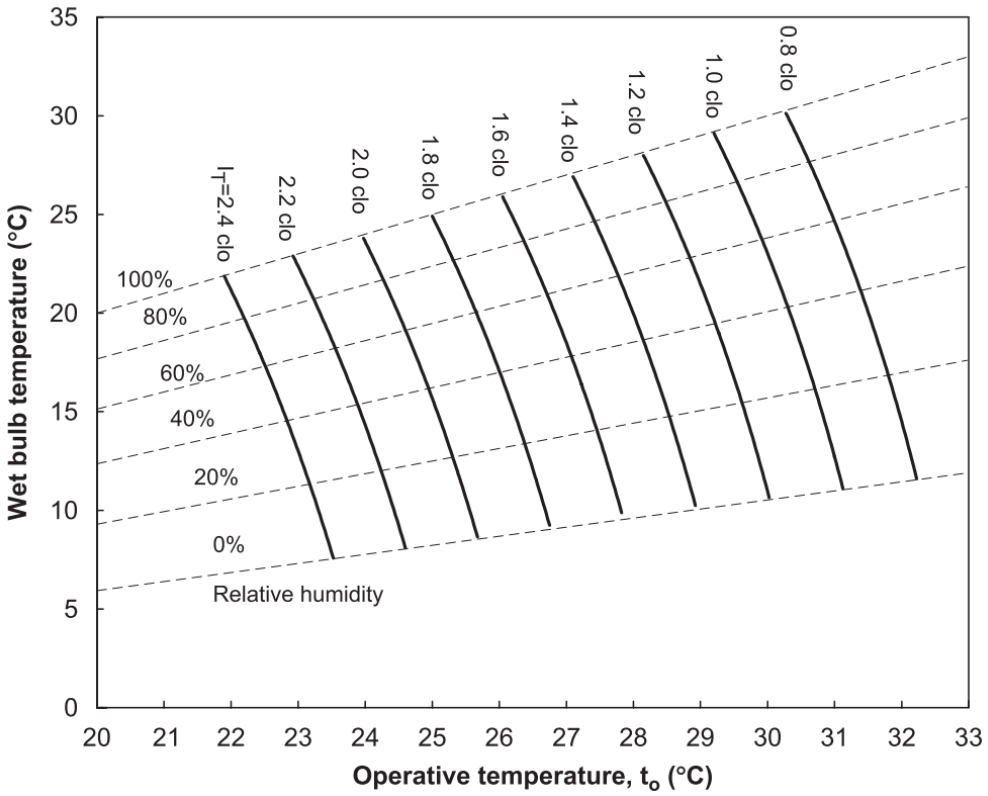

Fig. 2.4 Comfort lines (operative temperature vs. wet bulb temperature) with an indoor air velocity of not greater than 0.15 m/s (Lin and Deng 2008)

On the other hand, the total insulation value provided by a bedding system could significantly affect the operative temperature for a sleeping person. It can be seen that there was a linear relationship between the operative temperature and the total insulation value, as shown in Fig. 2.5.

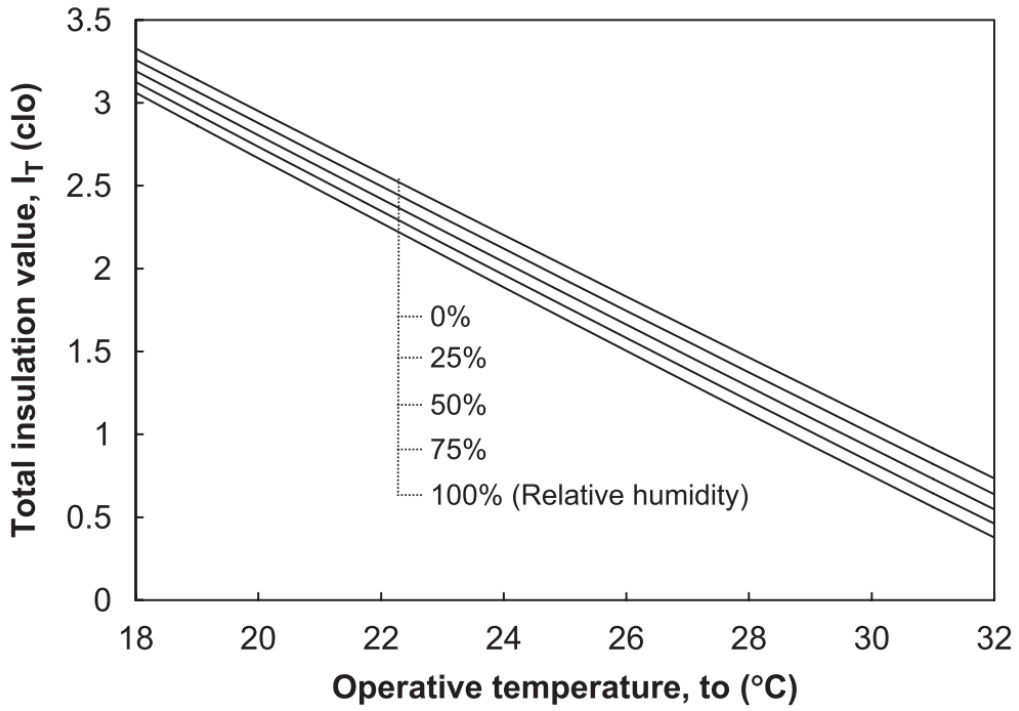

Fig. 2.5 Relationship between operative temperature and the total insulation value with an indoor air velocity of not greater than 0.15 m/s (Lin and Deng 2008)

Based on Gagge's two-node model (Gagge 1973), Pan et al. (2012) developed a four-node thermoregulation model to predict the thermoregulatory responses of a sleeping person as shown in Fig. 2.6. The model was firstly experimentally validated, which could be used to predict the thermoregulatory responses of a sleeping person with an acceptable accuracy. Moreover, the validated model could be used to predict different indoor thermal parameters, such as air temperature and humidity, in a sleeping environment and different bedding systems on the thermoregulatory responses of a sleeping person. Therefore, the model was expected to be a useful tool for carrying out on thermal comfort studies in sleeping environments.

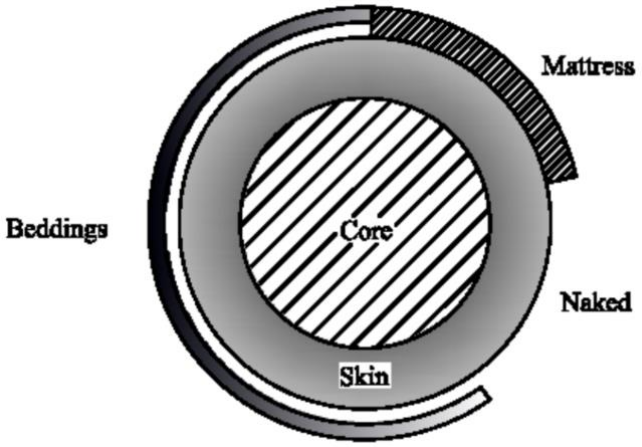

(a) The four-node thermoregulation model (Pan et al. 2012)

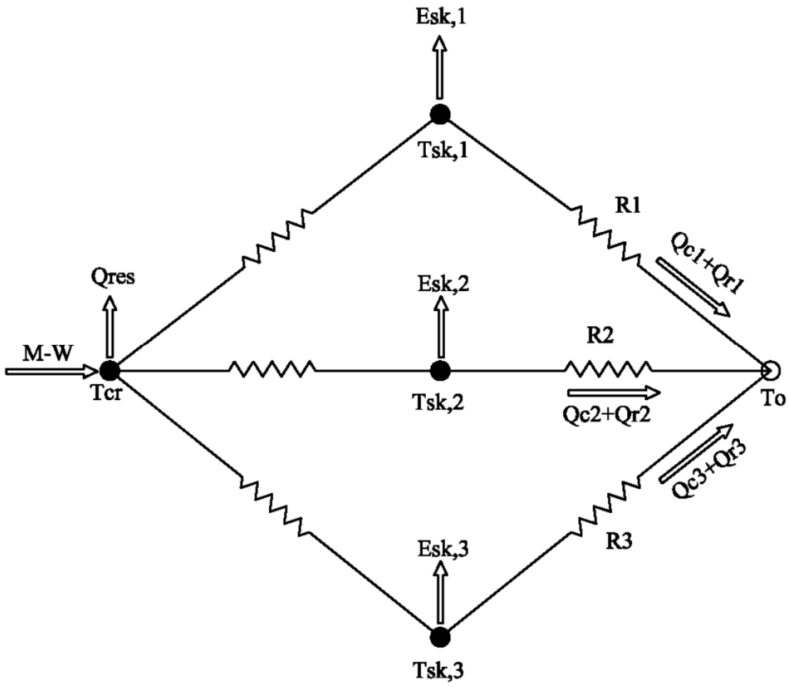

(b) Thermal resistance network (Pan et al. 2012)

Fig. 2.6 Schematic diagrams of the four-node thermoregulation model for sleeping applications (Pan et al. 2012)

2.5.2.2 Thermal comfort models applicable to heated sleeping environments

Based on Fanger's *PMV-PDD* scheme (Fanger 1970) and Lin and Deng's sleeping thermal comfort model (Lin and Deng 2008), a partial thermal sensation-whole predicted percentage of dissatisfaction (*PTS-WPD*) model applicable to heated sleeping environments has been previously developed by Song et.al (2018a). The *PTS-WPD* may be used for measuring the predicted percentage of dissatisfaction for a sleeping person under space heating conditions, by considering the differences in the thermal environments requirements exposed by a head region and the other body parts covered by quilt of a sleeping person, respectively, as seen in Fig. 2.7.

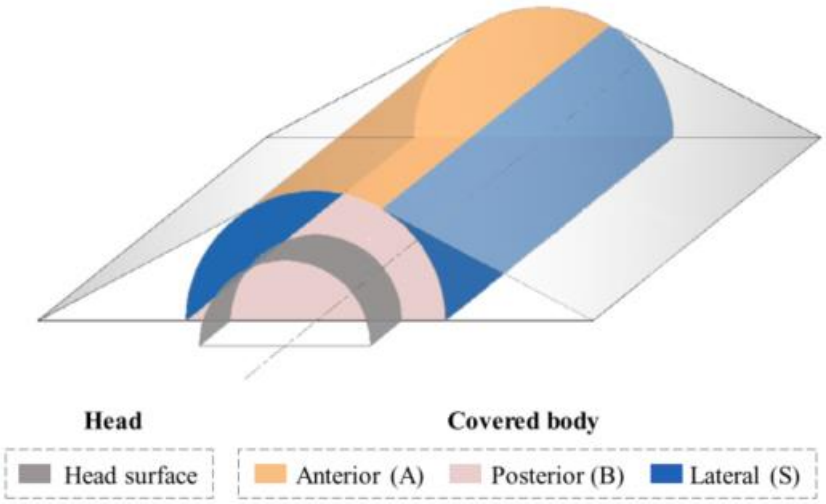

Fig. 2.7 A simplified model of a covered sleeping body in three parts (Song et al. 2018a)

The *PTS-WPD* model is expressed as follows (Song et al. 2018a):

$$WPD = 26.27 + 31.40PTS_H - 38.21PTS_{CB} + 13.12PTS_H{}^2 + 20.09PTS_{CB}{}^2 - 18.67PTS_H \cdot PTS_{CB} \tag{2.4}$$

Where PTS_H and PTS_{CB} are the calculated partial thermal sensation (*PTS*) of the head region, which is exposed to the ambient environment in a bedroom directly, and the other body parts covered by quilt, respectively, expressed by:

$$PTS_H = 0.9701 + 0.2317L_H + 0.0329\Delta L \tag{2.5}$$

$$PTS_{CB} = 2.0948 + 0.2184L_{CB} - 0.1663\Delta L \tag{2.6}$$

Where L_H and L_{CB} are the thermal load on the head region and the other body parts covered by a quilt, respectively, W, expressed as follows:

$$L_H = 0.176MA_W - \left\{ \begin{array}{l} 0.5\times\left[0.0014M(34-t_a)+0.0173M(5.87-p_a)\right]A_W \\ +0.99h_{c,H}(0.256t_{sk,H}-3.373-p_a)A_H + h_{c,H}(t_{sk,H}-t_a)A_H \\ +h_{r,H}(t_{sk,H}-\overline{t_r})A_H \end{array} \right\} \quad (2.7)$$

$$L_{CB} = 0.824MA_W - \left\{ \begin{array}{l} 0.5\times\left[0.0014M(34-t_a)+0.0173M(5.87-p_a)\right]A_W \\ +\dfrac{(t_{sk,A}-t_{a,A})A_A}{R_{cl}} + \dfrac{(t_{sk,B}-t_{a,B})A_B}{R_{cl}} \\ +\dfrac{(t_{sk,S}-t_{a,S})A_S}{R_{cl}+\dfrac{1}{f_{cl}h_{c,C}}} + \dfrac{(t_{sk,S}-t_{a,S})A_S}{R_{cl}+\dfrac{1}{f_{cl}h_{r,C}}} \\ +\dfrac{0.06(0.256t_{sk,A}-3.373-p_{a,A})A_A}{R_{ecl}} \\ +\dfrac{0.06(0.256t_{sk,B}-3.373-p_{a,B})A_B}{R_{ecl}} \\ +\dfrac{0.06(0.256t_{sk,S}-3.373-p_{a,S})A_S}{R_{ecl}+\dfrac{1}{16.5f_{cl}h_{c,C}}} \end{array} \right\} \quad (2.8)$$

$$\Delta L = L_{CB} - L_H \quad (2.9)$$

Where p_a is the water vapor pressure in ambient air, kPa, set at a value when relative humidity was 30 %; $t_{sk,q}$ the averaged skin temperature in contact with quilt, ^{o}C; $t_{sk,mat}$ the averaged skin temperature in contact with mattress, ^{o}C.

According to the established *PTS-WPD* model (Song et al. 2018a), the use of both PTS_H and PTS_{CB} was similar to that of the *PMV* model developed by Fanger (1970). PTS_H at 0 reflected a thermally neutral environment for the head region and PTS_{CB} at 0 that for the other body parts covered by quilt. Furthermore, when the calculated *WPD* values was lower than 10 %, a thermal environment may be regarded as being thermally comfort for a sleeping person.

2.5.2.3 Other related studies

Except studies on establishing thermal comfort models applicable to sleeping environments, other related studies have been carried out such as studying the effects of indoor air temperatures on human sleep stages, adopting different thermal neutral temperatures in sleeping environments, etc. (Karacan et al. 1978, Haskell et al. 1981, Candas et al. 1982, Macpherson 1973, Di Nisi et al. 1989, Dewasmes et al. 2000). Table 2.1 (Mao 2015) shows different thermal neutral temperatures demonstrated by the related studies. It can be seen that there is a fairly great range of thermal neutral temperature. Therefore, there is not a universal thermal neutral temperature applied to all circumstances due to different experimental conditions.

Table 2.1 Different thermal neutral temperatures adopted in studies related to sleeping thermal environments (Mao 2015)

Literature	Thermal neutral temperature (^{o}C)	Condition of sleeping subjects	Remark
Macpherson 1973	29 - 32	Naked	Air temperature
Karacan et al. 1978	22.2	Covered	Air temperature
Haskell et al. 1981	29	Naked	Air temperature
Candas et al. 1982	32	Naked	Operative temperature
Palca 1986	29	Naked	Air temperature
Sewitch et al. 1986	20 - 22	Covered	Air temperature
Di Nisi et al. 1989	30	Naked	Operative temperature
Dewasmes et al. 2000	28	Naked	Air temperature

In addition, Pan et al. (2011) carried out a numerical study to determine the thermal neutral temperatures in a conditioned bedroom. As shown in Fig. 2.8, the thermal resistance of beddings could significantly affect the thermal neutral temperature of a sleeping person, i.e., at a higher thermal resistance of bedding, the lower the thermal neutral temperature. The study results also suggested that the supply air velocity did not significantly affect the thermal neutral temperature when people were fully covered by beddings.

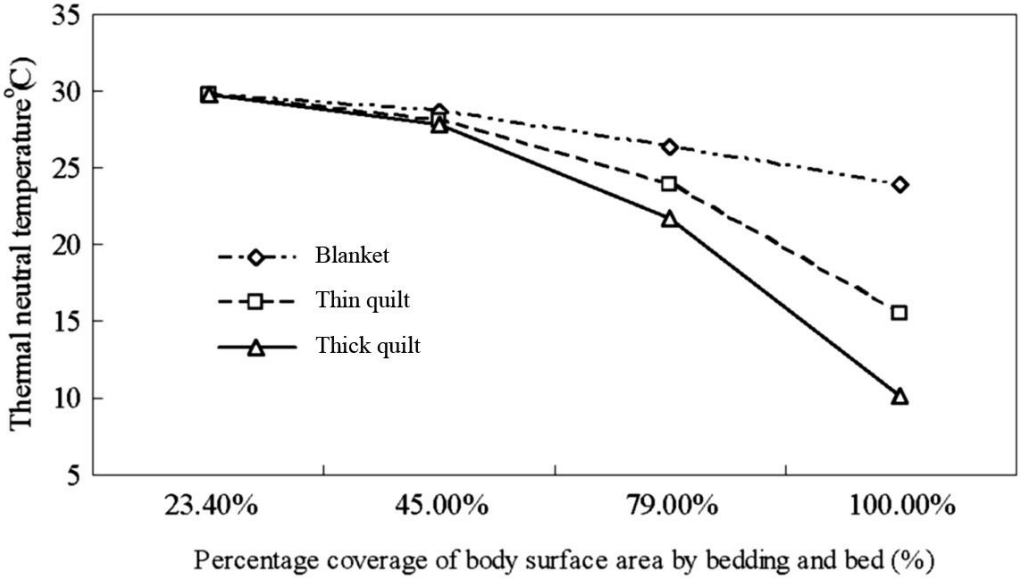

(a) at a supply air velocity of 0.12 m/s

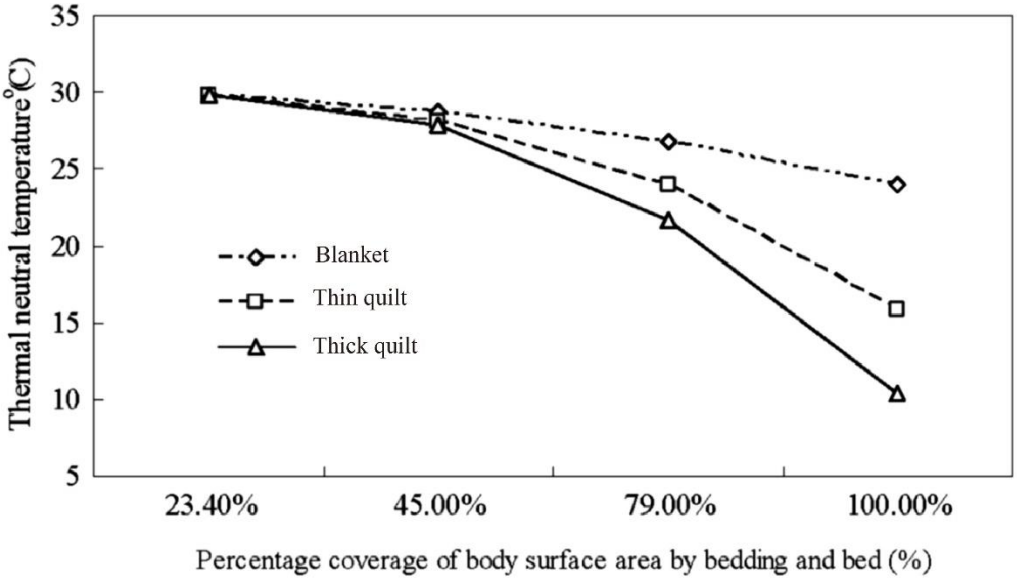

(b) at a supply air velocity of 0.24 m/s

Fig. 2.8 The relationship between thermal neutral temperature and percentage coverage of body surface area by bedding and bed at the three different beddings (Pan et al. 2011)

2.6 Using CFD methods for indoor thermal environment study

Computational fluid dynamics (CFD) based numerical methods are widely used in investigating the thermal environment of a conditioned indoor space such as room air distribution, air flow pattern and indoor air quality (Myhren and Holmberg 2008, Seyam et al. 2014, Zhou and He 2015), so as to optimize the design/operating parameters of HVAC systems and to improve system performances.

2.6.1 Governing equations

The flow field can be evaluated by three-dimensional and steady-state Reynolds averaged Navier-Strokes (RANS) equations, combined with continuity and energy equations. The governing equations are as follows:

Continuity equation:

$$\frac{\partial \rho}{\partial t} + \nabla \cdot \left(\rho \vec{v} \right) = 0 \tag{2.10}$$

Momentum equation:

$$\frac{\partial}{\partial t}\left(\rho \vec{v} \right) + \nabla \cdot \left(\rho \vec{v} \vec{v} \right) = -\nabla P + \nabla \cdot \left(\bar{\bar{\tau}} \right) + \rho \vec{g} \tag{2.11}$$

Where p is the static pressure, $\bar{\bar{\tau}}$ is the stress tensor and $\rho \vec{g}$ is the gravitational body force.

Energy equation:

$$\frac{\partial}{\partial t}(\rho E) + \nabla \cdot (\vec{v}(\rho E + p)) = \nabla \cdot (\rho k_{eff} \nabla T - h + (\overline{\overline{\tau}}_{eff} \cdot \vec{v})) \qquad (2.12)$$

Where k_{eff} is the effective conductivity, h the enthalpy and $\overline{\overline{\tau}}_{eff}$ the deviatoric stress tensor. The total energy, E, is expressed by:

$$E = h - \frac{p}{\rho} + \frac{|\vec{v}|^2}{2} \qquad (2.13)$$

2.6.2 Turbulence models and applications

In general, there are three approaches for predicting the turbulence flow using CFD methods: Direct Numerical Simulation (DNS), Large Eddy Simulation (LES), and Reynolds-Averaged Navier-Stokes (RANS) equation simulation, respectively, as shown in Table 2.2 (Mao 2015).

Table 2.2 Turbulence models for predicting airflows in enclosed environments (Mao 2015)

<table>
<tr><th colspan="3">Turbulence model classification</th><th>Primary turbulence models used in indoor air simulations</th></tr>
<tr><td colspan="3">DNS</td><td>(Orszag 1970)</td></tr>
<tr><td colspan="3">LES</td><td>LES-Sm (Smagorinsky 1963)
LES-Dyn (Germano et al. 1991, Lilly 1992)
LES-Filter (Zhang and Chen 2000, Zhang and Chen 2005)</td></tr>
<tr><td rowspan="6">RANS</td><td rowspan="5">EVM</td><td>Zero-equation</td><td>Zero-equation (Chen and Xu 1998)</td></tr>
<tr><td rowspan="3">Two-equation</td><td>Standard k-e (Launder and Spalding 1974)
RNG k-e (Victor Yakhot and Orszag 1986)
Realizable k-e (Shih 1995)</td></tr>
<tr><td>LRN-LS (Launder and Sharma 1974)
LRN-JL (Jones and Launder 1973)
LRN-LB (Lam and Bremhorst 1981)</td></tr>
<tr><td>LRN k-w (Wilcox 1994)
SST k-w (Menter 1994)</td></tr>
<tr><td>Multiple-equation</td><td>v2f-dav (Davidson et al. 2003)
v2f-lau (Laurence et al. 2005)</td></tr>
<tr><td colspan="2">RSM</td><td>RSM-IP (Gibson and Launder 1978)
RSM-EASM (Gatski and Speziale 1993)</td></tr>
</table>

Airflow inside buildings is characterized by displaying of various flow elements. For example, the airflow inside a room may be divided into natural convection, forced convection, or mixed convection according to its driving force. However, certain turbulence models are only good at dealing with certain flow elements. It has been almost impossible so far to identify a single model that can be used to evaluate all room airflow patterns economically and accurately. To choose a suitable turbulence

model is therefore a compromise considering the following factors: the physics encompassed in the flow, the established practice for a specific class of issues, the level of accuracy needed, the available computing powers, and the urgency for project completion, etc.

Nowadays, k-e models are still widely adopted for engineering applications. A standard k-e model is only feasible for predicting fully turbulent flow. In the near-wall region around the solid surfaces, the model should be carefully treated with a selected wall function considering the dominant effects of viscosity. The accuracy of the solution would be significantly affected by the location of the first layer of the mesh adjacent to the wall boundaries (Niu and Van der Kooi 1992). For predicting the airflow around a human body, the RNG k-e model and the low Reynolds number k-e model are commonly used. Murakami et al. (Murakami et al. 1995) demonstrated that the accuracy when using the standard k-e turbulence model to simulate the airflow around a thermal manikin was relatively low. However, due to the complication of the manikin physical model, it was impossible to achieve a good convergence using the low Reynolds number k-e model (Voigt et al. 2001).

Apart from the k-e model, the k-w model (Menter 1994, Wilcox 1994) is attracting increasing attentions for industrial and scientific applications in the past 10 years. To improve the robustness of the k-w model for predicting the flow in wake region and free shear flows, a shear stress transport (SST) k-w model was developed by Menter (1994) by combing the advantages of both the k-e and the k-w models, and the numerical results were in good agreement with the experimental data . For example, by comparing the use of three advanced turbulence models, i.e., RNG k-e model,

Reynolds stress model and SST k-w model, respectively, Arun and Tulapurkara (2005) demonstrated that the SST k-w model could capture the details of the complex flow features such as the movement of vortices downstream of the partition, flow in reverse direction in the top portion of the enclosure, and the exit of flow with swirl. Moreover, Stamou and Katsiris (2006) compared the use of SST k-w model, standard k-e model, RNG k-e model and a laminar flow model, respectively, for predicting air velocity and temperature distributions in an office room with a task ventilation system. The numerical study results showed that although the three turbulence models could satisfactorily capture the main qualitative features of the air flow, the SST k-w model performed better at predicting the air flow at near-wall region. Kuznik et al. (2007) used Realizable k-e model, RNG k-e model, standard k-w model and SST k-w model, respectively, for predicting the air temperature and velocity in a mechanically ventilated room. By comparing the numerical study results with experimentally measured data, it was found that the k-w models showed a better accuracy and robustness. Therefore, the SST k-w model (Menter 1994) seemed to have a better overall performance than other models for predicting the air flow inside an indoor space.

2.6.3 Mesh generation

Apart from choosing a suitable turbulence model, mesh quality could also significantly affect the accuracy of simulation results. The mesh quality is impacted by grid topology, grid shape, grid size and the consistency of grids with geometry, etc.

In general, there are four methods to discretize a space: cartesian co-ordinates, cylinder co-ordinates, body-fitted co-ordinates and unstructured grids, respectively. For

predicting the airflow near complicated geometries such as the region around a human body, body-fitted co-ordinates and unstructured grids are commonly used, and unstructured grids are more preferable.

The meshes for numerical studies inside an occupied indoor space are usually separated into 2 computing regions: a cuboid for housing the manikin and the space outside the cuboid. The cuboid region is therefore generated with unstructured grids due to complicity of the manikin and the rest of space with structured grids due to the simplicity of its geometry, respectively (Gao and Niu 2005, Mao et al. 2014a).

2.6.4 Related numerical studies on the thermal environment around a person

In order to correctly evaluate the thermal comfort of an individual, the thermal environment around a human body should be measured including air temperature, air velocity, etc. In the related studies, digital thermal manikins (DTMs) are widely used due to the advantages of operation safety, controllable and stability (Holmér 2004).

Gao and Niu (2005) reviewed several important issues related to CFD studies on predicting the thermal environment around a human body, including geometric complexity, boundary conditions and related simulation results obtained, respectively. Firstly, the review showed that it was necessary to choose a suitable manikin model with appropriate size, posture and the level of geometric complexity, which depended on the purpose of study (Gao and Niu 2004, Sørensen and Voigt 2003, Pan et al. 2011). Using simplified DTMs required fewer computing powers and solution time. However, DTMs with higher geometric complexity could provide more details. Secondly, two methods were commonly adopted for the boundary conditions of a DTM, i.e., at a

fixed surface temperature or at a fixed surface heat flux. Normally, the surface temperature of a DTM was set between 31 ^{o}C (Murakami 1997) and 33.7 ^{o}C (Sørensen and Voigt 2003), and the convective heat flux was set between 20 W/m^2 (Hayashi et al. 2002) and 25 W/m^2 (Brohus and Nielsen 1995), respectively. Finally, heat transfer through radiation and convection from a DTM could be numerically evaluated for predicting the thermal comfort level of a person (Murakami et al. 2000, Silva and Coelho 2002, Yang et al. 2002, Sørensen and Voigt 2003, Gao and Niu 2004).

On the other hand, by using a DTM to simulate a sleeping person, both convection-based (Mao et al. 2014b) and radiation-based (Du et al. 2017) bed-based task/ambient air conditioning (C-TAC and R-TAC) systems were numerically studied, and the sleeping thermal environment around the DTM analyzed.

2.7 Conclusions

In this Chapter, an extensive review on the previous related studies on the use of ASHPs and Chinese Kangs for space heating, the thermal comfort for a sleeping person and the use of CFD technologies for evaluating indoor thermal environments is presented. The key findings from this review are summarized as follows. Firstly, as shown in Section 2.2, air source heat pumps (ASHPs) have been increasingly used for space heating because they are highly energy efficient and flexible in installation. However, when using a conventional ASHP system for space heating, its fan-powered convection-based indoor heating terminals are usually located at a higher level in a heated room. This results in an undesired vertical indoor air temperature gradient and thermally discomfort to occupants as a result of directly blowing warm air to their upper bodies including heads. Furthermore, as shown in Section 2.3, in many rural

areas in northern Chinese provinces, Kangs, a kind of traditional biofuel-burning heating systems, are still being widely used for space heating in winter. A Kang-bed in a Chinese Kang-based heating system serves as not only a space heating terminal at daytime for daytime activities but also a heated bed for sleeping at nighttime. However, employing such a Chinese Kang-based heating system can also lead to a number of operational, environmental and safety problems. Although some novel Kang-based heating systems have been developed, there were also a number of additional issues of concerns, making them technically less attractive.

Secondly, as presented in Section 2.4, the factors influencing sleeping quality may include the personal mental-physical factors of a sleeping person, and the environmental factors in a sleeping environment, such as noise level, lighting and thermal environment. However, as presented in Section 2.5, there have been only a limited number of previous studies on investigating the appropriate thermal parameters in a sleeping environment, developing thermal comfort models applied to both air conditioned and heated sleeping environments and determining thermally neutral temperature for a sleeping environment, in particular for a winter condition.

Finally, in Section 2.6, a review on using CFD methods to predict indoor thermal environment and energy performances in buildings is presented. The CFD method is powerful to study thermal comfort, energy utilization efficiency and ventilation effectiveness in the field of HVAC engineering.

Through the extensive literature review reported in this Chapter, a number of the problems of applying both conventional ASHPs and traditional Chinese Kang-based

heating systems to space heating have been identified. These problems will be addressed in the research project reported in this thesis.

Chapter 3 Proposition

3.1 Background

It is evident from the literature review presented in Chapter 2 that, due to the distinguished advantages of high energy efficiency and flexibility in installation, ASHPs have been widely applied worldwide. However, when using a conventional ASHP system for space heating, its fan-powered convection-based indoor heating terminals are usually located at a higher level in a heated room. This would lead to a number of operational problems such as an undesired vertical indoor air temperature gradient and thermally discomfort to occupants as a result of directly blowing warm air to their upper bodies including heads. On the other hand, Chines Kangs are still being widely used for space heating in the rural areas in Northern China in winter. However, employing such a Chinese Kang heating system may also lead to a number of operational, environmental and safety problems.

Therefore, it is highly necessary to propose and develop a novel bed-based ASHP (B-ASHP) space heating system by combing the merits from both an ASHP space heating system and a Chinese Kang-based space heating system. In this novel B-ASHP system, refrigerant tubes of the condenser in an ASHP can be placed on the surface of a bed based heating terminal which is to be operated in a similar way to the Kang-bed in a Chinese Kang heating system. Refrigerant being circulated in an ASHP unit is directly used as the heating medium for better ASHP operating efficiency and more uniformed bed surface temperature. Therefore, a research project to experimentally and numerically study operational characteristics an experimental B-ASHP system and to

optimize its design and operation was carried out and the project results are presented in this Thesis.

3.2 Project title

This research project was divided into three parts: firstly, experimentally evaluating the operating performances and indoor thermal environment when using an experimental B-ASHP system; Secondly, numerically studying the effects of varying the design/operating parameters of the bed-based heating terminal of the experimental B-ASHP system on indoor thermal environment and system operating efficiecncy; Finally, further numerically studying the thermal comfort of a person sleeping on the bed-based heating terminal of the B-ASHP system. Therefore, the research project presented in this Thesis is entitled “Experimental and Numerical Studies for a Novel Bed-based Air Source Heat Pump (B-ASHP) Heating System for Improving Indoor Thermal Environments in Winter”.

3.3 Aims and objectives

The aims and objectives of the research project are as follows:

- To experimentally evaluate the operating performances and indoor thermal environment when using the experimental B-ASHP system;
- To numerically investigate the effects of design/operating parameters of the bed-based heating terminal of the B-ASHP system on indoor thermal environment and operating efficiency;

- To further numerically study the sleeping thermal comfort of a person sleeping on the bed-based heating terminal of the B-ASHP system;

3.4 Research methodologies

Experimental and numerical methods are employed in this research project. The technical block diagram of the research project are shown in Fig. 3.1. Firstly, in the first part of the research project, an experimental approach will be used to evaluate the operating performances of the experimental B-ASHP system and indoor thermal environment in an experimental indoor space where the bed-based heating terminal was placed. The surface temperatures of the bed-based heating terminal, refrigerant pressures and mass flow rate in the experimental ASHP system and air temperature, globe temperature, surface temperature, indoor air velocity distribution in the experimental indoor space, respectively, will be measured. Using the measured parameters, the operating characteristics of the experimental B-ASHP system, and the thermal environments inside the experimental indoor space will be evaluated.

Then, in the second part of the research project, a numerical approach will be used to study the effects of varying the design/operating parameters of the bed-based heating thermal of the B-ASHP system on indoor thermal environment and operating efficiency. A CFD method for predicting indoor air temperature and air flow fields will be developed and experimentally validated using the experimental results obtained in the first part of the research project. Using the validated CFD method, the influences of varying a number of design/operating parameters of the bed-based heating terminal of the B-ASHP system, including the location, dimension, surface

temperature and surface emissivity, on the thermal environments of the indoor space and the operating efficiency of the experimental B-ASHP system will be studied.

Finally, in the last part of the research project, also a numerical approach, using a digital thermal manikin (DTM), will be employed to study the effects of a number of factors, including the operating modes of the bed-based terminal, bed surface temperature (t_{bed}), and thermal resistances of a mattress (R_{mat}) and a quilt (R_q), on the thermal comfort of a person sleeping on the bed-based heating terminal. A revised CFD method for predicting indoor air temperature and air flow fields will be developed and experimentally validated. Using the revised CFD method, the influences of these factors on the thermal comfort of a sleeping person when using the B-ASHP system will be numerically evaluated.

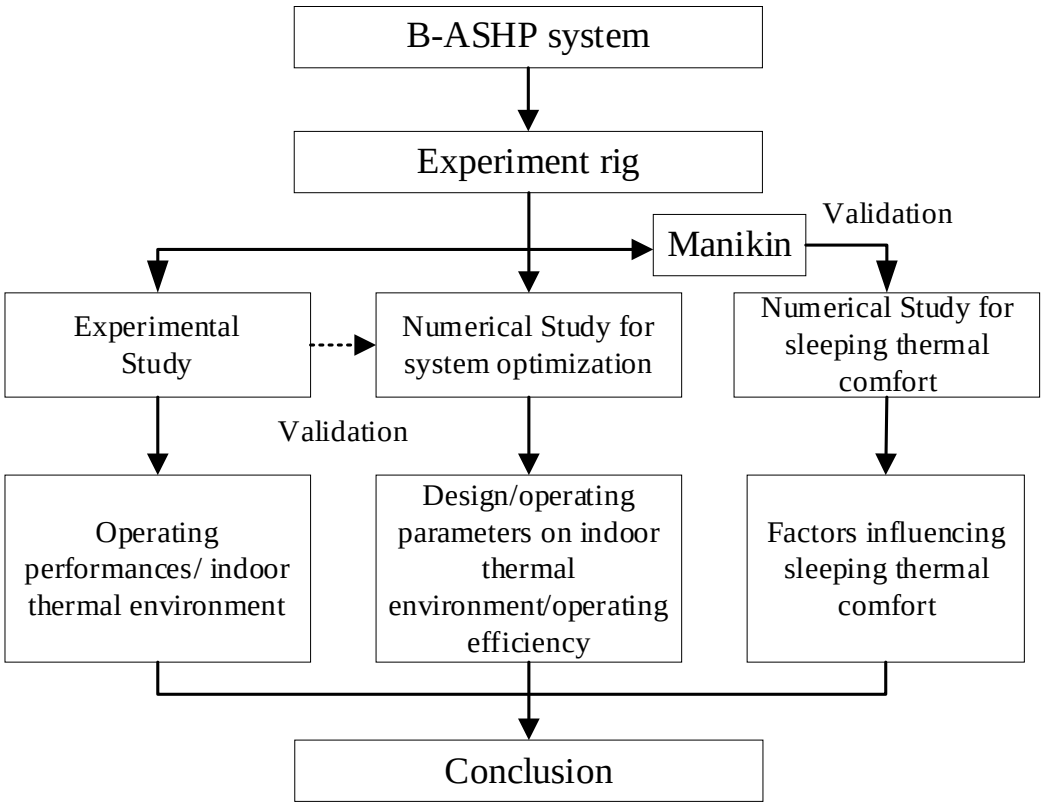

Fig. 3.1 Technical block diagram of the research project

Chapter 4 An experimental study on the operating performances of a novel bed-based air source heat pump (B-ASHP) system

4.1 Introduction

Air source heat pumps (ASHPs) have been widely applied worldwide due to their distinguished advantages of higher energy efficiency and installation flexibility (Dong et al. 2012). Conventionally, when using ASHPs for space heating, convection-based fan-powered indoor heating terminals are used (Lin et al. 2016). These terminals are usually located at a higher level in heated rooms, which is particularly true when the ASHPs are also used for space cooling in summer seasons. This would lead to a number of problems such as an undesired indoor air temperature gradient (Imanari et al. 1999) and thermally discomfort to occupants as a result of directly blowing warm air to their upper bodies including heads as reported in Chapter 2.

On the other hand, in many rural areas of northern China, currently, Chinese Kangs or heated beds (Cao et al. 2011) are still being used in nearly 85 % of village houses to maintain a warmer indoor thermal environment in winter. Traditionally, a Chinese Kang-based heating system is powered by burning biofuel such as stalk or firewood, even coal in a cooking stove normally placed in a kitchen adjacent to a heated room. Inside the heated room, the heated Kang-bed maintains a warm space where occupants could either sit or sleep on bed top. Hence, a Chinese Kang-based heating system not only provides a multifunctional living area, but also serves as a space heating terminal at both daytime and nighttime. However, employing such a Chinese Kang-based

heating system may also lead to a number of problems, such as local air pollutions, as described in Chapter 2.

As seen, while ASHP based space heating systems with fan-powered convection-based heating terminals and Chinese Kang-based heating systems, are widely used, they have their own pros and cons. Therefore, a novel bed-based ASHP (B-ASHP) space heating system has been proposed by combining the merits of both an ASHP and a traditional Chinese Kang-based heating system. In this novel B-ASHP system, refrigerant tubes of the condenser in an ASHP can be embedded on to the surface of a Kang bed to enable the bed to be operated in a similar way to a Chinese Kang-based heating system. In addition, refrigerant being circulated in an ASHP is directly used as the heating medium for better ASHP operating efficiency and more uniform Kang surface temperature. With the proposed B-ASHP system, the operating problems associated with a Chinese Kang-based heating system such local air pollutions and that with a conventional convection-based ASHP system such as unfavorable vertical indoor air temperature distribution and direct warm air blow to occupants' upper bodies may be avoided. Therefore, an experimental study for the operating performances of the proposed B-ASHP system, as the first part of the research project reported in this Thesis, has been carried out and the study results are reported in this Chapter. Firstly, an experimental setup for an experimental B-ASHP system is described, and the measurement methods specified. Secondly, the operating performances of the experimental B-ASHP system were experimentally investigated and are presented. Thirdly, a comparison analysis on the indoor thermal comfort between using the experimental B-ASHP system and a conventional convection-based ASHP unit is included. Finally, discussions and conclusions are given.

4.2 The experimental B-ASHP system

4.2.1 Description of the system

The schematic diagram for the experimental B-ASHP system is shown in Fig. 4.1. As seen, the major components in the experimental B-ASHP system included a compressor, an outdoor coil, an electronic expansion valve (EEV) and a bed-based heating terminal. The bed-based heating terminal consisted of two sections, a horizontal section (H-Section) and a vertical section (V-Section). Refrigerant R-410A was used as the working fluid in the experimental B-ASHP system. The detailed specifications of the major components are given in Table 4.1.

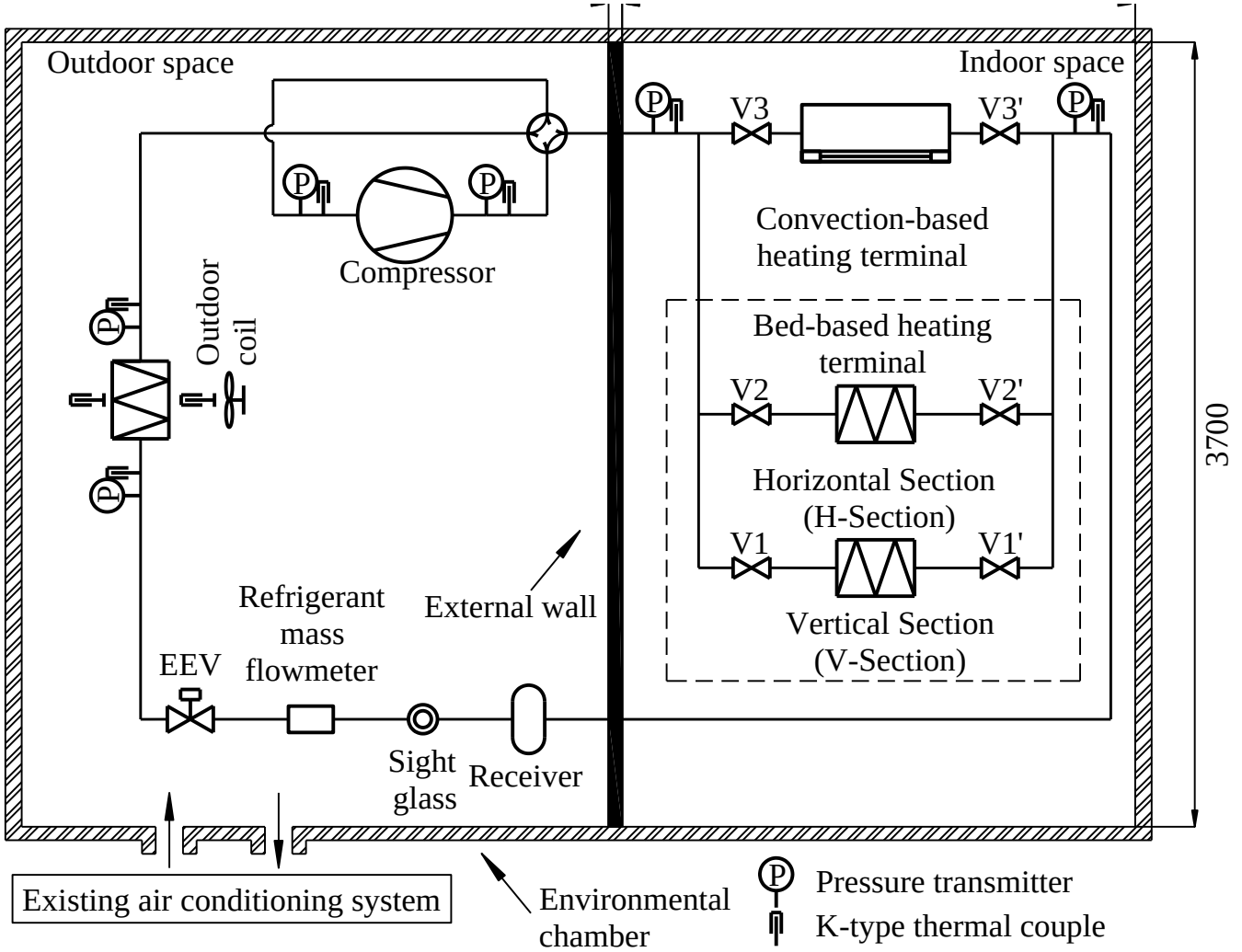

Fig. 4.1 The schematics of the complete setup for the experimental B-ASHP system installed in an environmental chamber (unit: mm)

The experimental B-ASHP system was placed in an environmental chamber having a simulated heated indoor space (3700 mm × 2600 mm × 3290 mm) and a simulated cold outdoor space. The bed-based heating terminal was placed inside the experimental indoor space, while the rest of the system in the outdoor space. The two spaces were separated by a simulated external wall. There was a window (1220 mm × 1220 mm) on the external wall. The heat transfer due to the temperature difference between the two spaces provided the experimental indoor space with space heating load. In addition, the envelope of the chamber was thermally insulated and could be regarded as adiabatic. On the other hand, the environment in the outdoor space was jointly controlled by an existing air conditioning system for the chamber (Xia et al. 2017, Yan et al. 2018), and the outdoor coil of the experimental B-ASHP system placed there, to maintain a stable low-temperature experimental outdoor environment. Moreover, to enable the comparison between using the experimental B-ASHP system and a conventional convection-based ASHP system, one more convection-based heating terminal was also installed on an internal surface of the experimental indoor space at 2500 mm high.

Table 4.1 Specifications of the major components in the experimental B-ASHP system

Component	Parameter	Value	Unit
Compressor	Power type	DC inverter	
	Allowable Frequency	1500-6300	rpm
	Rated Capacity	2200	W
Receiver	Volume	1.0	L
Bed-based heating terminal (H-Section)	Number of circuits	3	
	Surface area	3.00	m^2
Bed-based heating terminal (V-Section)	Number of circuits	2	
	Surface area	4.95	m^2
Convection-based heating terminal	Air flow rate	0.172	m^3/s
	Surface area	9.52	m^2
	Rated Capacity	3400	W
Circulating fan	Air flow rate	0.024	m^3/s
EEV	Pulse range	1-480	pulse
	Rated capacity	4.1	kW
	Port diameter	1.4	mm

4.2.2 Details of the bed-based heating terminal

The bed-based heating terminal, functioning like a Kang, in the experimental B-ASHP system, was made of hollow cuboid structure with a metal frame and filled with neoprene foam. To ensure an adequate bed surface area for heating purpose, the cuboid was designed to be measured at 2000 mm × 1500 mm × 900 mm, as illustrated in Fig. 4.2 (a). It should be mentioned that the height of 900 mm was slightly higher than that of a typical Kang at 600 - 700 mm (Zhuang et al. 2009b), so as to provide sufficient heat transfer area of the V-Section. Nonetheless, further optimizations on the dimension should be carried out to bring the height close to 700 mm.

As seen from Fig. 4.2 (b) and Fig. 4.2 (c), rows of refrigerant tubes were placed on both the top and side surfaces of the cuboid, to form the H-Section and the V-Section respectively, as mentioned earlier. The H-Section consisted of three refrigerant circuits, sandwiched by two aluminum plates measured at 2000 mm × 1500 mm, to form a

smooth bed surface of 3.00 m^2. The V-Section consisted of two refrigerant circuits, also sandwiched by aluminum plates and installed vertically on each side of the bed structure, with a total heat transfer area of 4.95 m^2, as shown in Fig. 4.2 (c).

In addition, in Fig. 4.2 (d), the details of fixing refrigerant tubes to the aluminum plates for both the H-Section and V-Section are shown. Refrigerant tubes were sandwiched between an outer aluminum plate and an inner plate to form a bed-surface assembly, with the outer surfaces of the outer aluminum plates being uncovered. Inside an assembly, heat conducting silicone grease was injected into the space among the aluminum plates and the refrigerant tubes. There were in total three assemblies, one for the H-Section and the other two for the V-Section. The three assemblies were then fixed to the bed structure, as shown in Fig. 4.2 (a). A neoprene foam thermal insulation layer of 30 mm thick was provided between an assembly and the bed structure, as shown in Fig. 4.2 (d), and the material properties details of the bed-based heating terminal are listed in Table 4.2.

Table 4.2 Material properties details of the bed-based heating terminal

Material	Specific heat / J/(g·K)	Density / kg/m^3	Thermal conductivity / W/(m·K)
Aluminium plate	0.900	2600	237
Refrigerant tube (copper)	0.386	8960	401
Thermal insulation layer	2.996	110	0.050
Heat-conducting silicone grease	2.5	2400	1.5

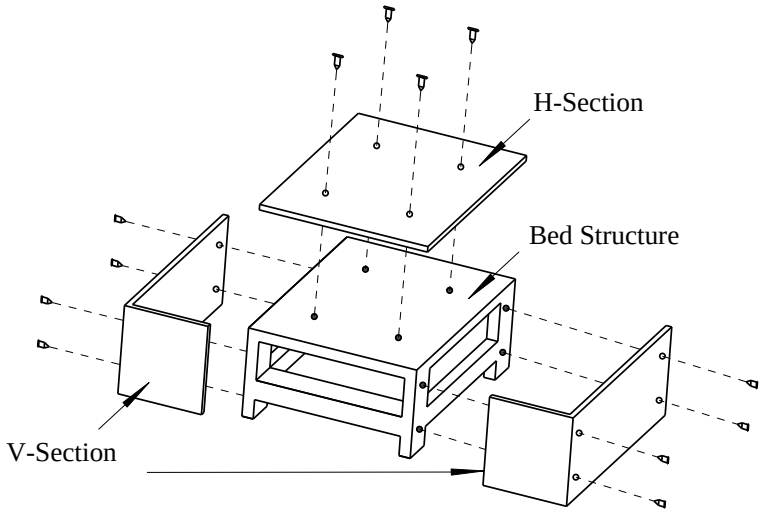
H-Section
Bed Structure
V-Section

(a)

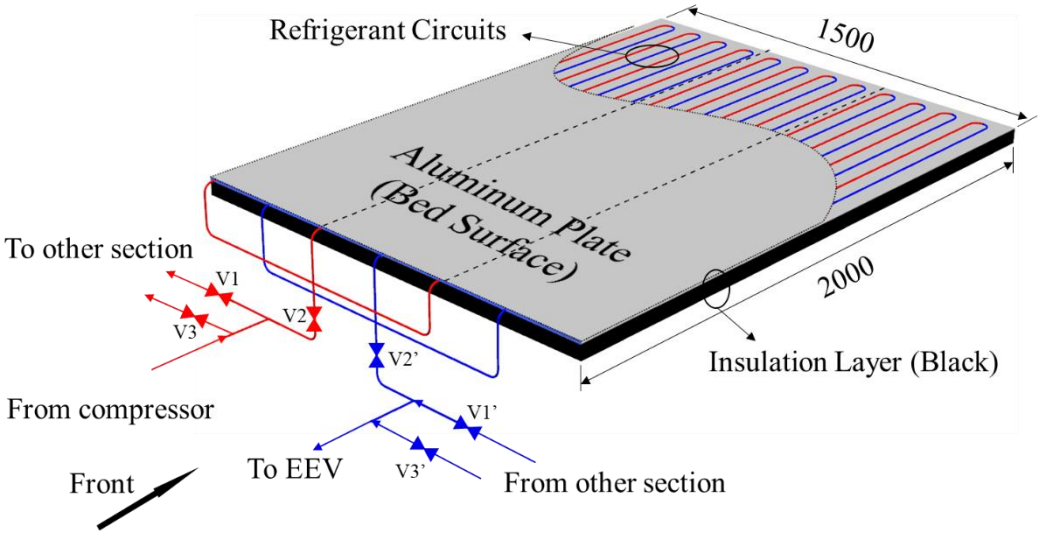
Refrigerant Circuits
1500
Aluminum Plate
(Bed Surface)
2000
To other section
V1
V2
V3
V2'
Insulation Layer (Black)
From compressor
V1'
To EEV
V3'
From other section
Front

(b)

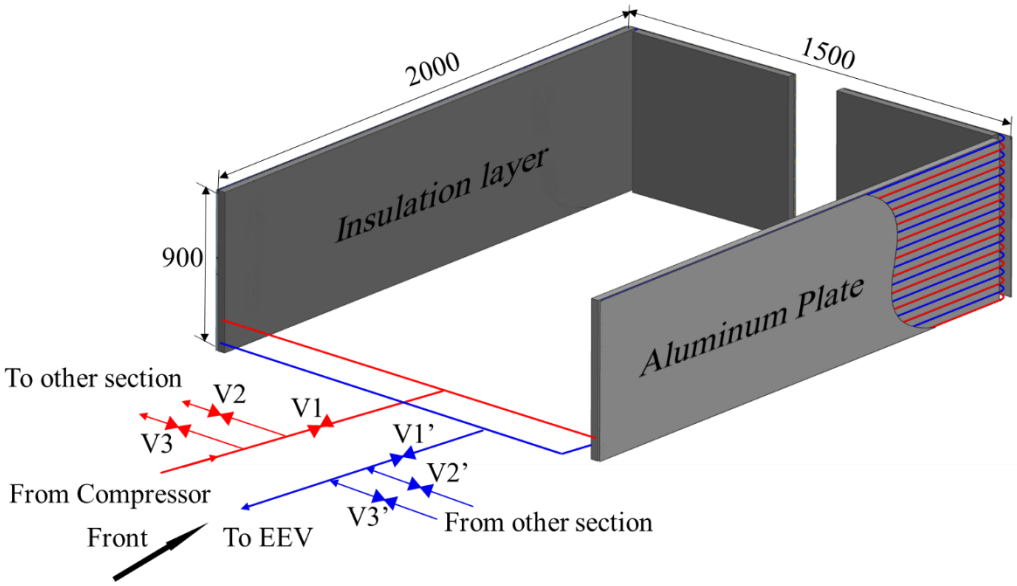
2000
1500
900
Insulation layer
Aluminum Plate
To other section
V2
V1
V3
V1'
V2'
V3'
From Compressor
From other section
Front
To EEV

(c)

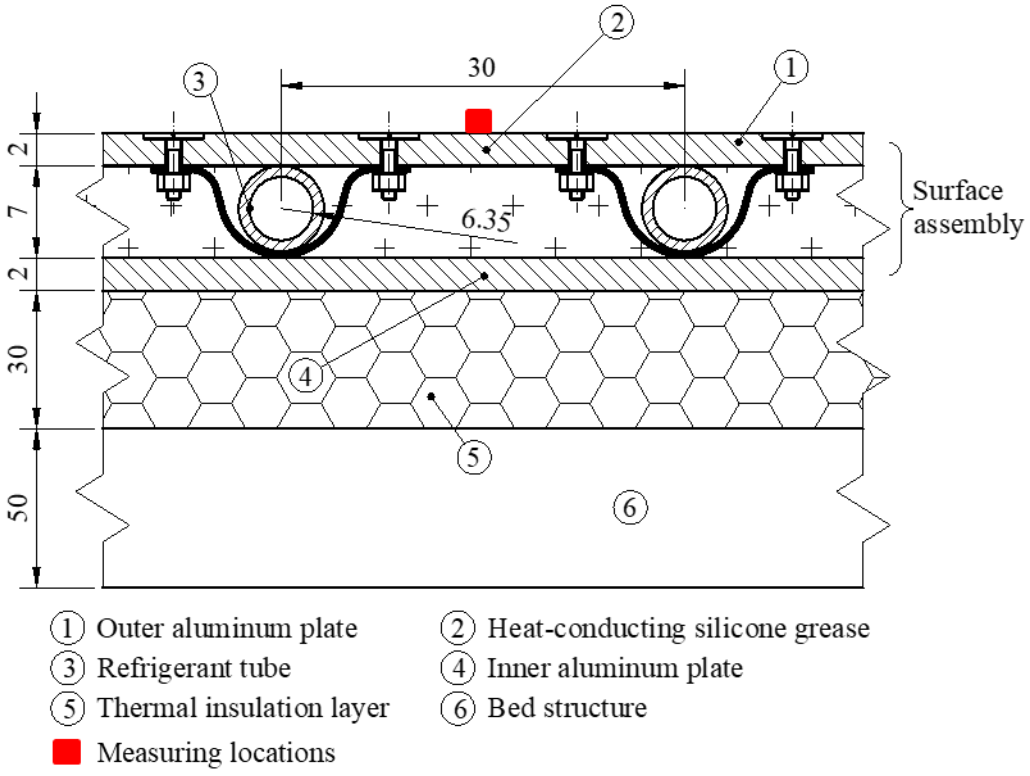
30
6.35
Surface assembly
2
7
2
30
50
1 Outer aluminum plate
2 Heat-conducting silicone grease
3 Refrigerant tube
4 Inner aluminum plate
5 Thermal insulation layer
6 Bed structure
Measuring locations

(d)

Fig. 4.2 Construction details of the bed-based heating terminal (a) 3-D view of the bed-based heating terminal and assembling method (b) the H-Section (c) V-Section (d) a surface assembly (unit: mm)

The experimental B-ASHP system may be operated at two operating modes, i.e., a nighttime mode and a daytime mode. At the nighttime mode, only the H-Section was operated when valve V2 was opened and V1 and V3 closed, for achieving localized heating during sleeping. At daytime mode, either the V-Section or H+V-Section may be operated to achieve full space heating at daytime.

4.2.3 Measurement methods

The experimental B-ASHP system was fully instrumented with high precision sensors and transducers to enable the experimental evaluation of its operating performances. Signals from sensors/transducers were collected by a computerized data acquisition system, and recorded at an interval of 10 s.

Measuring points in the experimental B-ASHP system for refrigerant tube surface temperatures, pressures and mass flow rate are indicated in Fig. 4.1. Refrigerant tube surface temperatures were measured by K-type thermocouples of 1 mm diameter, with an accuracy of ± 0.3 °C, pressures by pressure sensors (± 0.005 MPa), and mass flow rate by a mass flowmeter (± 0.05 %). The input power to the compressor in the experimental B-ASHP system was measured by a power meter (± 2.0 W). The thermocouples for measuring refrigerant tuber surface temperatures were attached firmly to the tube surface and wrapped with insulating tape, so that the measured

surface temperatures may be taken approximately as the refrigerant temperature inside the tube.

At the nighttime mode, the experimental indoor space was divided into two zones for better thermal comfort evaluation. A cuboid (2000 mm × 1500 mm × 600 mm) right above the bed surface was designated as an occupied zone (OZ). The rest of the experimental indoor space, on the other hand, was designated as an unoccupied zone (UZ). At nighttime mode, occupants normally slept and the localized heating inside the OZ was essential, while the full heating for the rest of the experimental indoor space was not of main concern.

Inside the OZ, air temperature (t_a) and air velocity were measured at 18 sampling points, i.e., at three height of 1000 mm, 1200 mm and 1500 mm above the floor level of the six horizontal locations marked as OA to OF in Fig. 4.3 (a), respectively. The measured 18 values for each of the two parameters were averaged to be their respective mean value in the OZ (ASHRAE 2017). Similarly, for the UZ, t_a were recorded at five different heights, 100 mm, 600 mm, 1100 mm, 1700 mm and 2500 mm above the floor level, respectively, at the six locations marked by UA to UF, also shown in Fig. 4.3 (a). Totally, 30 measured values were averaged to be the averaged t_a in the UZ. In addition, four globe thermometers were placed at four locations of OA, OB, OE and OF at a height of 1500 mm above the floor level for measuring the $\overline{t_r}$.

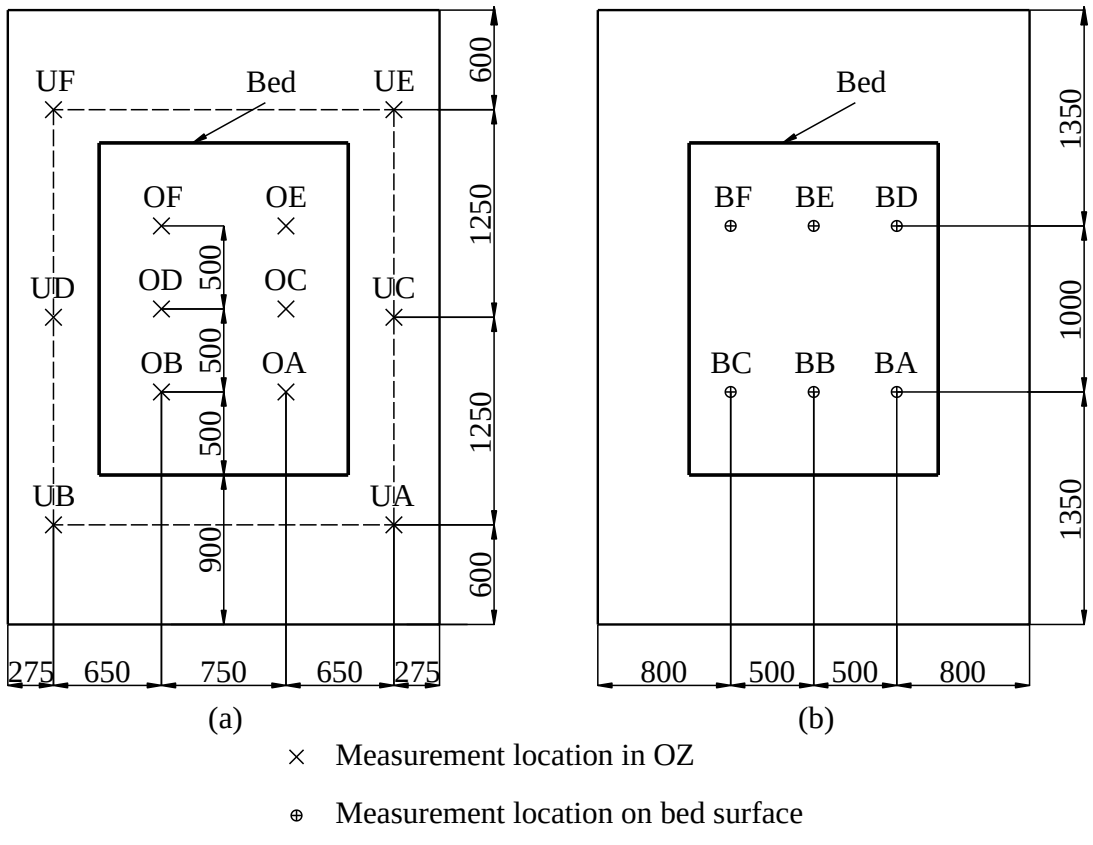

Fig. 4.3 Measurement locations for (a) OZ and UZ; (b) on the bed surface (unit: mm)

Bed surface temperatures were measured at the six locations marked as BA to BF as shown in Fig. 4.3 (b). The six measured values were averaged to be the mean bed surface temperature. The t_a inside both OZ and UZ, and bed surface temperatures were measured using the same type of K-type thermocouples in previous section and the air velocity inside the OZ using an air velocity transducer (± 1 %).

4.2.4 Description of test cases

With the availability of the above described experimental B-ASHP system, extensive experiment work has been carried out to evaluate its operating performances at both nighttime and daytime modes. Based on the ISO 5151 (2017) and GB/T 7725 (2004), t_{out} was set at 2, 7, 10 ^{o}C, respectively. Totally, there were four test cases and their

respective experimental conditions are given in Table 4.3. Since the purpose of the current experimental study was to obtain the operating performances of the experimental B-ASHP system, the experimental outcomes from the four test cases would demonstrate the actual measured steady-state and dynamic operating performances of the experimental B-ASHP system at different operating modes. Firstly, the dynamic operating performances of the experimental B-ASHP system after starting up were evaluated under the standard space heating condition at nighttime mode in Case 4.1. Secondly, in Cases 4.2 and 4.3, steady state performances of the experimental B-ASHP system under three different testing t_{out} at both the nighttime and daytime modes were respectively evaluated. Finally, in Case 4.4, comparative studies between using the experimental B-ASHP system and the convection-based heating terminal were carried out, so as to demonstrate the advantages of the proposed B-ASHP system. In each of the four test cases, compressor speed was fixed at 6300 rpm.

Table 4.3 Experimental conditions of four test cases for the experimental B-ASHP system

Test case	Testing t_{out}	Operating mode / heating section (s) of the B-ASHP system used	Objective	Experimental results shown in Section
4.1	7 °C	Nighttime / Horizontal	Dynamic performances of the B-ASHP system after starting up	4.3.1
4.2	2 °C, 7 °C, 10 °C	Nighttime / Horizontal	Steady state operating performances at various t_{out}	4.3.2.1
4.3	2 °C, 7 °C, 10 °C	Daytime / Vertical and vertical + horizontal	Steady state operating performances at various t_{out}	4.3.2.2
4.4	2 °C	Daytime / Vertical + horizontal	Comparative study between using the experimental B-ASHP system and the convection-based heating terminal	4.3.3

4.3 The experimental results

4.3.1 Measured dynamic operating performances of the experimental B-ASHP system after starting up (Case 4.1)

The dynamic operating performances of the experimental B-ASHP system at nighttime mode were experimentally investigated both after starting up and when a change in heating load was introduced to examine its starting up performances in Case 4.1. The measured results are reported in this section.

The experiment work in Case 4.1 lasted for 5 hours after starting up the experimental B-ASHP system. The variation profiles of refrigerant temperatures and averaged t_a in both OZ and UZ and t_{bed} are shown in Fig. 4.4. As seen, the refrigerant temperature at compressor discharge was quickly increased from 8 °C at the onset to 60 °C within the first 15 minutes. Then, it was increased slowly to 73.5 °C at 60 min and stayed at around 74.0 °C for the rest of the 5-hour test duration. The refrigerant temperature leaving the bed-based heating terminal which was actually the condensing temperature minus the degree of refrigerant sub-cooling was also increased quickly in the first 15 minutes of the test and stabilized at 36 °C at about 60 min into the experiment.

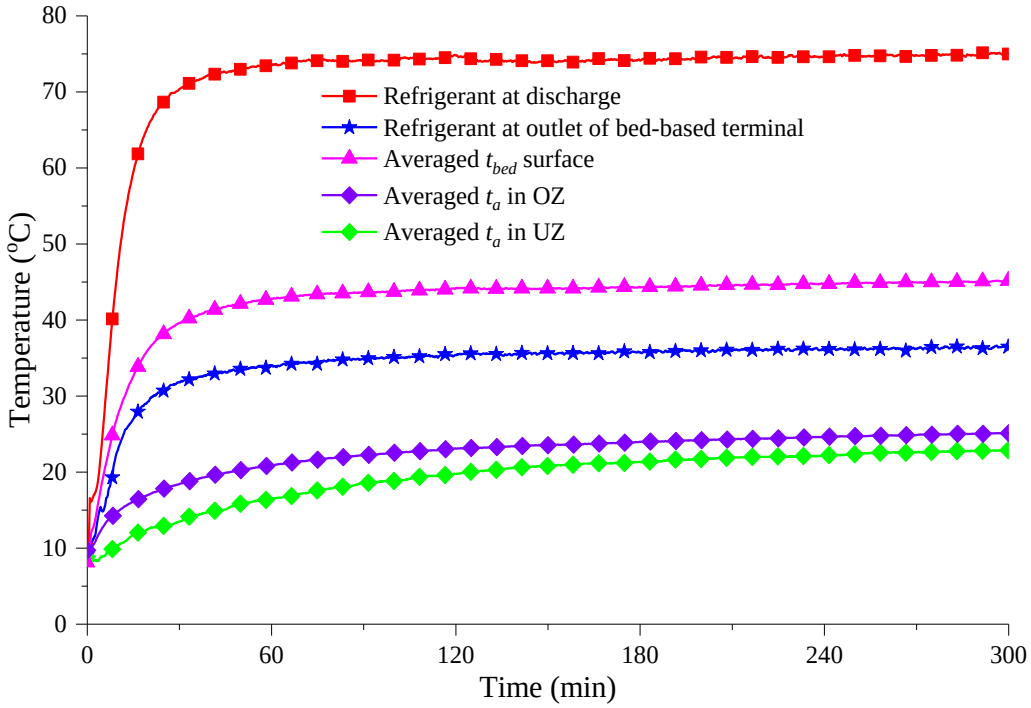

Fig. 4.4 Variations in various temperatures in Case 4.1

Furthermore, the variation profiles of the averaged t_a in the OZ and UZ are also shown in Fig. 4.4. At nighttime mode, it was important to maintain an appropriate thermal environment in the OZ. It took 10 minutes for the B-ASHP system to warm up the air

in the OZ from around 8 °C to 16.2 °C. The averaged t_a in the OZ gradually approached to 18 °C at 25 min and stayed stable at around 25 °C till the end of the test.

However, no significant t_a changes could be observed in the UZ for the first 6 minutes. Thereafter, t_a was increased gradually, with the similar increasing trend to that in the OZ and finally stayed stable at 23.0 °C. This suggested that a warmer environment could be created in the OZ at nighttime mode, which was beneficial to maintaining a thermally better sleeping environment.

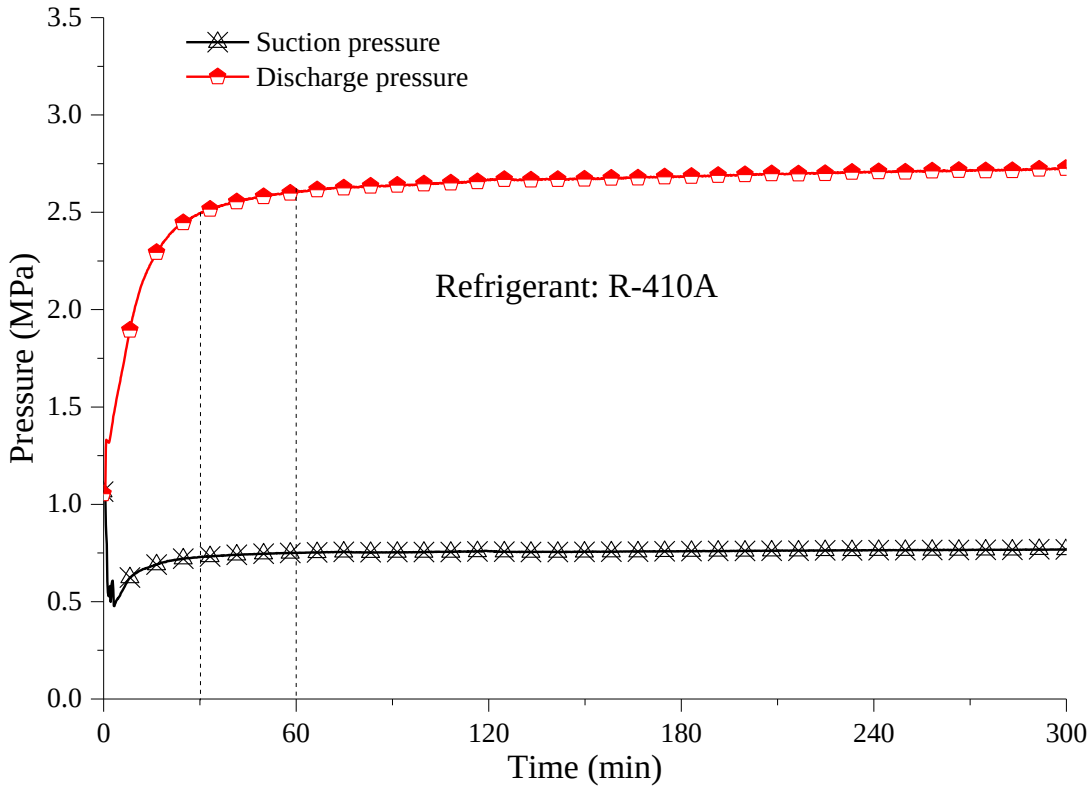

Fig. 4.5 Time variations in refrigerant pressures in Case 4.1

Fig. 4.5 shows the time variations in compressor suction and discharge pressures in the experimental B-ASHP system in Case 4.1. As seen, the suction pressure dropped

to 0.49 MPa at 4 min after starting up but was then slowly increased to 0.76 MPa at 30 min into the test. The discharge pressure, on the contrary, was significantly increased from 1.13 MPa to 2.64 MPa at 30 min, then gradually approached to 2.73 MPa at the end of the 5-hour long test.

The test results reported in this Section show that the experimental B-ASHP system can be satisfactorily and stably operated, during the 5-hour long test. The test results suggested that the use of the B-ASHP system can lead to a quicker increase in the t_a in the OZ and bed surface temperature, than the use of either a hot water based Kang system (Wang et al. 2014, Li et al. 2018) that may require up to 4 hours, or a traditional biofuel based Kang heating system that may require up to 5 hours (Zhuang et al. 2015, Zhuang et al. 2009b) to heat up indoor air to its setting.

4.3.2 Measured steady state performances of the experimental B-ASHP system (Cases 4.2 and 4.3)

The steady state performances of the experimental B-ASHP system in terms of the output heating capacity and *COP* were investigated under three different t_{out}, 2 °C, 7 °C and 10 °C, in both nighttime mode and daytime mode, respectively.

The output heating capacity, *Q*, was evaluated by:

$$Q = \dot{m} \times (h_{in} - h_{out}) \tag{4.1}$$

where $\dot{m}$ is the measured refrigerant mass flow rate, h_{in} and h_{out} the refrigerant enthalpy at the inlet and outlet of the bed-based heating terminal, evaluated based on

the measured refrigerant tube surface temperatures and refrigerant pressures, respectively.

The *COP* was then evaluated by:

$$COP = \frac{Q}{P_{com}} \tag{4.2}$$

where P_{com} is the measured input power to the compressor of the experimental B-ASHP system.

4.3.2.1 Steady state performances – nighttime mode (Case 4.2)

At nighttime mode, only the H-Section of bed-based heating terminal was operated. As seen in Fig. 4.6 (a), the output heating capacity at t_{out} of 2 °C was 2303 W, and increased to 2566 W and 2732 W at 7 °C and 10 °C, respectively. At a fixed compressor speed and surface area of the heating terminal, an increase in t_{out} would result in a higher evaporating pressure, leading to a greater output heating capacity and a higher system efficiency. As shown in Fig. 4.6 (b), the evaluated system *COP* was increased from 2.62 to 2.88 when t_{out} was increased from 2 °C to 10 °C.

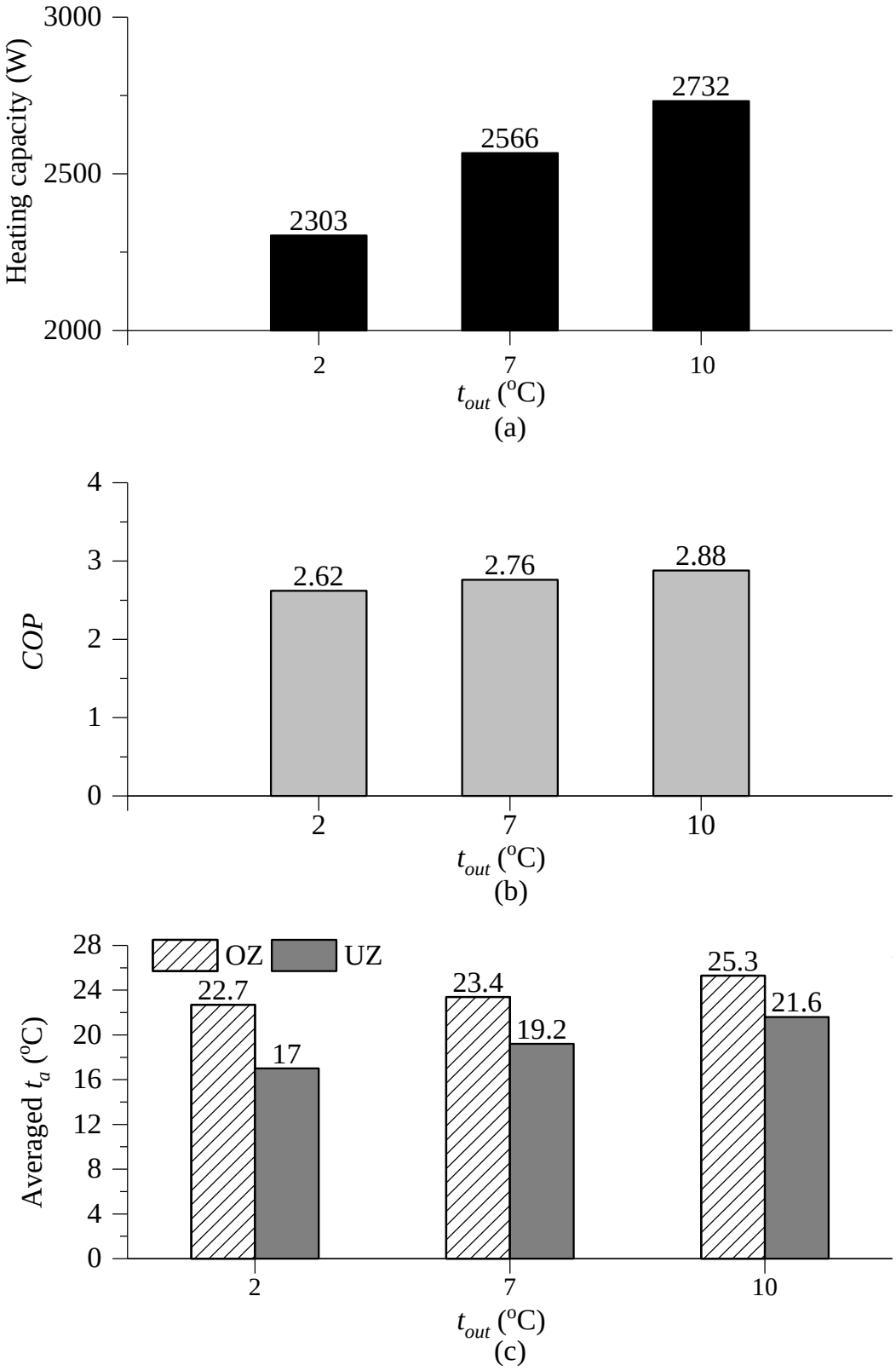

Fig. 4.6 Steady state operating performances at nighttime mode (a) Output heating capacity; (b) *COP*; (c) Averaged t_a (Case 4.2)

t_a at various t_{out} in both the OZ and the UZ are plotted in Fig. 4.6 (c). The t_{out} inside the OZ was increased from 22.7 °C to 25.3 °C as t_{out} was increased from 2 °C to 10 °C, owing to a higher output heating capacity and a lower space heating load. Furthermore, the t_a inside the OZ was 3.6 °C to 5.7 °C higher than that in the UZ, reflecting a cooler environment outside the OZ.

4.3.2.2 Steady state performances – daytime mode (Case 4.3)

To provide the maximum operating flexibility, full space heating may also be provided by the experimental B-ASHP system through operating only the V-Section, or H+V-Section of the bed-based heating terminal. In Case 4.3, the steady state performances of the experimental B-ASHP system when using the V-Section only or H+V-Section of the bed-based heating terminal at various t_{out} were experimentally studied.

The test results in Case 4.3 are shown in Fig. 4.7. As seen in Fig. 4.7 (a), when only the V-Section was used, the output heating capacities at different t_{out} were about 10 % higher than those shown in Fig. 4.7 (a), but about 6 - 10 % less than those when H+V-Section were used. This was because different bed surface areas were involved in these different situations, when all others operating conditions remained unchanged.

Furthermore, in Fig. 4.7 (b) and Fig. 4.7 (c), *COP* values and the averaged t_a in the experimental indoor space, at different t_{out} of 2 ^{o}C, 7 ^{o}C and 10 ^{o}C, using either the V-Section or H+V-Section, respectively, are given. As seen, both *COP* values and averaged t_a values had similar variations trends to that for the output heating capacity, also because of the differences in the surface areas involved in these different situations.

Furthermore, the test results at 2 ^{o}C t_{out} in Cases 4.2 and 4.3 showed that under a fixed compressor speed, the output heating capacities were 2303 W , 2549 W and 2717 W, when the H-Section, V-Section and H+V-Section of the bed-based heating terminal at 3 m^2, 4.95 m^2 and 7.95 m^2, respectively, were used. The differences among the three output heating capacities were therefore not significantly large, although the surface areas for heat transfer in these situations were significantly different. Moreover, Table 4.4 shows the normalized heating capacity comparison at different heating modes. As seen, with an increased heating surface area, the normalized heating capacity decreased. This suggested that to enable greater variations in output heating capacity, it was not adequate to only vary the heat transfer surface area, but varying compressor speed may be more effective.

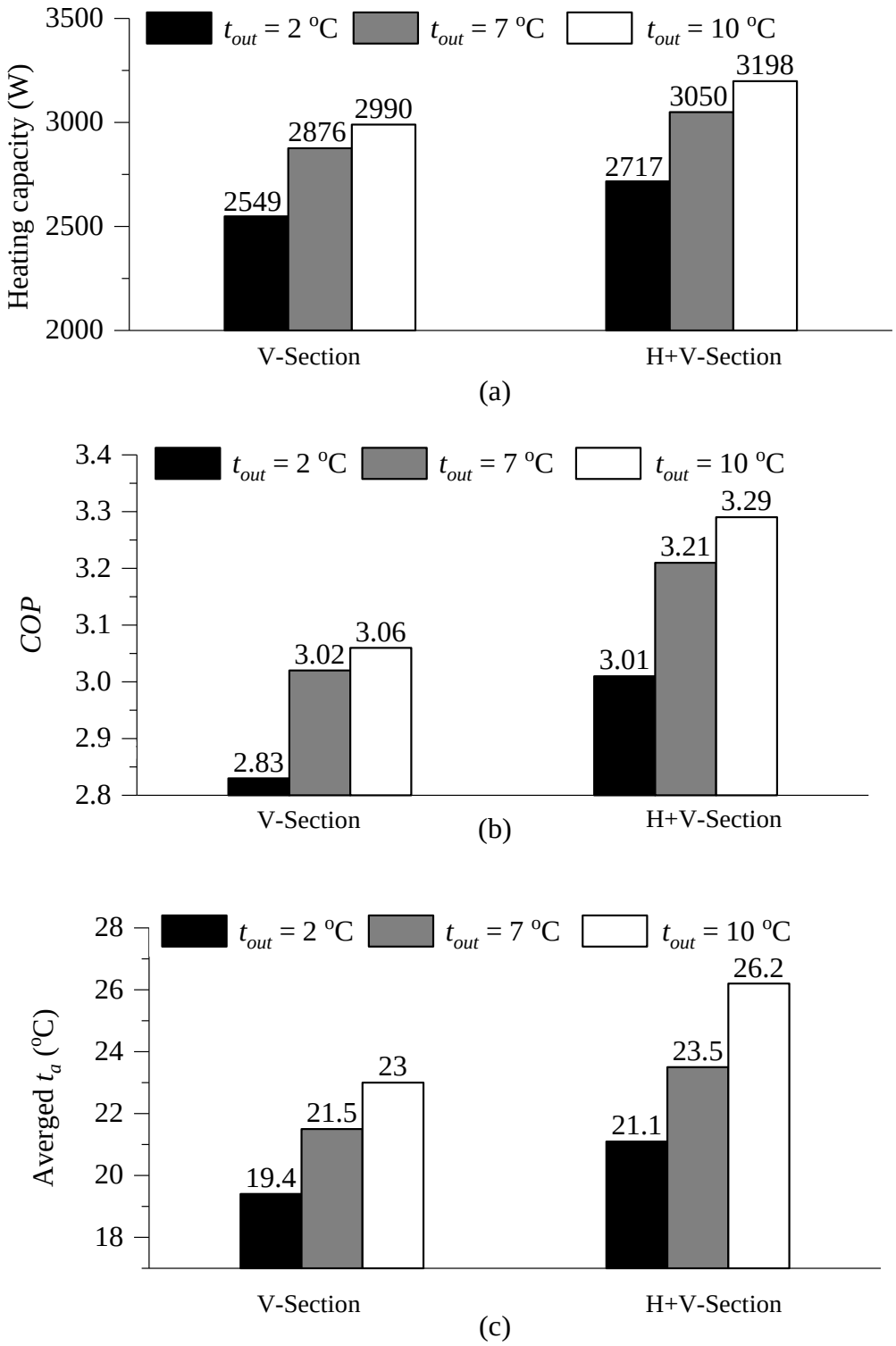

Fig. 4.7 Steady state operating performances at daytime mode (a) Output heating capacity; (b) *COP*; (c) Averaged t_a (Case 4.3)

Table 4.4 The normalized heating capacity at different heating modes

Mode		Daytime mode		Nighttime mode
Heating section		V-Section	H+V-Section	H-Section
Heating surface area (m^2)		4.95	7.95	3
Normalized heating capacity (W/m^2)	t_{out} = 2 °C	514.34	341.76	767.67
	t_{out} = 7 °C	581.01	383.65	855.33
	t_{out} = 10 °C	604.04	402.26	910.67

4.3.3 Comparative studies between using the bed-based terminal and convection-based heating terminal (Case 4.4)

To further reveal the merits of the experimental B-ASHP system, comparative studies between using the bed-based and the convection-based heating terminals were also conducted. The comparisons on the operating performances were carried out at daytime mode for the experimental B-ASHP system when H+V-Section of the bed-based heating terminal were operated. In the comparative studies, t_{out} was maintained at 2 °C.

Fig. 4.8 (a) shows the measured vertical distributions of averaged t_a, and Fig. 4.8 (b) the $\overline{t_r}$ and t_a in OZ using both bed-based heating terminal and the conventional convection-based terminals, where $\overline{t_r}$, was evaluated by (ASHRAE 2017):

$$\bar{t}_r = [(t_g + 273.15)^4 + \frac{1.1\times10^8 \left|\vec{v}\right|^{0.6}}{\varepsilon D^{0.4}} \times (t_g - t_a)]^{1/4} - 273.15 \quad (4.3)$$

Where t_g is the globe temperature at a measuring position (°C), $\left|\vec{v}\right|$ the measured air velocity (m/s), D the globe diameter (mm) and ε the globe emissivity.

As seen in Fig. 4.8 (a), a more uniformed vertical distribution between 18.5 °C and 22.4 °C when using the bed-based heating terminal than that between 15.8 °C and 22.3 °C when using the conventional convection-based terminal may be achieved. In Fig. 4.8 (b), the difference between t_a and $\bar{t}_r$ using the convection-based terminal was 0.1 °C and that was 1.0 °C when using the B-ASHP system. This suggested that radiative heat transfer would play a more important role than convective heat transfer when using the bed-based heating terminal.

Furthermore, a temperature gradient of 2.3 °C/m between head and feet when using the bed-based heating terminal and 4.0 °C/m when using the convection-based heating terminal were observed, respectively. According to ISO 7730 (2005), a vertical air temperature gradient larger than 3.0 °C/m would result in local discomfort, and also according to ASHRAE Standard 55 (2017), a 13 % dissatisfaction rate would result in at 4.0 °C/m air temperature gradient between head and feet. Therefore, the use of the bed-based heating terminal can lead to a more uniformed vertical temperature distribution in an indoor space and thus a higher level of thermal comfort, than the use of a conventional convection-based heating terminal.

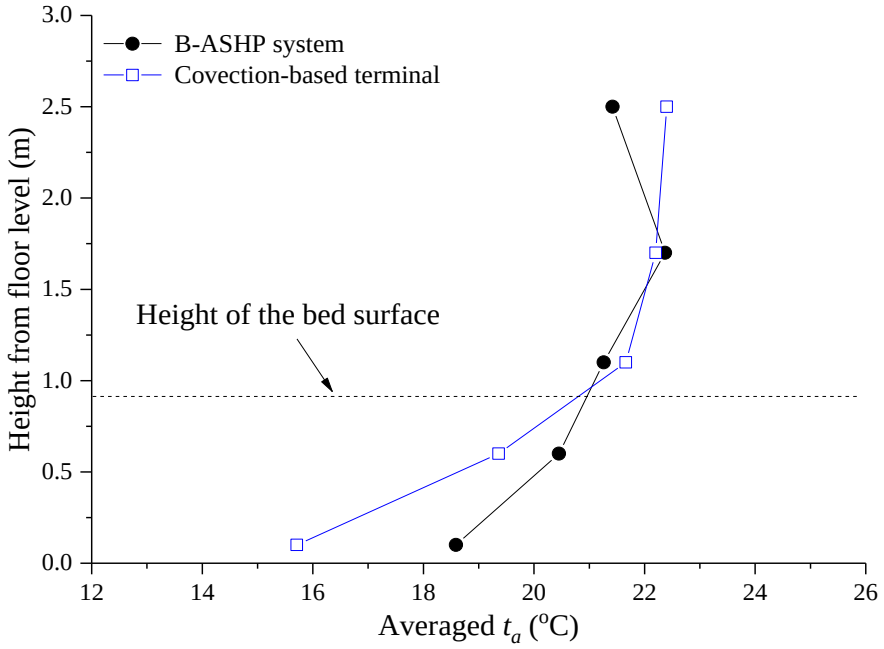

(a)

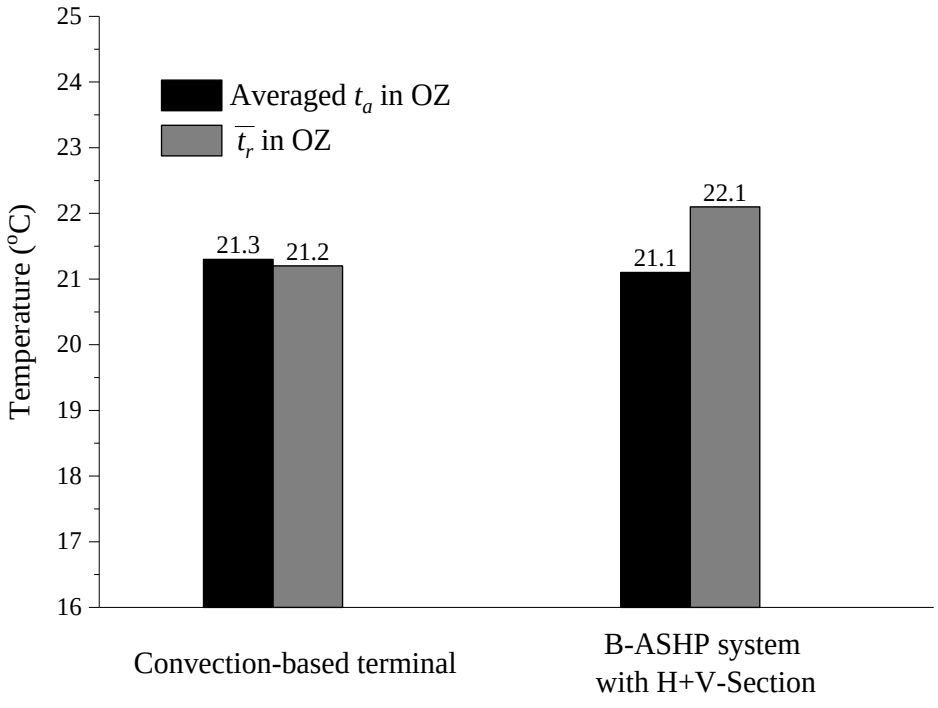

(b)

Fig. 4.8 (a) Vertical temperature gradients (b) $\overline{t_r}$ and t_a values in the experimental indoor space in OZ when using the B-ASHP system and the convectional convection-based terminals in Case 4.4

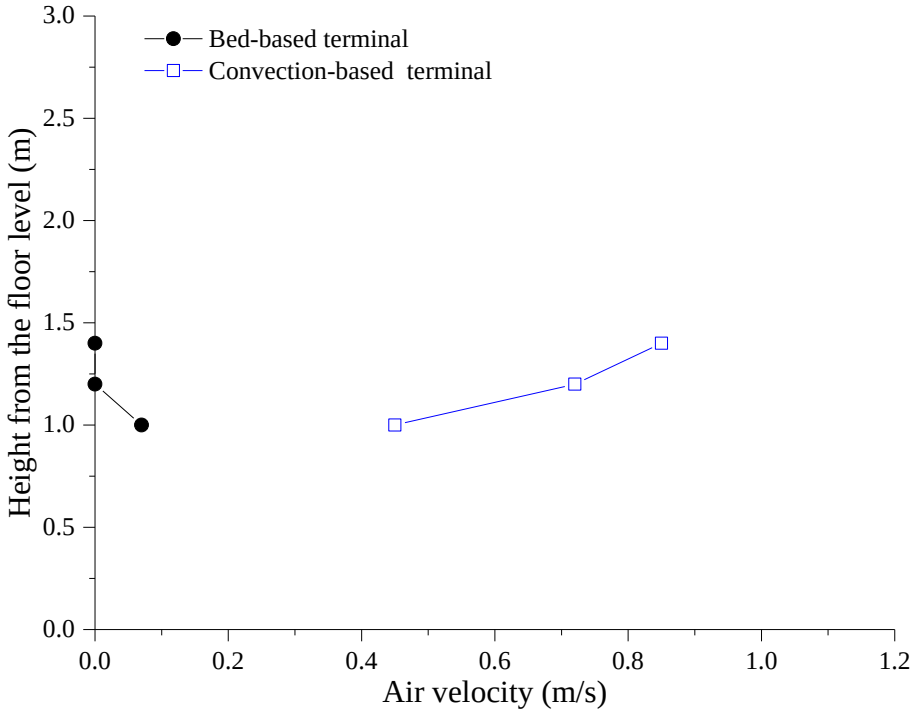

Fig. 4.9 Measured air velocity in the experimental indoor space when using the two different terminals in Case 4.4

In addition, Fig. 4.9 shows the measured air velocity in the experimental indoor space when the two terminals were used. As seen, a much higher air velocity at 0.45 to 0.85 m/s was resulted in when using the convection-based heating terminal, due to the use of a supply fan in the terminal. On the contrary, when using the bed-based terminal, indoor air velocity was very low, with its maximum value of less than 0.1 m/s, mainly due to the natural convection. Therefore, at a higher air velocity and a high t_a at a higher level, the use of a conventional convection-based heating terminal would lead to a less thermally comfortable indoor environment than the use of the bed-based heating terminal in the experimental B-ASHP system.

Moreover, Table 4.4 shows the measured *COP* values for both the B-ASHP and the conventional convection-based terminal at a t_{out} of 2 ºC. As seen, the averaged

measured *COP* of the convection-based terminal reached at 3.78. However, the averaged maximum measured *COP* of the B-ASHP system was only 3.01. Therefore, the experimental B-ASHP system would have a lower energy efficiency than the conventional convection-based terminal. However, this lower efficiency also suggested there were rooms for energy efficiency improvement for the experimental B-ASHP system since its current designs were preliminary and should be optimized in future.

Table 4.5 Comparisons of measured *COP* values between the B-ASHP system and the convection-based terminal

Heating System	Measured *COP* values at a t_{out} of 2 °C
B-ASHP system with the terminal of:	
V-Section	2.67
H-Section	2.83
H+V-Section	3.01
Convection-based terminal	3.78

4.3.4 Uniformity of bed surface temperature

Fig. 4.10 shows the measured t_{bed} at the six points, marked as BA, BB, BC, BD, BE and BF in Fig. 4.2 (b) in Case 4.1 when the experimental B-ASHP system was operated at the steady-state condition at the end of the test. As seen, the six temperatures were close to one another, with the maximum deviation of 0.3 °C among

them. This reflected that the use of refrigerant directly in the bed-based heating terminal could result in a highly uniformed temperature distribution on bed surface. However, when a traditional biofuel based Chinese Kang-based heating system (Zhuang et al. 2015, Zhuang et al. 2009b) and a hot water based Kang heating system (Wang et al. 2014, Li et al. 2018) were respectively used, their maximum bed surface temperature deviations were at between 0.53 and 5.01 ^{o}C and between 4.1 and 10.6 ^{o}C, respectively.

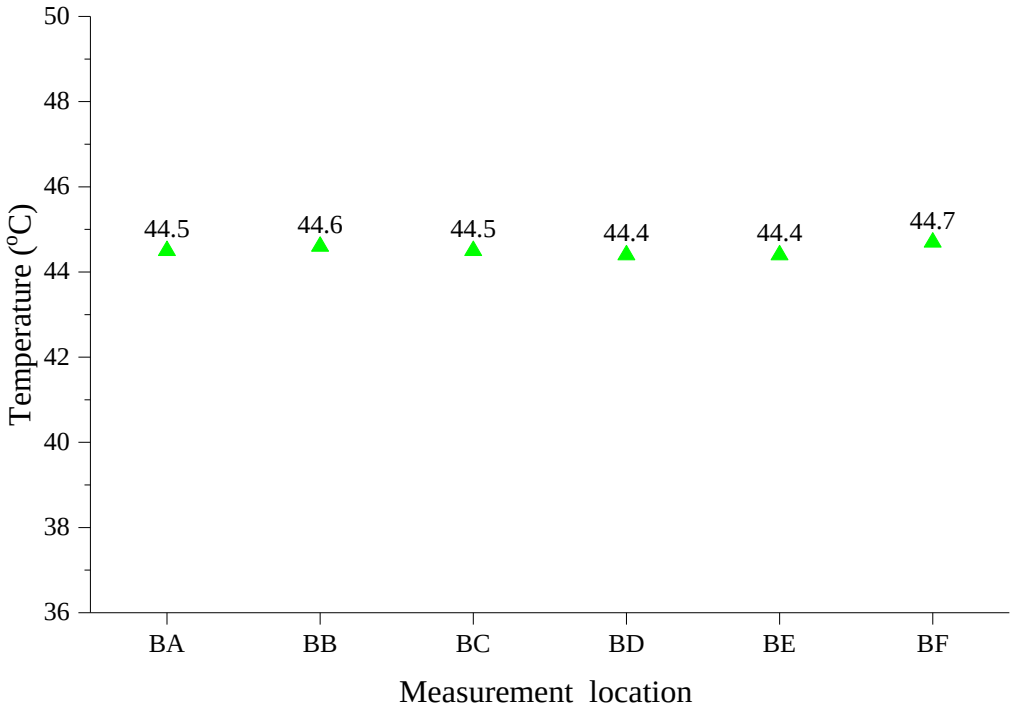

Fig. 4.10 Measured t_{bed} at six points

4.4 Discussions

The experimental results from the four test cases reported in Section 4.3 demonstrated that the experimental B-ASHP system can be operated satisfactorily. However, with

reference to the current design of the experimental B-ASHP system, there were a few issues that required careful considerations for the efficient and safe operation.

- Refrigerant R-410A with a relatively high operating pressure was used as working fluid. For example, its condensing pressure was as high as 2.73 MPa in Case 4.1 as shown in Fig. 4.5, nearly 27 times of the barometric pressure. Although in the current design, R-410A was directly used in the bed-based heating terminal for better heat transfer, a refrigerant with a high operating pressure may be disadvantageous by imposing a stricter refrigerant sealing requirement. Alternative refrigerants with a lower operating pressure should be preferred.

- The refrigerant tubes were integrated with a bed using surface assemblies, so that the bed could not be easily moved once installed. Furthermore, the current layout of refrigerant tubes was not optimized, and a large refrigerant drop through the bed-based heating terminal at ~ 0.1 MPa can be identified. Optimization and modularization on the layout of the bed-based heating terminal with appropriate tube diameter should be considered.

- In the current studies, the surface of the H-Section of the bed-based heating terminal in the experimental B-ASHP system was not covered with any beddings. However, in reality, bed surfaces were usually covered with beddings. Therefore, future test cases using different types of beddings on bed surfaces should be organized.

- The heat transfer from the surface of the bed-based heating terminal in the experimental B-ASHP system was mainly via natural convection and radiation. Hence a lager surface area may be required, as compared to an ASHP system using forced convection, such as a conventional convection-based heating terminal. Consequently, the matching between compressor's capacity and heat exchangers' surface area in a B-ASHP system should be carefully investigated, so as to provide the required output heating capacity while not unnecessarily enlarging the size of a bed-based heating terminal.

- The work reported in Section 4.3 has opened up a new application field of ASHP technology, by replacing traditional Chinese Kangs with the proposed B-ASHP systems in rural areas in China to achieve clean and energy efficient space heating. In addition, the novel B-ASHP system was bed-based to provide localized heating during nighttime. Therefore, its use can help reduce the applications of electrical blankets which are less energy efficient.

4.5 Conclusions

By combining the merits from both a conventional ASHP and a traditional Chinese Kang-based heating system, an experimental B-ASHP system was proposed, and its operating performances experimentally evaluated and the results are reported in this Chapter. Four test cases were organized, for both dynamic and steady state performance evaluation and comparisons. The following conclusions may be drawn:

1. The dynamic test results in Cases 4.1 and 4.2 suggested that the use of the experimental B-ASHP system can lead to a quicker increase in the t_a in the OZ and

t_{bed}, than the use of Kang heating systems, and that a B-ASHP system was also responsive to the change in space heating load.

2. The tests on the steady state performances of the experimental B-ASHP system in Cases 4.2 and 4.3 showed that the system can be satisfactorily operated at both nighttime and daytime modes. However, the test results also suggested that only varying the surface area for heat transfer may not be an effective way to varying output heating capacity of a B-ASHP system, but varying compressor system can be more effective.

3. The test results in Case 4.4 demonstrated that compared to using a conventional convection-based heating terminal, the use of the bed-based heating terminal in the B-ASHP system can lead to a more uniformed vertical indoor air temperature gradient, thus a better occupants' thermal comfort.

4. The use of a B-ASHP system can lead to a more uniformed t_{bed}, than the use of Kang-based heating systems.

Although the current experimental B-ASHP system can be satisfactorily operated, there were still a number of issues requiring further considerations for its efficient and safe operation, such as the selection of a suitable refrigerant, optimizations of refrigerant tube layouts, and the use of a variable speed compressor for improved capacity control. Nevertheless, the current work reported in this Chapter has adequately paved the way for the further development and optimizations of a B-ASHP system.

Hence, a follow-up numerical study on further optimizing a number of design and operating parameters of the bed-based heating terminal was carried out and is reported in Chapter 5.

Chapter 5 A numerical study on the impacts of the optimization of the bed-based heating terminal on indoor thermal environment using the B-ASHP system

5.1 Introduction

From the experimental study presented in Chapter 4, it can be seen that the novel bed-based ASHP (B-ASHP) space heating system has been proposed by combining the merits of both an ASHP unit and a traditional Chinese Kang-based heating system, and was experimentally studied. A bed-based heating terminal was used inside an experimental heated indoor space to replace a convection-based fan powered heating terminal, using R-410A as the refrigerant. The experimental study results showed that compared to using a conventional convection-based indoor heating terminal, the use of the bed-based heating terminal could lead to a more uniformed vertical air temperature gradient, thus an indoor environment with a higher thermal comfort level. The study results also suggested a relatively high operating efficiency of the experimental B-ASHP system, with a maximum *COP* of 3.21 at an outdoor temperature of 7 ^{o}C. However, in the experimental study reported in Chapter 4, as constrained physically by the experimental conditions, the three design parameters, i.e., the location, dimension and surface emissivity, and one operating parameter, i.e., the surface temperature (t_{bed}), of the bed-based heating terminal, were fixed. Therefore, to optimize the design and operation of the B-ASHP system for better indoor thermal environmental control and higher operating efficiency, it became highly necessary to further numerically study the indoor thermal environment in the space served by the B-ASHP when the above design/operating parameters were varied.

On the other hand, computational fluid dynamics (CFD) based numerical methods have been increasingly popular in optimizing the design and operating characteristics of HVAC systems and predicting air flow pattern and temperature distribution inside an indoor space (Mao et al. 2018, Pan et al. 2011). For an indoor space using radiant heat transfer-based environmental control systems, CFD methods have also been used to study the indoor thermal environmental parameters, such as room air distribution, air flow pattern and indoor air quality (Myhren and Holmberg 2008, Seyam et al. 2014, Zhou and He 2015), so as to improve system performances.

Therefore, as a follow-up to the experimental study reported in Chapter 4, a numerical study on the impacts of varying the location, dimension, t_{bed} and surface emissivity of the bed-based heating terminal on indoor thermal environment and the operating efficiency of the B-ASHP system, as the second part of the research project presented in this Thesis, was carried out, and the numerical study results are reported in this Chapter. The organization of this Chapter is as follows: firstly, a geometry model for the experimental indoor space and a CFD method developed are described in detail, and the boundary conditions for the indoor space used in the experimental study presented in Chapter 4 and the objectives of each study group detailed. Secondly, the experimental validation of the CFD method using the measured indoor air temperatures and velocities obtained in the experimental study reported in Chapter 4 is reported. Thirdly, the results and the related analysis of the numerical study on the effects of varying the above design/operating parameters on the indoor thermal environment and operating efficiency of the B-ASHP system are presented. Finally, a conclusion is given.

5.2 Development of the CFD method

5.2.1 Geometry model

A geometry model for the experimental indoor space used in the experimental study presented in Chapter 4 was built. The experimental indoor space was located inside an environmental chamber which was consisted of the indoor space and a simulated outdoor space used as the plant room to house the outdoor unit of the B-ASHP system. The schematics of the complete setup for the experimental B-ASHP system installed in the chamber, is shown in Fig. 4.1.

A three-dimensional view and two sectional views of the experimental indoor space used in this numerical study are shown in Fig. 5.1 (a) and Fig. 5.1 (b), respectively. A cuboid of 2000 mm × 1500 mm × 600 mm (L×W×H) right above the bed-based heating terminal was designed as an occupied zone (OZ) for the purpose of results analysis. The rest of the experimental indoor space, on the other hand, was designed as an unoccupied zone (UZ). In addition, a convection-based heating terminal was placed on an internal surface of the experimental indoor space at the height of 2500 mm. It should however be noted that the convection-based heating terminal was not part of this numerical study, but the space it occupied may impact on the indoor air flow field, which cannot be neglected.

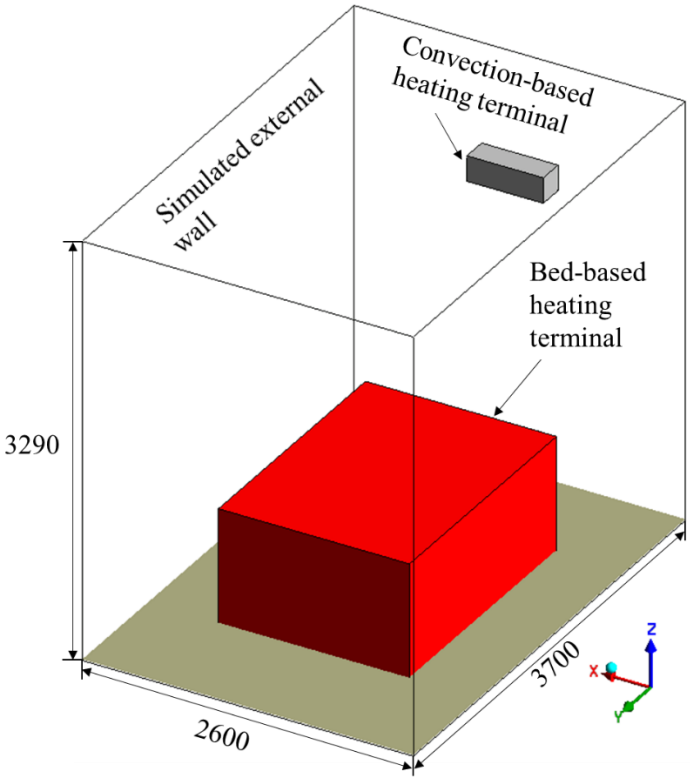

Fig. 5.1(a) A 3-D view of the experimental indoor space and the bed-based heating terminal of the B-ASHP system (unit: mm)

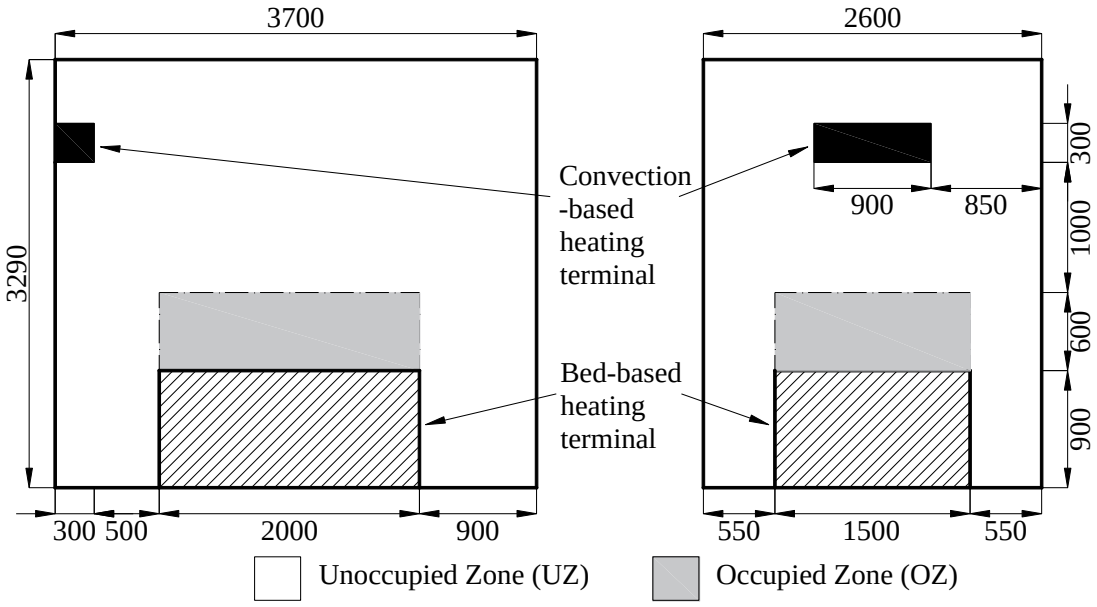

Fig. 5.1(b) Sectional views of the experimental indoor space and the bed-based heating terminal of the B-ASHP system (unit: mm)

5.2.2 Mesh generation and CFD method

Grids were generated using ICEM CFD (2010) with structured mesh. For the experimental indoor space, the sectional views of the mesh for the computational domain corresponding to the section views shown in Fig. 5.1, are shown in Fig. 5.2 (a) and Fig. 5.2 (b), respectively.

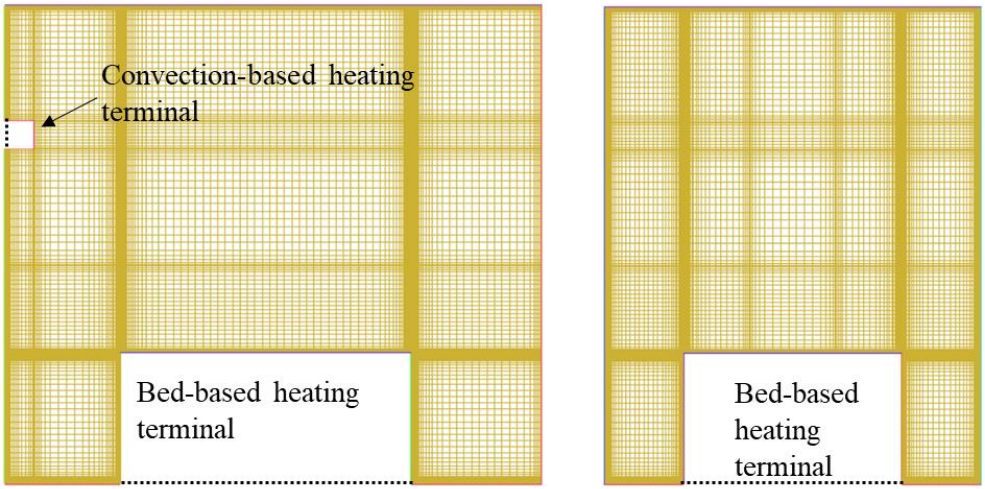

Fig. 5.2 Sectional views of the mesh generation for the experimental indoor space from (a) x-axis direction (b) y-axis direction

A commercial CFD code (ANSYS Fluent 2010) was used to solve the following these steady state, governing equations for continuity, momentum and energy to obtain the air flow field inside the experimental indoor space. Since the Rayleigh number evaluated around the bed-based heating terminal was greater than 10^{10}, turbulence was expected at the near wall region. The Boussinesq approximation was used to simulate the natural convection in the experimental indoor space considering buoyance term

(ANSYS Fluent 2010). The Coupled algorithm was used with a second order scheme for the convective terms.

In addition, in this numerical study, the steady state, viscous and 3D governing equations for the flow field inside the experimental indoor space are given as Equations (2.10) - (2.14) in Chapter 2.

5.2.3 Boundary conditions and numerical cases

A constant t_{out} of 7 ^{o}C was set for the outdoor space, which was used in the experimental study presented in Chapter 4. The boundary conditions for the experimental indoor space are given in Table 5.1. It needs to be noticed that in a real building, the envelope materials are with higher emissivity than those in the experimental study, and could not be treated as adiabat. Therefore, the heating load in a real bedroom is higher than that in the experimental study.

Table 5.1 Boundary conditions of the experimental indoor space used in the numerical study

Boundary	Material	Emissivity	Thermal conditions (^{o}C)
External wall	Gypsum plaster	0.9	7
Floor	Anodized aluminum	0.3	Adiabatic
Other walls (including ceiling)	Aluminum	0.07	Adiabatic

In the current numerical study reported in this Chapter, a baseline case was designated where all the settings strictly followed the parameters and conditions used in the experimental study presented in Chapter 4, i.e., bed-based terminal placed at the center

of the experimental indoor space; bed surface temperature of 43 ^{o}C, surface emissivity of 0.7; and bed dimension of 2000 mm × 1500 mm × 900 mm (L×W×H). Then, in other study cases, different bed locations, dimensions, bed surface temperature and emissivity, as detailed in Table 5.2, were used. As seen, two more t_{bed} values of 25 ^{o}C and 35 ^{o}C were included, so as to evaluate the impacts of different bed surface temperature on indoor thermal environments and the operating efficiency of the B-ASHP system. In addition, three more bed surface emissivities were also added: 0.1, for metal surface, 0.5 and 0.9 for the surface of common bedding materials, respectively, to evaluate the impacts of different bed surfaces on indoor thermal environment. Consequently, a total of 12 study cases including the baseline case, separated into 4 groups, were designated, as detailed in Table 5.2. The purposes of each group were as follows. Firstly, the baseline case in Group 5.1 was used for the validation of the CFD method, and as a basis for performances comparisons. Secondly, the cases in Group 5.2 were used to investigate the influence of bed locations on indoor thermal environment. Thirdly, the cases in Group 5.3 were used to study the effects of dimensions of the bed-based heating terminal on indoor thermal comfort and the operating efficiency of the B-ASHP system. Lastly, the cases in Group 5.4 were used to investigate the effects of different t_{bed} values and bed surface emissivities on indoor thermal environment, and the operating efficiency of the B-ASHP system.

Table 5.2 Cases used in the numerical study

Group	Cases	Bed location	Bed dimension (L×W×H) (mm)	t_{bed} (^{o}C)	Bed surface emissivity
5.1	Baseline/ 5.1.1	Center	2000 × 1500 × 900	43	0.7
5.2	5.2.1	Corner	2000 × 1500 × 900	43	0.7
	5.2.2	Wall			
5.3	5.3.1	Center	2000 × 1500 × 400	43	0.7
	5.3.2		2000 × 1500 × 600		
	5.3.3		2000 × 1000 × 900		
	5.3.4		2000 × 2000 × 900		
5.4	5.4.1.1	Center	2000 × 1500 × 900	25	0.7
	5.4.1.2			35	
	5.4.2.1			43	0.1
	5.4.2.2				0.5
	5.4.2.4				0.9

5.2.4 Validation of the CFD method

Because the flow mechanism inside the experimental indoor space and the heat transfer characteristics were similar among different study cases, Case 5.1.1 (baseline case) was therefore used to validate the CFD method, following the recommended validation procedures and criteria in a previous study (Chen and Srebric 2002). The measured t_a and velocities at two locations inside the unoccupied zone (U1 and U2)

obtained in the experimental study presented in Chapter 4, were compared with the numerical results in Case 5.1.1 in order to validate the CFD method.

5.2.4.1 Mesh sensitivity

To ensure the grid independence of the numerical results, the thermal environments in Case 5.1.1 were first numerically studied from three different mesh sizes of 0.6 million, 1.8 million and 3.2 million. The predicted t_a and velocities at the above two locations are shown in Fig. 5.3. As seen, the obtained results at 1.8 million and 3.2 million mesh sizes were very close to each other, within an averaged deviation of 0.49 ^{o}C for the t_a and that of 0.026 m/s for air velocity. On the other hand, the numerical results at 0.6 million mesh sizes showed noticeable differences as compared with those at the other two mesh sizes. Hence, the numerical results at mesh size of 1.8 million were considered to be grid independent and thus used in this numerical study.

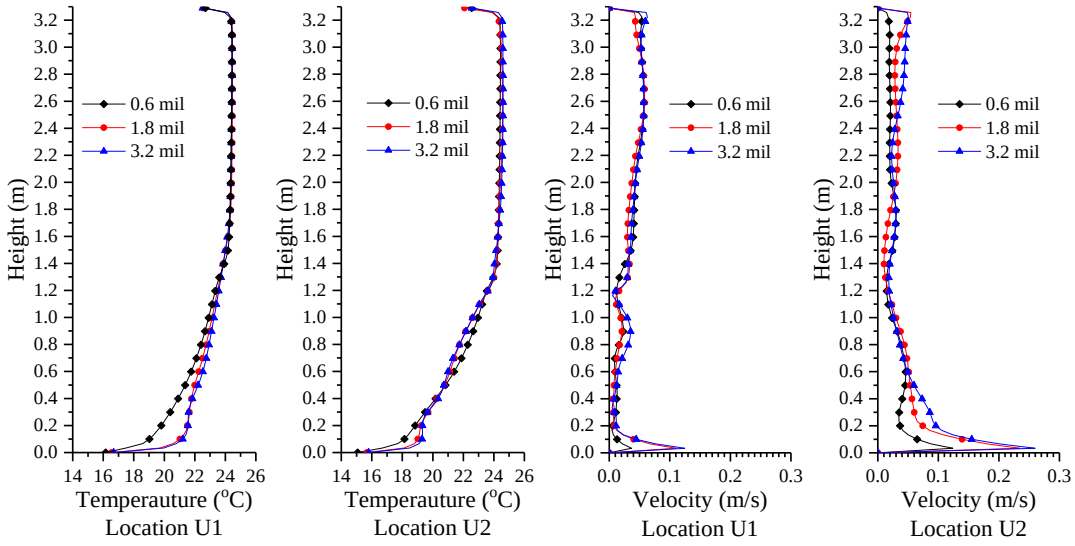

(a) t_a (b) Air velocity

Fig. 5.3 The simulated t_a and air velocities at two different locations using three different mesh sizes

5.2.4.2 Selection of a turbulence model

Fig. 5.4 compares the measured and the simulated t_a and velocities at the two different locations using three different available turbulence models: SST k-w model, Standard k-epsilon (STD-ke) model and RNG k-epsilon (RNG-ke) model, respectively. As seen, the RNG-ke model performed better than the other two in predicting both t_a and air velocity profiles, with an averaged absolute difference between the measured and the predicted t_a at 0.06 °C, and that between the measured and the predicted air velocities 0.023 m/s, respectively, when using the RNG-ke model.

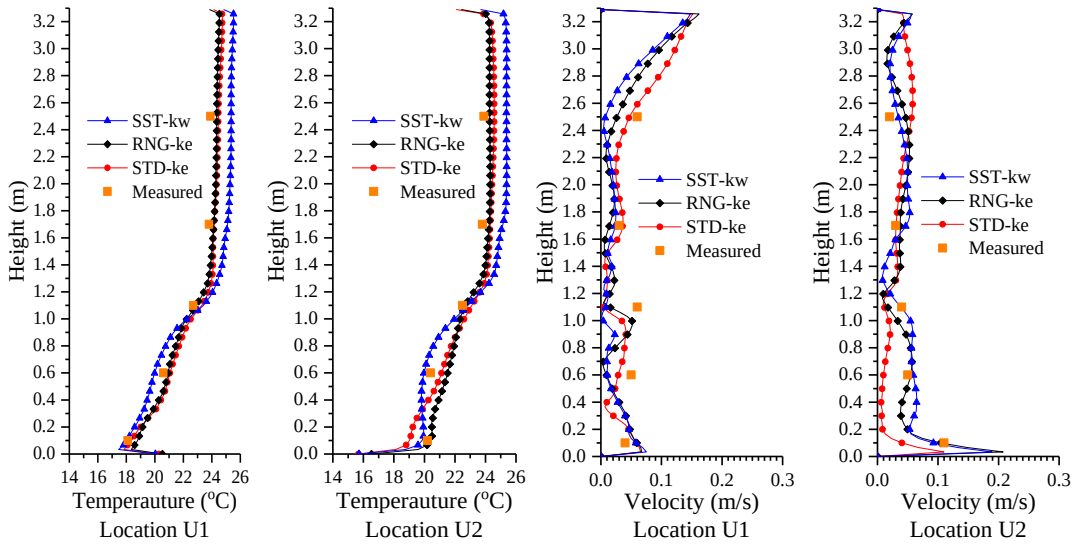

(a) t_a (b) Air velocity

Fig. 5.4 Comparisons between the measured and the simulated t_a and air velocities at two different locations using three different turbulence models

5.2.4.3 Selection of a radiation model

The use of three different radiation models, P1 model, surface-to-surface (S2S) model and discrete ordinate (DO), was examined and the simulated results of t_a and air

velocities at the two locations were compared with the experiment data. For the P1 model, it was easy to solve with less computing power demand. However, it may not work well when the optical thickness of radiation heat transfer media was small. The S2S model was commonly used to calculate radiation heat transfers in buildings as an enclosure for radiative heat transfer with non-participating media. Furthermore, the DO model was widely known for its high accuracy, especially for the heat transfer media with a thin optical thickness such as air (ANSYS Fluent 2010). Fig. 5.5 shows the comparisons between the experimental data and simulated results obtained with the three radiation models. As seen, a better agreement between the measured data and the numerical results when using S2S model may be observed. The maximum absolute differences between the measured and simulated t_a was 0.5 ^{o}C, and that between the measured and simulated air velocities 0.06 m/s, respectively, when using the S2S model. Therefore, the S2S model was selected to calculate radiation heat transfer in this numerical study.

Consequently, in the CFD method developed, the followings were adopted: mesh sizes of 1.8 million, RNG-ke turbulence model and S2S radiation model. Following the suggestions in a previous CFD study (Chen and Srebric 2002), and based on the comparison results shown in the sub-sections 5.2.4.1 to 5.2.4.3, it was considered that the CFD method developed was validated.

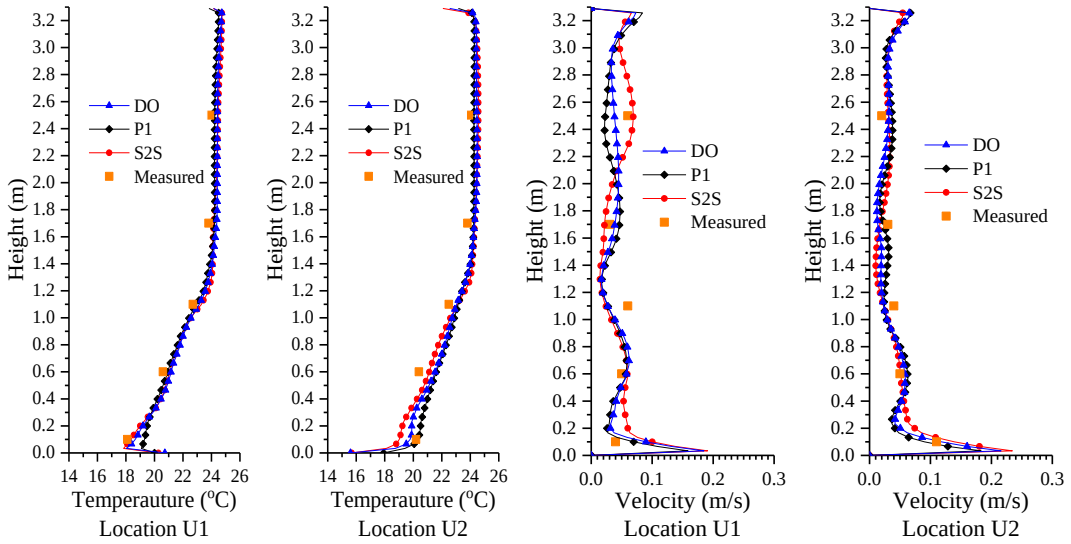

(a) t_a (b) Air velocity

Fig. 5.5 Comparison between the measured and the simulated t_a and air velocities using the three different radiation heat transfer models

5.3 Numerical results and the related analysis

The thermal environments in the experimental indoor space have been numerically studied using the validated CFD method, and the study results are presented in this section. In addition, where appropriate, the operating efficiencies of the B-ASHP system at different settings were also qualitatively evaluated, and the evaluated results are also included in this section. In study Groups 5.2 - 5.4, detailed performance parameters, including the t_a and air velocity fields inside the experimental indoor space were compared with those in Case 5.1.1. To present the numerical study results, two sectional planes inside the experimental indoor space were used to illustrate the numerical results of t_a and flow fields, as shown in Fig. 5.6. The planes were perpendicular to X-axis and Y-axis, respectively, and placed cross the center point of

the experimental indoor space. In presenting the numerical results, the simulated values in both OZ and UZ were volume averaged.

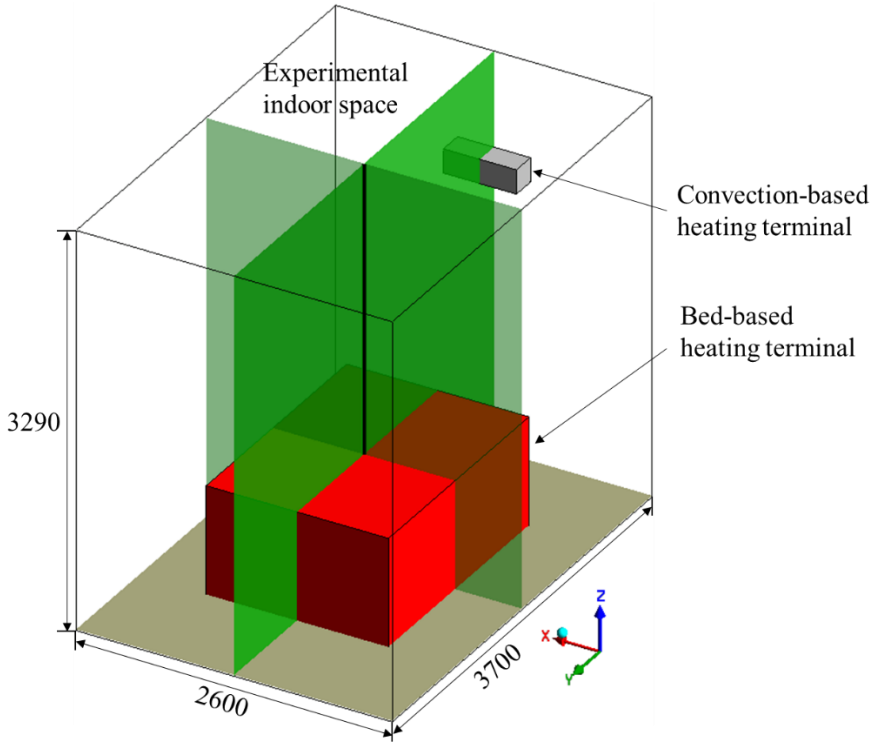

Fig. 5.6 Two sectional planes for presenting the numerical results in the experimental indoor space (unit: mm)

In Sections 5.3, operative temperature (t_{op}) and averaged air velocity ($\overline{v}$) are used to illustrate the effects of varying the location, dimensions of the bed-based heating terminal on the indoor thermal environment. t_{op} was a comprehensive index commonly used for thermal environmental analysis (ASHRAE 2017).

t_{op} is expressed as follows:

$$t_{op} = \frac{h_r \bar{t}_r + h_c t_a}{h_r + h_c} \tag{5.1}$$

where $\bar{t}_r$ is the mean radiant temperature, °C; h_r radiative heat transfer coefficient, W/m$^{2\cdot}$°C, which was determined at 4.7 W/m$^{2\cdot}$°C for most calculations; h_c convective heat transfer coefficient, W/m$^{2\cdot}$°C, calculated by (ASHRAE 2017):

$$\begin{aligned} h_c &= 2.7 + 8.7v^{0.67} (0.15 < \bar{v} < 1.5) \\ h_c &= 5.1 (0 < \bar{v} < 0.15) \end{aligned} \tag{5.2}$$

5.3.1 Location of the bed-based heating terminal

The impacts of the locations of the bed-based heating terminal inside the experimental indoor space on indoor thermal environment were studied using the study cases in Group 5.1. The numerical study results from the two study cases, where the bed-based heating terminal was placed at a corner in Case 5.1.1 and attached to a wall in Case 5.1.2, as shown in Fig. 5.7, respectively, were compared to those from Case 5.1.1 in Fig. 5.8.

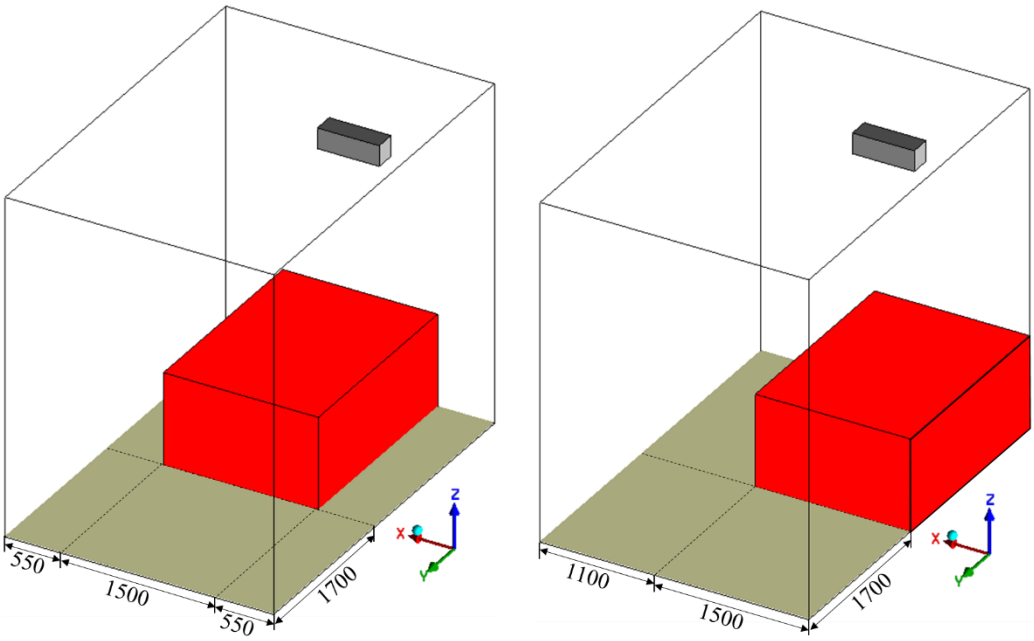

(a) (b)

Fig. 5.7 3-D views of the experimental indoor space and the bed-based heating terminal placed in (a) Case 5.1.1 (b) Case 5.1.2 (unit: mm)

Fig. 5.8 shows the variations in the total heat output from the bed-based heating terminal in Case 5.1.1, Cases 5.2.1 and 5.2.2. As seen, at a fixed t_{bed} of 43 °C, the difference between the total output heating capacity from Case 5.2.2 and that from the Case 5.1.1 was smaller at around 41 W, compared to that between Case 5.2.1 and Case 5.2.2 at around 190 W. To visualize the effects of location of the bed-based heating terminal on indoor thermal environment, the simulated t_{op} fields and air velocity vectors at the two sectional planes in the three cases are shown in Fig. 5.9. It can be seen that there were significant differences between the operative temperature in the occupied zone, $t_{op,oz}$, and that in the unoccupied zone, $t_{op,uz}$. Furthermore, the vertical temperature gradients were 1.51 °C/m in Case 5.1.1, 1.75 °C/m in Case 5.2.1 and 1.56 °C/m in Case 5.2.2, respectively, as summarized in Table 5.3, suggesting an insignificant vertical variation in indoor t_a in all study cases.

The numerical study results in Group 5.2 suggested that, when placing the bed-based heating terminal in the center, as in Case 5.1.1, a larger output heating capacity from the bed based terminal, a more uniformed indoor thermal environment and a better air velocity distribution could be achieved, as compared to placing the terminal at the other two locations. However, placing the indoor terminal at different locations may imply different installation space requirements for the bed-based terminal, and should therefore be carefully evaluated, depending on the available indoor space.

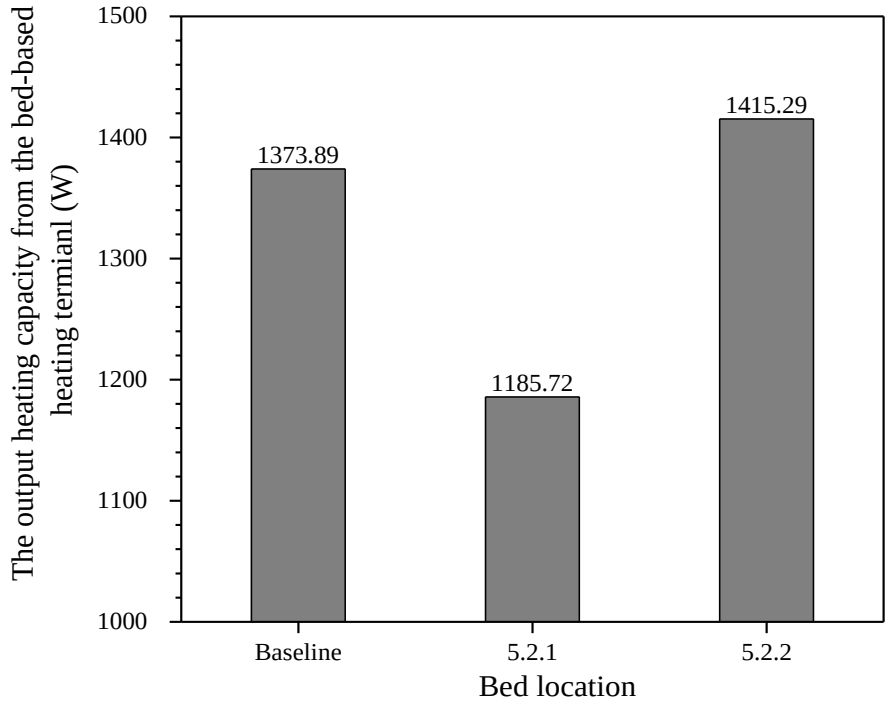

Fig. 5.8 The output heating capacity variations from the bed-based heating terminal in Group 5.2 study cases

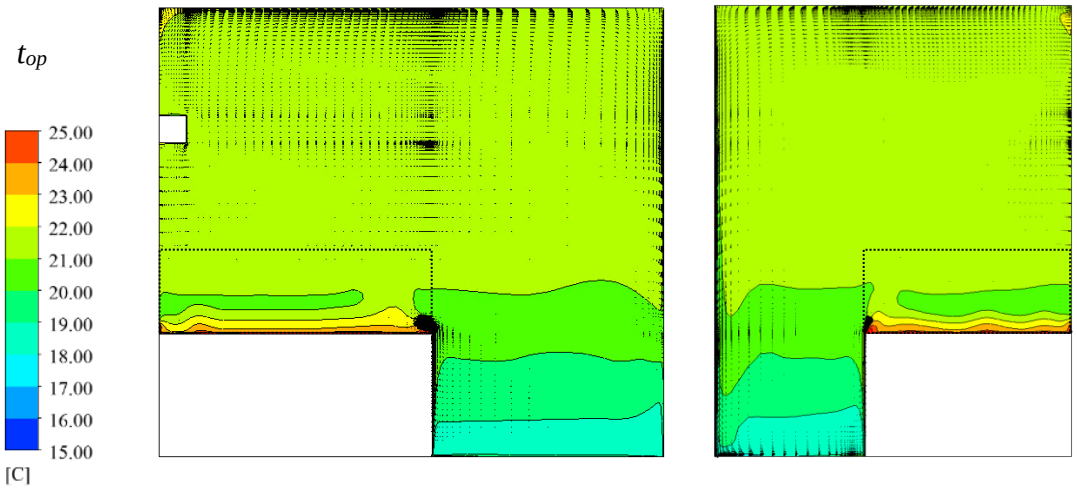

(a) Case 5.2.1

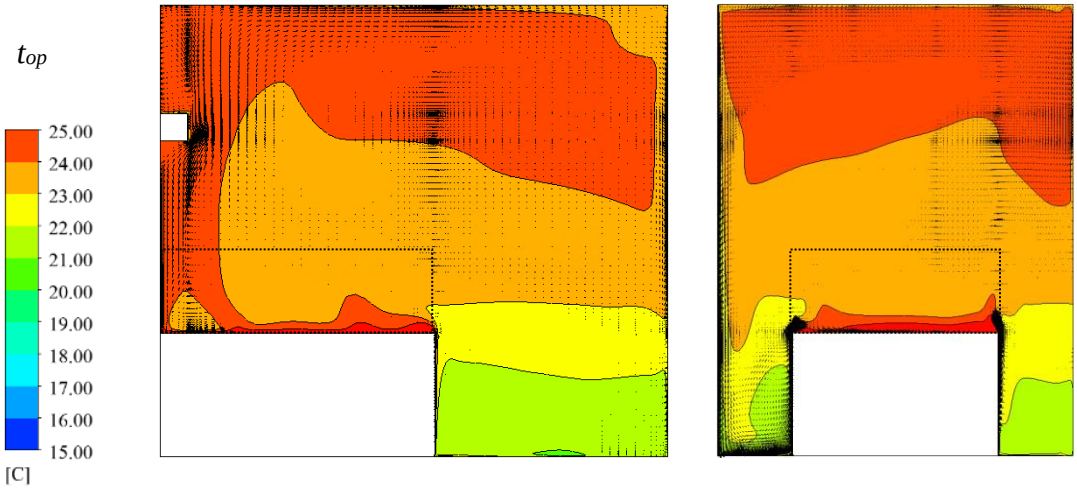

(b) Case 5.2.2

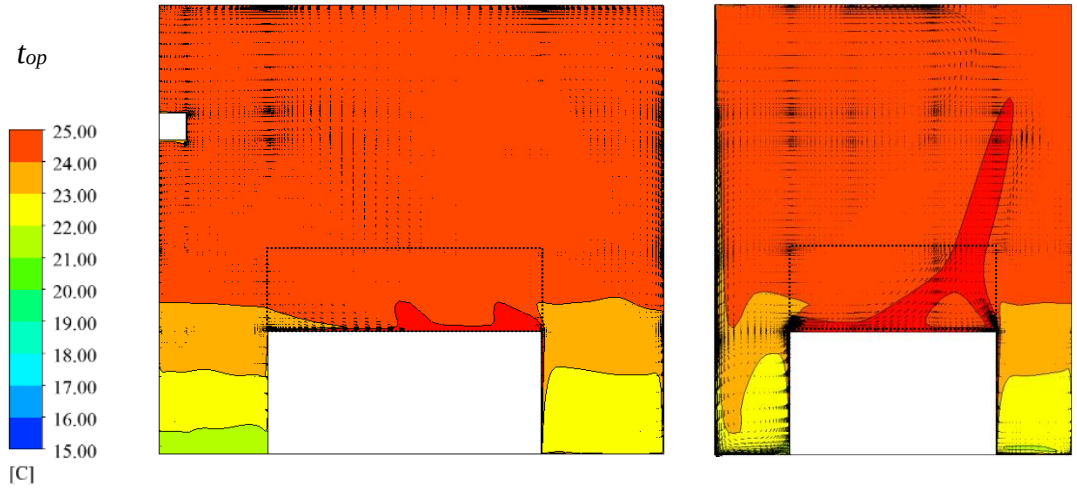

(c) Case 5.1.1

Fig. 5.9 Simulated indoor air temperature fields and air velocity vectors in Group 5.2 study cases

Table 5.3 Simulated vertical indoor air temperature gradients in Group 5.2 study cases

Case	Location of the bed-based heating terminal	Vertical temperature gradient (°C/m)
5.1.1	At the center	1.56
5.2.1	At a corner	1.75
5.2.2	Attached to a wall	1.51

5.3.2 Dimensions of the bed-based heating terminal

The effects of the dimension of the bed-based heating terminal on indoor thermal environment were numerically studied using Group 5.3 study cases. Fig. 5.10 shows, at a fixed t_{bed} of 43 °C, the total output heating capacity released from the bed-based heating terminal at different study cases including Case 5.1.1. As seen, with an increased height or width of the bed-based heating terminal, the total output heating capacity was increased from 1177.76 W in Case 5.3.1 to 1515.91 W in Case 5.3.4. To visualize the effects of the dimension of the bed-based heating terminal on indoor thermal environment, the simulated operative temperature fields and air velocity vectors at the two sectional planes are shown in Fig. 5.11. It can be seen that there were significant differences between $t_{op,oz}$ and $t_{op,uz}$ at different terminal dimensions. Furthermore, the vertical temperature gradients ranged from 1.02 to 1.79 °C/m, as shown in Table 5.4, suggesting an insignificant vertical temperature variation.

It may be seen from the numerical study results from cases in Group 5.3 that, the use of a larger dimension for the bed-based heating terminal would lead to a larger output heating capacity. In addition, with a larger surface area, the operating efficiency of the

B-ASHP system may also be increased. However, a larger bed would occupy more indoor space, and be more costly. Hence, care must be taken in choosing suitable bed dimension by considering all influencing factors.

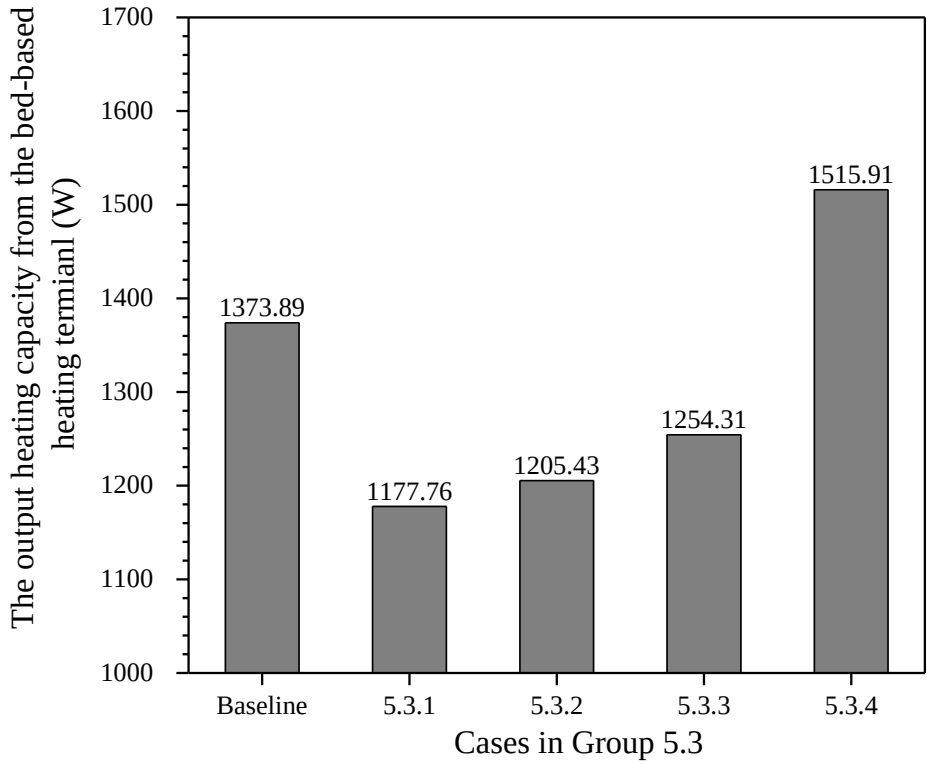

Fig. 5.10 Simulated output heating capacity from the bed-based heating terminal at different bed dimensions

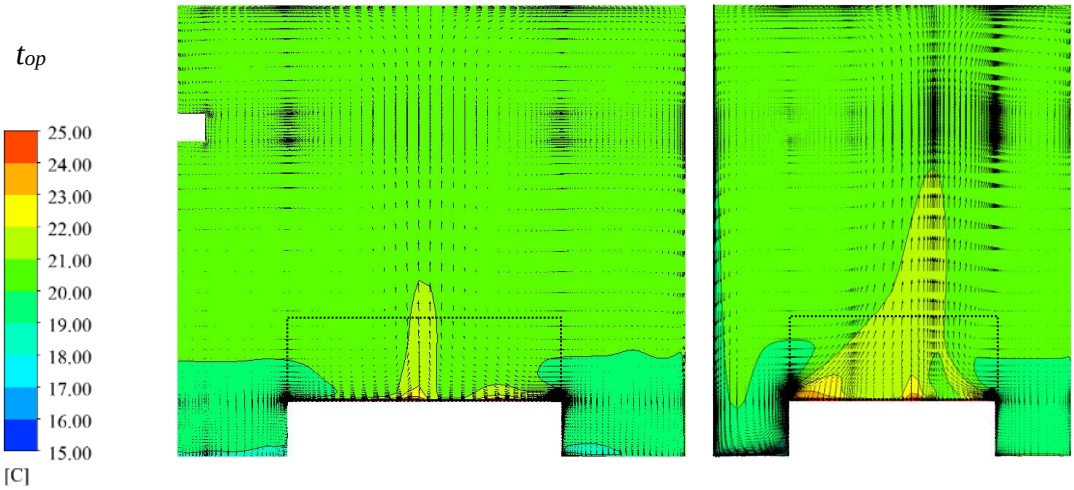

(a) Case 5.3.1

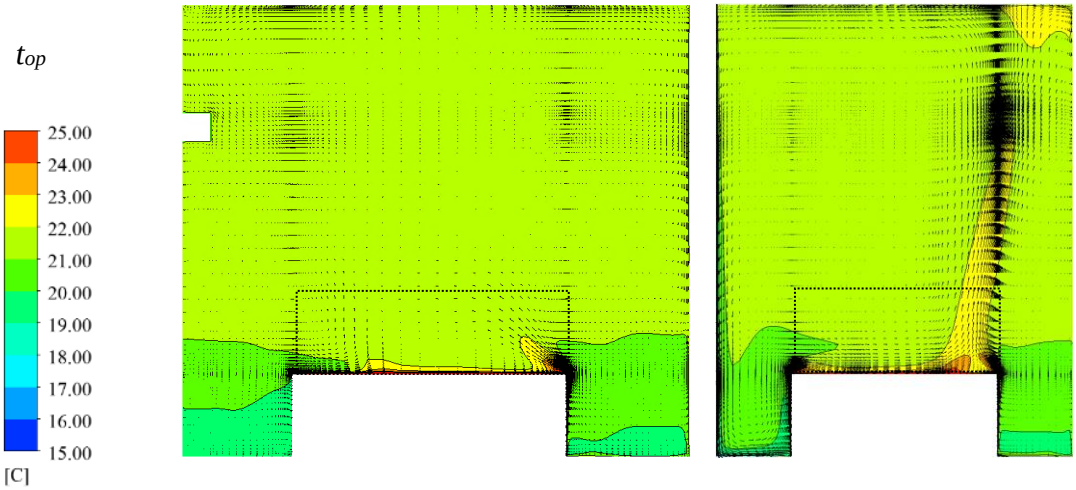

(b) Case 5.3.2

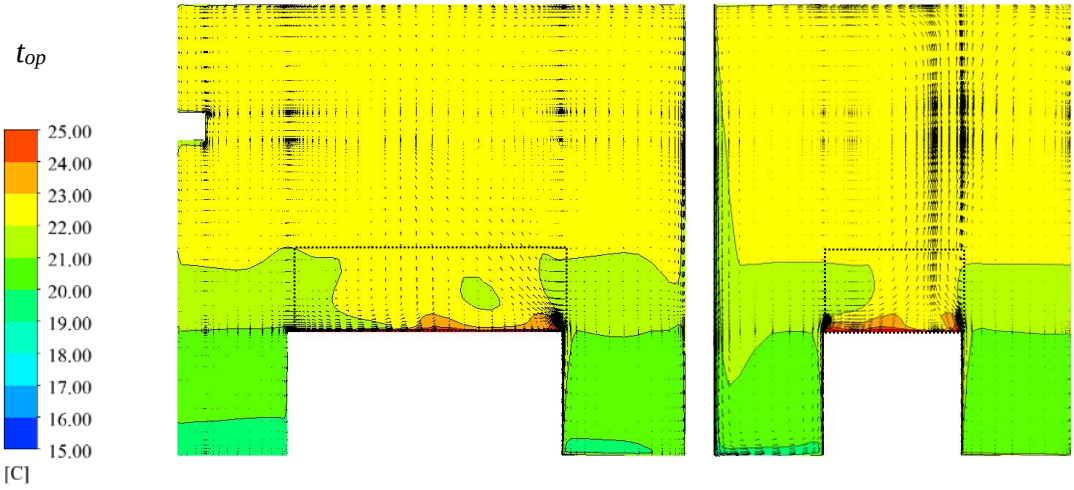

(c) Case 5.3.3

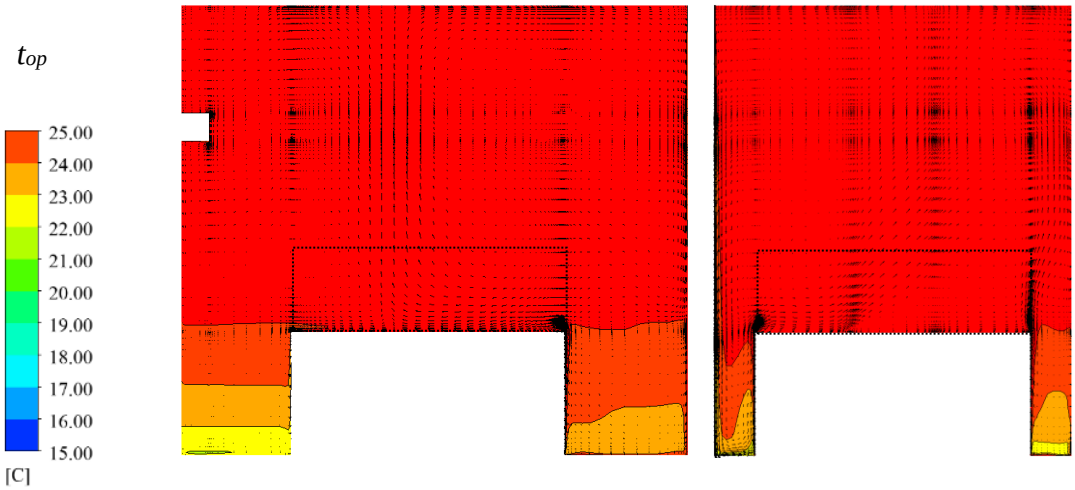

(d) Case 5.3.4

Fig. 5.11 Simulated temperature fields and air velocity vectors in Group 5.3

Table 5.4 Simulated vertical indoor air temperature gradients in Group 5.3 study cases

Case	Bed dimension (L×W×H) (mm)	Vertical temperature gradient (°C/m)
5.1.1	2000 × 1500 × 900	1.56
5.3.1	2000 × 1500 × 400	1.02
5.3.2	2000 × 1500 × 600	1.26
5.3.3	2000 × 1000 × 900	1.79
5.3.4	2000 × 2000 × 900	1.21

5.3.3 Surface temperature

Fig. 5.12 shows the simulated averaged t_{op} and $\bar{v}$ in Cases 5.4.1.1 and 5.4.1.2, as well as in Case 5.1.1. As seen, with an increase in t_{bed}, there was an obvious rise in t_{op}. At a t_{bed} of 25 °C , $t_{op,oz}$ was at 15.83 °C, but at a t_{bed} of 35 °C, $t_{op,oz}$ was actually at 20.78 °C, which can satisfy the Chinese National Standard for domestic space heating at 18 - 24 °C (GB 50736 2012). However, at 43 °C t_{bed}, $t_{op,oz}$ was at 24.76 °C, which was over that required in the Chinese National Standard thus unnecessary. The $\bar{v}$ values in all the cases ranged from 0.06 to 0.09 m/s in the OZ and 0.04 to 0.06 m/s in the UZ, respectively, suggesting a low air movement environment. Hence, in order to both maintain an acceptable indoor thermal environment and achieve the best possible operating efficiency of the B-ASHP system, the t_{bed} may be set at around 35 °C.

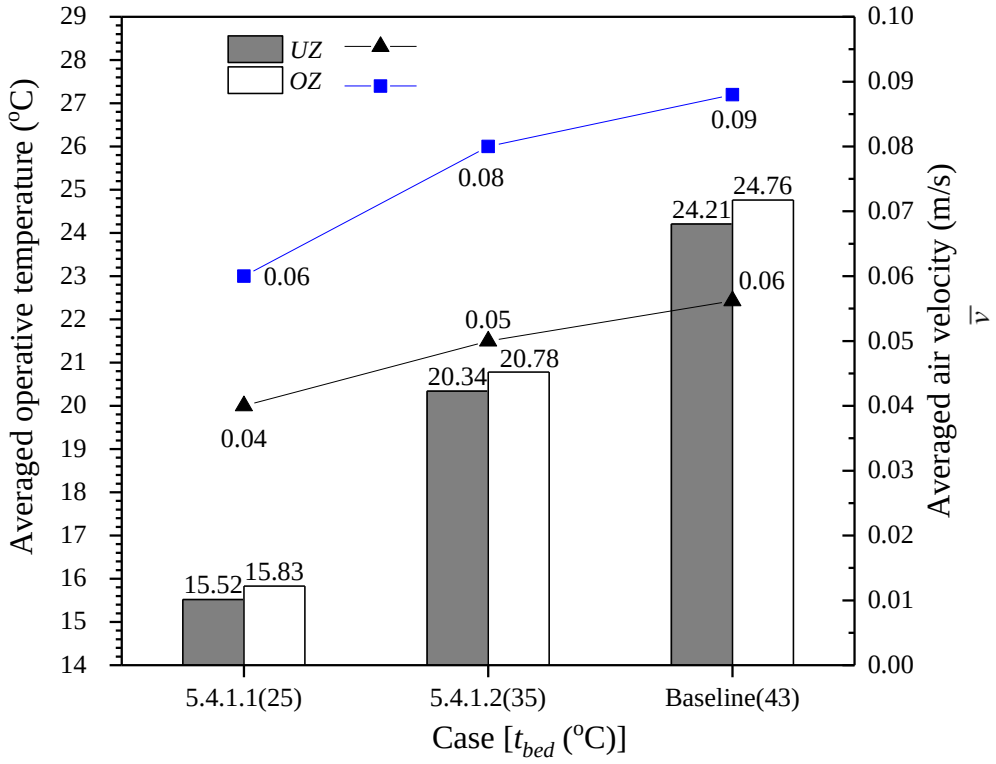

Fig. 5.12 Simulated averaged $t_{op,oz}$ and $t_{op,uz}$ values, and $\bar{v}$ values at different t_{bed} values

5.3.4 Surface emissivity of the bed-based heating terminal

Fig. 5.13 shows, at a fixed t_{bed} of 43 ^{o}C, the simulated t_{op} and $\bar{v}$ at different surface emissivities of the bed-based heating terminal, i.e., in Cases 5.2.1 to 5.2.3, as well as in Case 5.1.1. As seen, at a t_{bed} of 43 ^{o}C, with an increase in the surface emissivity of the bed-based heating terminal, t_{op} was increased. However, at all emissivity values, $t_{op,oz}$ varied within a narrow range of 22.28 ^{o}C to 25.39 ^{o}C. These implied that the changes in surface emissivity did not significantly impact on indoor thermal environment, when t_{bed} was fixed. However, the variation trend would suggest that when a lower t_{bed} was used, a higher surface emissivity would be preferred. Hence, setting a t_{bed} value and surface emissivity should be considered together, to maximize the operating efficiency of a B-ASHP system, while not compromising indoor thermal environment. The averaged air velocity values, on the other hand, dropped from 0.07 to 0.05 m/s and 0.11 to 0.08 m/s in the OZ and UZ, respectively. However, $\bar{v}$ values in all cases were lower than 0.15 m/s (ASHRAE Standard 55 2017), suggesting a low air movement environment.

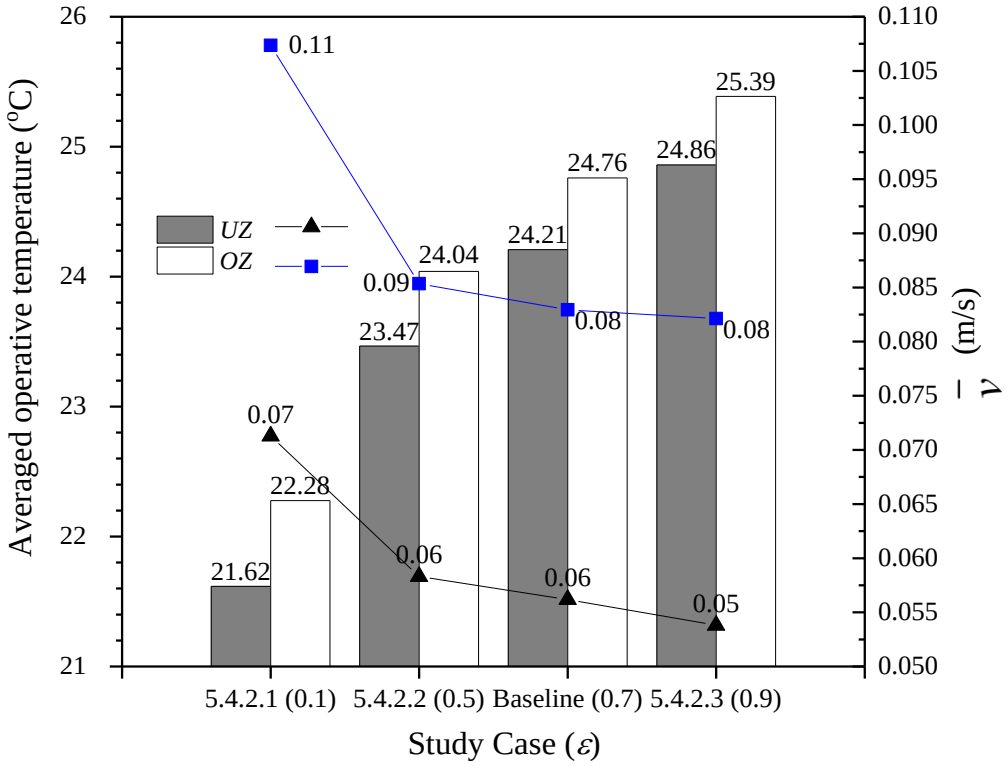

Fig. 5.13 Simulated averaged $t_{op,oz}$ and $t_{op,uz}$ values at different surface emissivity values (Cases 5.4.2.1 - 5.4.2.3, and the baseline case)

5.4 Conclusions

This Chapter reports on a numerical study on the effects of varying four design/operating parameters, i.e., location, dimension, t_{bed} and surface emissivity of the bed-based heating terminal in a B-ASHP system on indoor thermal environment and the operating efficiency of the B-ASHP system. A CFD method was firstly established and experimentally validated using the experimental data obtained in the experimental study reported in Chapter 4. The numerical results demonstrated that:

1. To place the bed-based heating terminal in the center, a larger output heating capacity, a more uniformed indoor thermal environment and a better air velocity

distribution could be achieved compared with other locations, however it may imply different installation space requirements.

2. To increase the width and height of the bed-based heating terminal would lead to a larger output heating capacity with a larger surface area, thus a better operating efficiency, however, a larger bed would occupy more indoor space and be more costly.

3. To both maintain an acceptable indoor thermal environment and achieve the best possible operating efficiency of the B-ASHP system, the t_{bed} of its bed-based heating terminal may be set at around 35 ^{o}C.

4. The changes in surface emissivity did not significantly impact much on indoor thermal environment at a fixed t_{bed}, however, the variation trend would suggest that when a lower t_{bed} was used, a higher surface emissivity would be preferred.

Chapter 6 A further numerical study on evaluating sleeping thermal comfort using the B-ASHP system

6.1 Introduction

In Chapter 5, the effects of varying four design/operating parameters, i.e., location, dimension, t_{bed} and surface emissivity of the bed-based heating terminal in a B-ASHP system on indoor thermal environment were numerically studied. The study results suggested that the variation in these design/operating parameters of the bed-based terminal, including location, dimension, surface temperature and surface emissivity, did impact both indoor thermal environment and the operating efficiency of the B-ASHP system, in terms of the uniformity of indoor thermal environment, indoor air velocity distribution and the output heating capacity, as well as the installation space requirement and cost implication.

Furthermore, it can be understood that in this B-ASHP system, a bed-based terminal was included. Such a terminal can virtually act as a bed, similar to a heated Chinese-Kang bed, to provide a sleeping person with a suitable micro-environment that was conducive to quality sleep. However, in the experimental and numerical studies presented in Chapters 4 and 5, the sleeping thermal comfort of person sleeping on the bed-based heating terminal and its influencing factors such as bed-surface temperature, thermal resistances of mattress and quilt were not considered.

Therefore, as a follow-up to the two studies presented in Chapters 4 and 5, a further numerical study based on a digital thermal manikin (DTM) on the influences of the

following four factors, i.e., the operating modes of the bed-based terminal, bed surface temperature (t_{bed}), and thermal resistance of a mattress (R_{mat}) and that of a quilt (R_q), on sleeping thermal comfort, as the third part of the research project reported in this Thesis, has been carried out, and the study results are reported in this Chapter. The organization of this Chapter is as follows: Firstly, a geometry model for the experimental indoor space with a DTM and a revised CFD method developed for use in this further numerical study are described in detail, and the boundary conditions for the experimental indoor space presented. Secondly, the experimental validation of the revised CFD method is reported. Thirdly, the numerical study cases, the numerical study results and the related analysis on the effects of varying the above four factors on the sleeping thermal comfort are presented. Finally, a conclusion is given.

6.2 Development of the Revised CFD method

6.2.1 Geometry model with a DTM

A geometry model for the experimental indoor space, which is described in Section 4.2, Chapter 4, with a DTM was built. A three-dimensional view and two sectional views of the experimental indoor space are shown in Fig. 6.1 (a) and Fig. 6.1 (b), respectively. As seen, the bed-based terminal was centered in the experimental indoor space. Except one simulated external wall between the indoor and outdoor spaces, all the other five envelope surfaces of the experimental indoor space can be regarded as adiabatic since they were well insulated, so that only the heat transfer through the simulated external wall took place. As also mentioned in Section 4.2, the bed-based terminal consisted of two sections, i.e., a horizontal section (H-Section) and a vertical section (V-Section) (see Fig. 6.1 (a)). In general, the use of H-Section only was to

provide localized heating for sleeping at nighttime and the use of H+V-Section to provide full space heating at daytime. In addition, a convection-based heating terminal was placed on an internal surface of the experimental indoor space at a height of 2500 mm. On top of the H-Section was a DTM (P.T. Teknik 2008), which was used to simulate a female sleeping person with a height of 1650 mm and in normal long sleeve sleeping wear with a thermal resistance of 0.054 $W/m^2 \cdot {}^oC$ (Du et al. 2017). The core temperature (t_{core}) of the DTM was set at 36.4 ^oC (Kreider et al. 1958), and the temperature of its skin compartment was left uncontrolled, but can vary in response to ambient thermal environment.

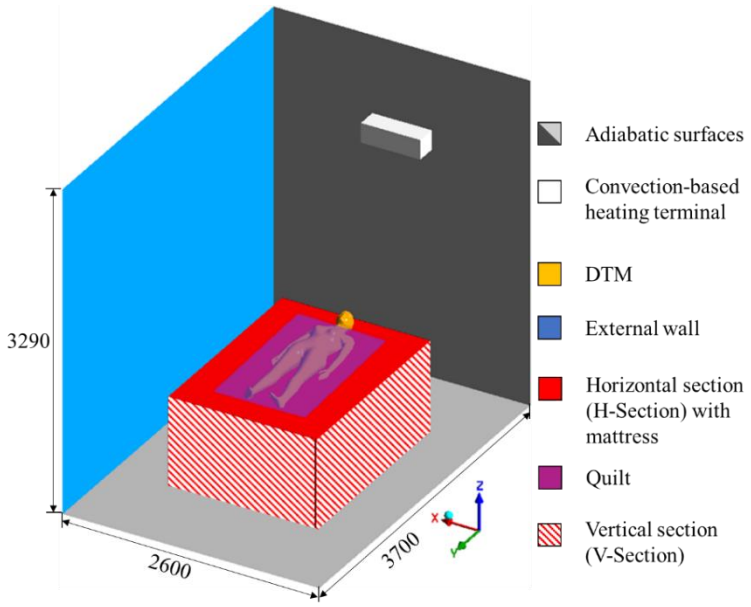

Fig. 6.1 (a) A 3-D view of the experimental indoor space, DTM and the bed-based terminal of the B-ASHP system (unit: mm)

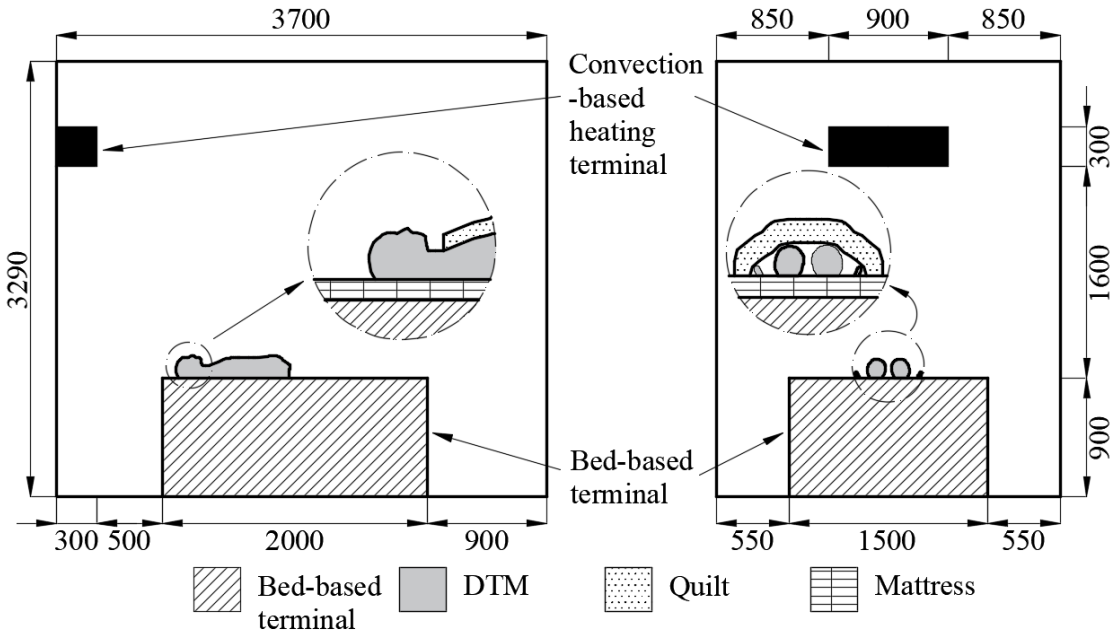

Fig. 6.1 (b) Sectional views of the experimental indoor space, and the bed-based terminal of the B-ASHP system and the DTM (unit: mm)

6.2.2 Mesh generation and CFD method with a DTM

Due to the geometry complexity of the DTM, the experimental indoor space was divided into two domains in this further numerical study. A cuboid of 2000 mm × 1500 mm × 600 mm (L×W×H) right above the bed-based terminal containing the DTM was defined as Domain 1. The rest of the experimental indoor space, on the other hand, was defined as Domain 2. Grids were generated using ICEM CFD (2010) with structured and unstructured mesh for the Domain 1 and Domain 2, respectively. For the experimental indoor space, the sectional view of the mesh for the computational domain corresponding to the sectional views shown in Fig. 6.1 (b), is shown in Fig. 6.2. Heights of 0.7 mm and 1.4 mm were used for the first layer of the DTM and that of the wall surfaces, respectively. Table 6.1 lists the mesh numbers in both Domain 1 and Domain 2 for sensitivity validation.

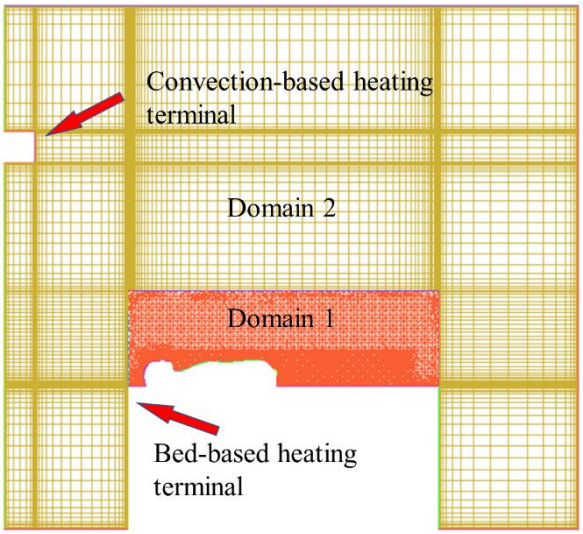

Fig. 6.2 Sectional view of the mesh generation for the two domains in the experimental indoor space

Table 6.1 The number of meshes for both Domain 1 and Domain 2 for mesh sensitivity validation (unit: million)

Total mesh number	Mesh number in Domain 1	Mesh number in Domain 2
1.95	0.98	0.97
2.26	1.07	1.19
2.60	1.13	1.47

The steady state, viscous and 3D governing equations for the flow field inside the experimental indoor space are given as Equations (2.10) - (2.14) in Chapter 2. A commercial CFD code (ANSYS Fluent 2010) was used to solve these governing equations to obtain the air flow field inside the experimental indoor space. Since the Rayleigh number evaluated around the DTM was greater than 10^{10}, turbulence was expected at the near wall region. The Boussinesq approximation was used to simulate the natural convection in the experimental indoor space considering buoyance term

(ANSYS Fluent 2010). The Coupled algorithm was used for pressure-velocity coupling scheme.

6.2.3 Revised boundary conditions for the experimental indoor space

The revised boundary conditions for the experimental indoor space are given in Table 6.2.

Table 6.2 Revised boundary conditions for the experimental indoor space

Boundary	Material	Emissivity	Thermal conditions
External wall	Gypsum plaster	0.9	7 ^{o}C
Floor	Anodized aluminum	0.3	Adiabatic
Other internal surfaces	Aluminum	0.07	Adiabatic
DTM	Plastic	0.9	36.4 ^{o}C

6.2.4 Validation of the revised CFD method

Following the recommended validation procedures and criteria in a previous study (Chen and Srebric 2002), although there would be many study cases using the revised CFD method, and since the flow mechanism and heat transfer characteristics in all study cases were similar, the validation of the revised CFD method for only one study case was sufficient. This particular study case was designated as Case 6.1. In Case 6.1, the following settings were used: 1) only the H-Section of the bed-based terminal was operated; 2) there was no mattress placed on the bed-surface, so the DTM was in direct contact with the bed surface; 3) Q2 type quilt whose the thermal resistance was 0.4774 W/m$^2 \cdot {}^{o}$C was used; 4) t_{bed} was set at 43 ^{o}C.

For validating the revised CFD method, with the same experimental setup in the experimental study presented in Chapter 4, validation experiments using the settings in Case 6.1 were carried out and experimental results were obtained. The experimentally measured air temperatures and velocities at two points inside Domain 1 ($D1_a$ and $D1_b$), and two inside Domain 2 ($D2_a$ and $D2_b$) were compared with those simulated using the revised CFD method.

6.2.4.1 Mesh sensitivity

The thermal environments in Case 6.1 were firstly studied using three different mesh sizes of 1.95 million, 2.26 million and 2.60 million. The simulated air temperatures and velocities at the above four locations are shown in Fig. 6.3 (a) and (b). As seen, the obtained results at 2.26 million and 2.60 million mesh sizes were very close to each other, within an averaged deviation of 0.06 ^oC for temperature and that of 0.084 m/s for air velocity. On the other hand, the numerical results at 1.95 million mesh sizes showed noticeable differences as compared with those at the other two mesh sizes. Secondly, as shown in Fig. 6.3 (c), the calculated y^+ value for the DTM using the selected mesh at the size of 2.26 million was below 1, which can ensure the numerical accuracy. Here, $y^+ = u^* \cdot y/v$, where y is the height of first mesh layer off the surface of the DTM, v the kinematic viscosity of air, and u^* the friction velocity, respectively (ANSYS Fluent 2010). Hence, the numerical results using mesh size of 2.26 million were considered to be grid independent and thus used in this further numerical study.

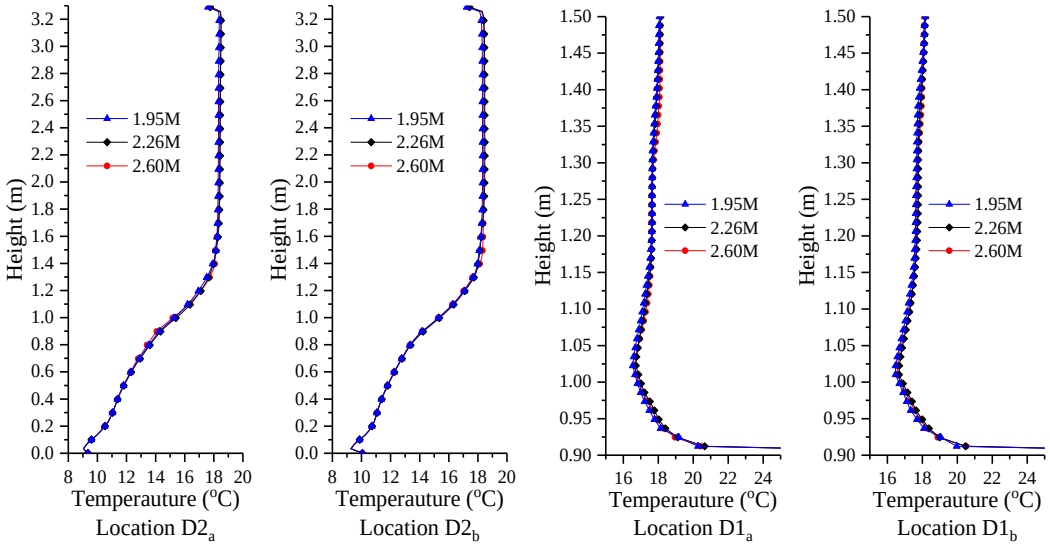

(a) Air temperature

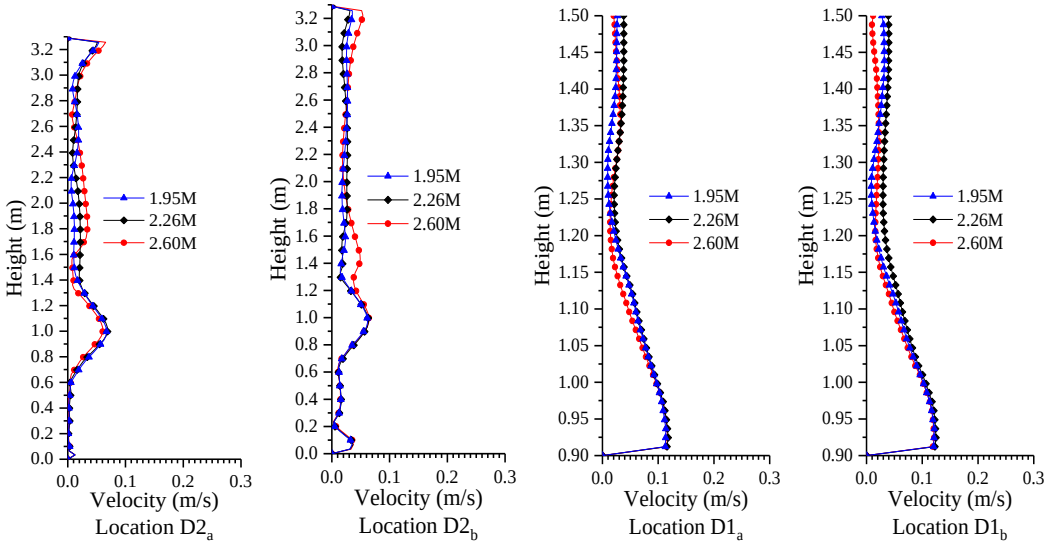

(b) Air velocity

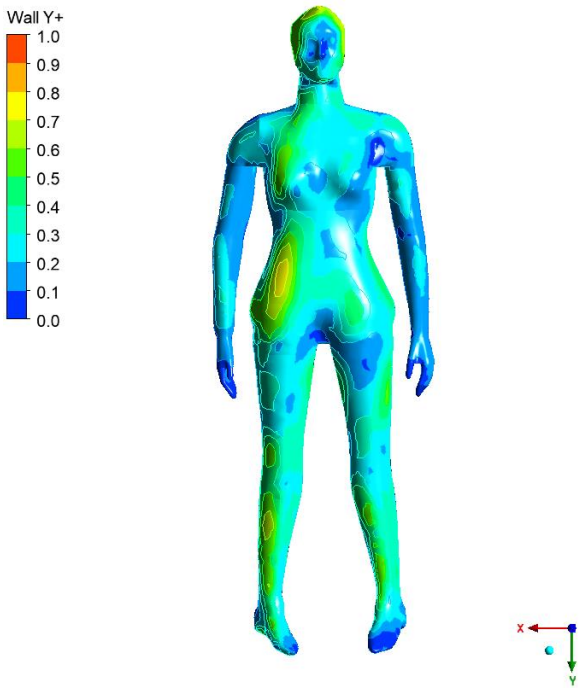

(c) y^+ distribution for DTM surface

Fig. 6.3 The simulated air temperatures and air velocities at four different locations using three different mesh sizes and y^+ distribution for DTM surface at mesh size of 2.26 million

6.2.4.2 Turbulence model

Fig. 6.4 compares the measured and the simulated air temperatures and velocities at the four different locations using three different available turbulence models: SST k-w model, Standard k-epsilon (STD-ke) model and RNG k-epsilon (RNG-ke) model, respectively. As seen, the SST k-w model performed better than the other two in simulating both air temperature and air velocity profiles, with an averaged absolute difference between the measured and the simulated temperatures at 0.16 °C, and that between the measured and the simulated air velocities 0.025 m/s, respectively, when using the SST k-w model.

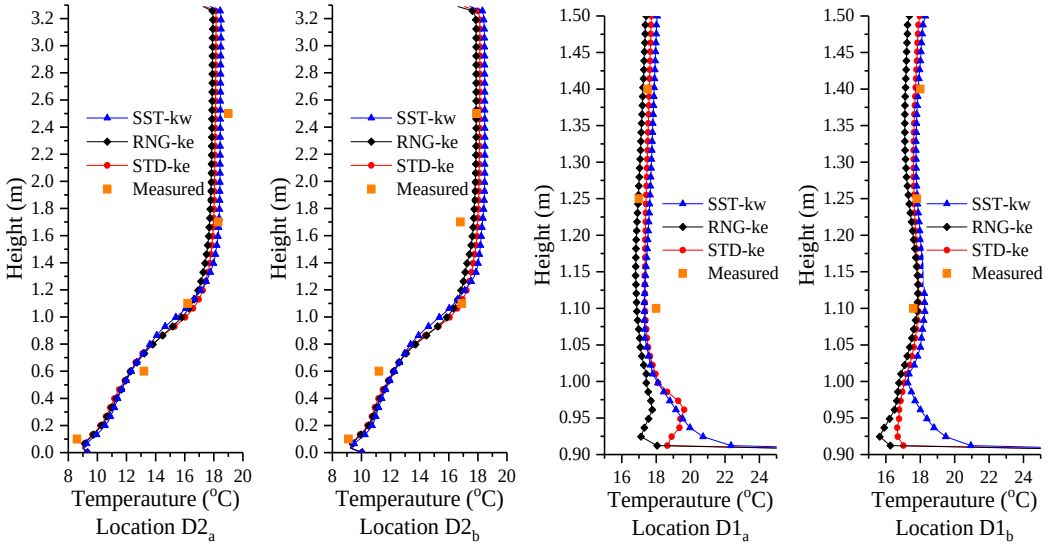

(a) Air temperature

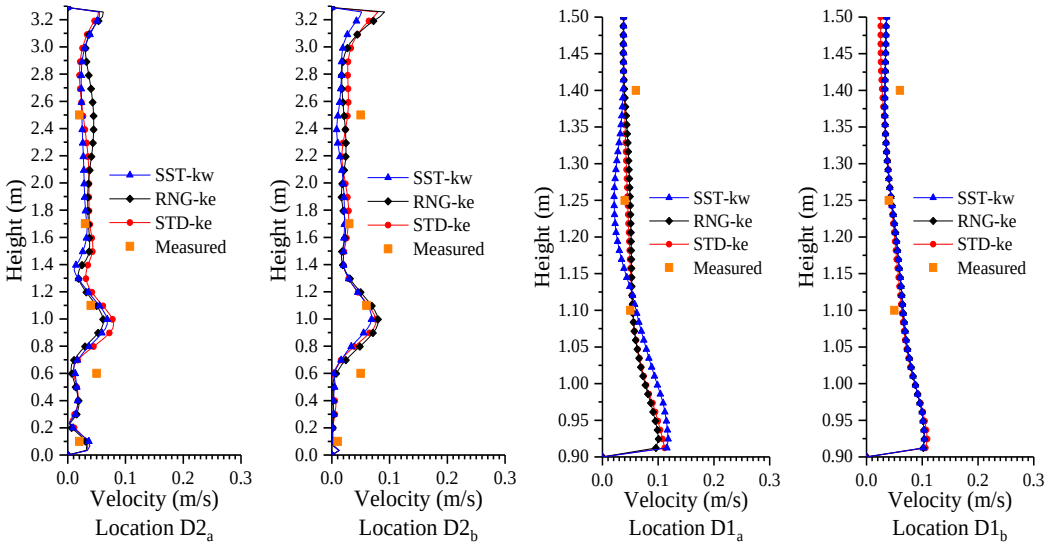

(b) Air velocity

Fig. 6.4 Comparisons between the measured and the simulated air temperatures and air velocities at four different locations using three different turbulence models

6.2.4.3 Radiation model

The use of two different radiation models, surface-to-surface (S2S) model and discrete ordinate (DO), was examined and the simulated results of air temperatures and air

velocities at the four locations were compared with the experimentally measured data. The S2S model was commonly used to calculate radiation heat transfer in buildings as an enclosure for radiative heat transfer with non-participating media. Furthermore, the DO model was widely known for its high accuracy especially for the heat transfer media with a thin optical thickness such as air (ANSYS Fluent 2010). Fig. 6.5 shows the comparisons between the measured experimental results and the simulated results obtained using the two radiation models. As seen, a better agreement between the measured data and the simulated results when using S2S model may be observed. The maximum absolute differences between the measured and simulated air temperatures and that between the measured and simulated air velocities were 0.8 ^{o}C and 0.05 m/s, respectively, when using the S2S model. Therefore, the S2S model was selected to calculate the radiation heat transfer in this numerical study.

Consequently, in the revised CFD method developed, the followings were adopted: mesh sizes of 2.26 million, SST-kw turbulence model and S2S radiation model. Following the suggestions in a previous CFD study (Chen and Srebric 2002), and based on the comparison results shown in the sub-sections 6.2.4.1 to 6.2.4.3, it was considered that the revised CFD method developed was validated.

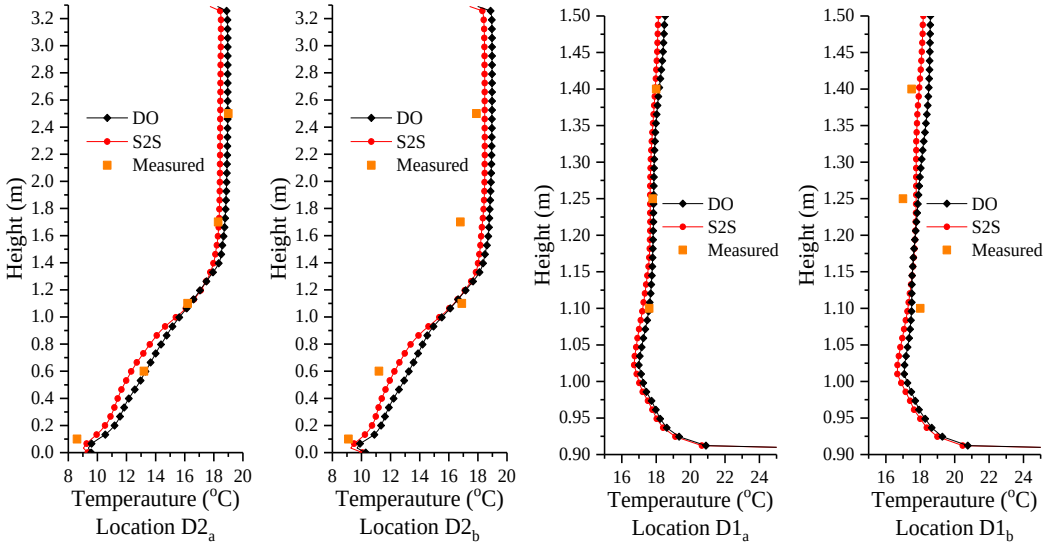

(a) Air temperature

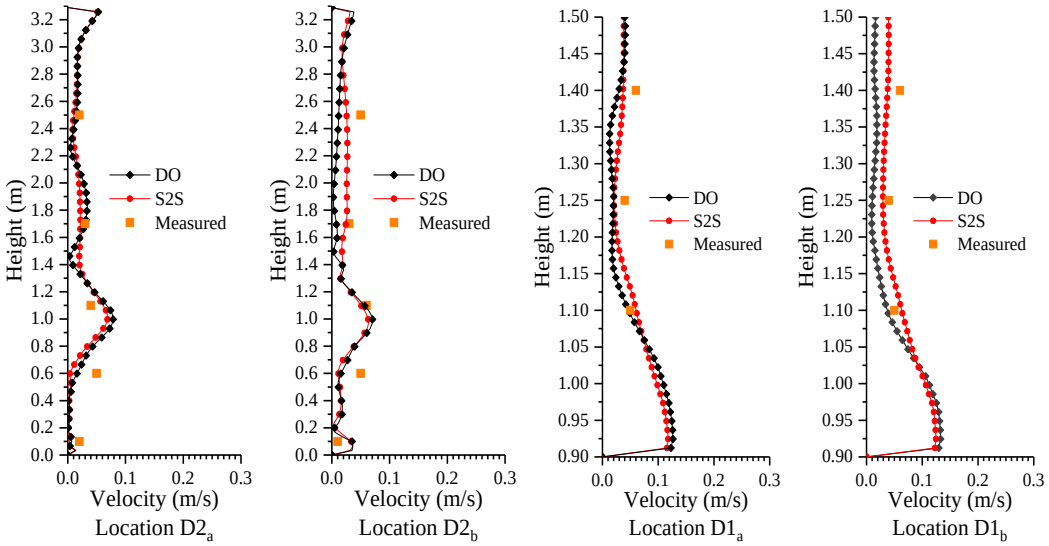

(b) Air velocity

Fig. 6.5 Comparison between the measured and the simulated air temperatures and air velocities at four different locations using the two different radiation heat transfer models

6.3 Numerical study results and the related analysis

6.3.1 Evaluation indexes and criteria

In this further numerical study, operative temperature (t_{op}) and the whole predicted percentage of dissatisfaction (*WPD*) (Song et al. 2018a) were used to evaluate the effects of both using different heating section of the bed-based terminal, and varying the values of t_{bed}, R_{mat}, and R_q on the thermal environment of a person sleeping on the bed-based heating terminal of the B-ASHP system. t_{op} as detailed already in Chapter 5, was a comprehensive index commonly used for thermal environmental analysis (ASHRAE 2017).

On the other hand, based on Fanger's *PMV-PDD* scheme (Fanger 1970) and Lin and Deng's sleeping thermal comfort model (Lin and Deng 2008), a *PTS-WPD* model was previously developed by Song et.al (2018a) for measuring the predicted percentage of dissatisfaction for a sleeping person under heating conditions, by considering the differences in the thermal environmental requirements exposed by a head region and the other body parts covered by quilt of a sleeping person, respectively. The *PTS-WPD* model is expressed as follows (Song et al. 2018a):

$$\begin{aligned} WPD = {} & 26.27 + 31.40PTS_H - 38.21PTS_{CB} + 13.12PTS_H{}^2 \\ & + 20.09PTS_{CB}{}^2 - 18.67PTS_H \cdot PTS_{CB} \end{aligned} \tag{6.1}$$

Where PTS_H and PTS_{CB} are the calculated partial thermal sensation of the head region, which is exposed to the ambient environment in a bedroom directly, and the other body parts covered by quilt, respectively, expressed by:

$$PTS_H = 0.9701 + 0.2317 L_H + 0.0329 \Delta L \tag{6.2}$$

$$PTS_{CB} = 2.0948 + 0.2184 L_{CB} - 0.1663 \Delta L \tag{6.3}$$

Where L_H and L_{CB} are the thermal load on the head region and the other body parts covered by a quilt, respectively, W, expressed as follows:

$$L_H = 10.0247 - \left\{ \begin{array}{l} 28.4794\left[0.0014(34 - t_a) + 0.0173(5.87 - p_a)\right] \\ +0.4090(5.9454 - p_a) + 0.4134(36.4 - t_a) + 0.3807(36.4 - \overline{t_r}) \end{array} \right\} \tag{6.4}$$

$$L_{CB} = 46.9341 - \left\{ \begin{array}{l} 28.4794\left[0.0014(34 - t_a) + 0.0173(5.87 - p_a)\right] + \\ 2.1099(0.256 t_{sk,q} - p_a) + 0.7765(0.256 t_{sk,mat} - p_a) \\ +Q_{cond} + Q_{conv} \end{array} \right\} \tag{6.5}$$

$$\Delta L = L_{CB} - L_H \tag{6.6}$$

Where p_a is the water vapor pressure in ambient air, kPa, set at a value when relative humidity was 30 %; $t_{sk,q}$ the averaged skin temperature in contact with quilt, ^{o}C; $t_{sk,mat}$ the averaged skin temperature in contact with mattress, ^{o}C; Q_{conv} the convective thermal load on a sleeping person, W; Q_{cond} the conductive thermal load on a sleeping person from a heated bed surface, W, which can be evaluated by:

$$Q_{cond} = \frac{t_{core} - t_{bed}}{R_{mat} + R_{clo} + R_{skin}} \cdot A_{back} \quad (6.7)$$

Where R_{mat}, R_{clo}, R_{skin} are the thermal resistance of mattress, clothing or sleeping wear in the current study, and skin, respectively; A_{back} the surface area of the back of a human body, m^2.

According to the established *PTS-WPD* model (Song et al. 2018a), the use of both PTS_H and PTS_{CB} is similar to that of *PMV*. PTS_H at 0 reflects a thermally neutral environment for the head region and PTS_{CB} at 0 that for the other body parts covered by quilt. Furthermore, when the calculated *WPD* values is lower than 10 %, a thermal environment may be regarded as being thermally comfort for a sleeping person.

6.3.2 Numerical cases and grouping

In this further numerical study, study cases were designated to evaluate the impacts of the four factors on the thermal comfort of a sleeping person. To designate the appropriate study cases, in addition to the settings used in Case 6.1, the followings different combinations of operating modes of the bed-based terminal, t_{bed} values and types of mattress and quilt were included: i) one more operating mode of the bed-based terminal using the H+V-Section; ii) different t_{bed} values of 25 ^oC, 36.4 ^oC, 44 ^oC, 46 ^oC, 50 ^oC and 55 ^oC when only using the H-Section, and B-ASHP system not operated, so that the bed-based terminal was not heated, or no heating was provided; iii) three different types of mattresses (M1, thin board mattress with an R_{mat} of 0.1519 $W/m^2 \cdot {}^oC$, M2, medium mattress with R_{mat} of 0.3038 $W/m^2 \cdot {}^oC$ and M3, thick mattress with R_{mat} of 0.9079 $W/m^2 \cdot {}^oC$); iv) three different types of quilt coverages (None with

R_q at 0, Q1, blanket with R_q at 0.25885 W/m$^2 \cdot$ ^{o}C and Q3, normal winter quilt with R_q at 0.75 W/m$^2 \cdot$ ^{o}C).

Consequently, a total of 16 study cases were designated and are detailed in Table 6.3. The 16 study cases were separated into 4 groups, as shown in Table 6.4. The study cases in these Groups were used to investigate the effects of using different heating sections of the bed-based heating terminal, adopting different t_{bed} values, varying R_{mat} values and varying R_q values, on the thermal comfort for a sleeping person, respectively.

Table 6.3 Cases used in the revised numerical study

Cases	Heating section	t_{bed} (^{o}C)	R_{mat}	R_q
6.1	H	43	None	Q2
6.2			M1	
6.3	H+V			
6.4	H	No heating		
6.5		25		
6.6		36.4		
6.7		44		
6.8		46		
6.9		50		
6.10		55		
6.11		44	None	
6.12			M2	
6.13			M3	
6.14			M1	None
6.15				Q1
6.16				Q3

Table 6.4 Study groups

Study group	Study cases involved	Study target
6.1	6.2, 6.3	Heating section
6.2	6.2, 6.4 to 10	t_{bed}
6.3	6.8, 6.11, 6.12, 6.13	R_{mat}
6.4	6.8, 6.14, 6.15, 6.16	R_q

6.3.3 Effects of using different heating sections on the sleeping thermal environment (Group 6.1)

Fig. 6.6 shows that the simulated total output heating capacity from the B-ASHP system using H-Section only in Case 6.2 was at ~ 306 W and that using H+V-Section in Case 6.3 at ~ 1160 W. Therefore, using H+V-Section would provide more output heating capacity at the expense of requiring more energy consumption. Moreover, in Fig. 6.7, detailed t_{op} distributions inside the experimental indoor space at two sectional planes across the center point of the space for the two cases are shown. As seen, the use of H+V-Section of the bed-based terminal could lead to an overall warmer thermal environment in the experimental indoor space. However, during sleep at nighttime, a higher t_{op} in the entire experimental indoor space of a bedroom may not be necessary. Therefore, during sleep, in order to both achieve a higher operating efficiency of the B-ASHP system and maintain a suitable sleeping thermal environment, the use of the H-Section only should be adequate. Consequently, in the study cases in other groups, i.e., Groups 6.2 - 6.4, only H-Section was operated.

Furthermore, it has been demonstrated that the temperature difference between two environments for a person could cause thermal disturbance (Xiong et al. 2017b, Nagano et al. 2005, Xiong et al. 2016a). This was also true for a sleeping person before and after a night-long sleep. Therefore, to reduce the temperature difference between inside and outside a micro-environment separated by a quilt, the H+V-Section of the bed-based heating terminal may be operated to provide full space heating an hour prior to bedtime and an hour before leaving the bed. However, only H-Section was operated during sleeping hours, leading to less energy consumption for the B-ASHP system.

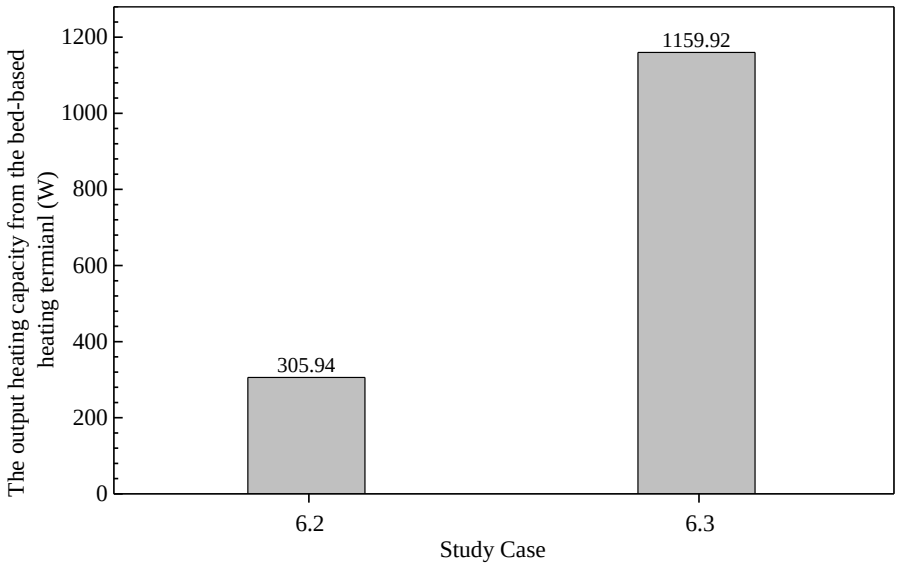

Fig. 6.6 The output heating capacity in the study cases in Group 6.1

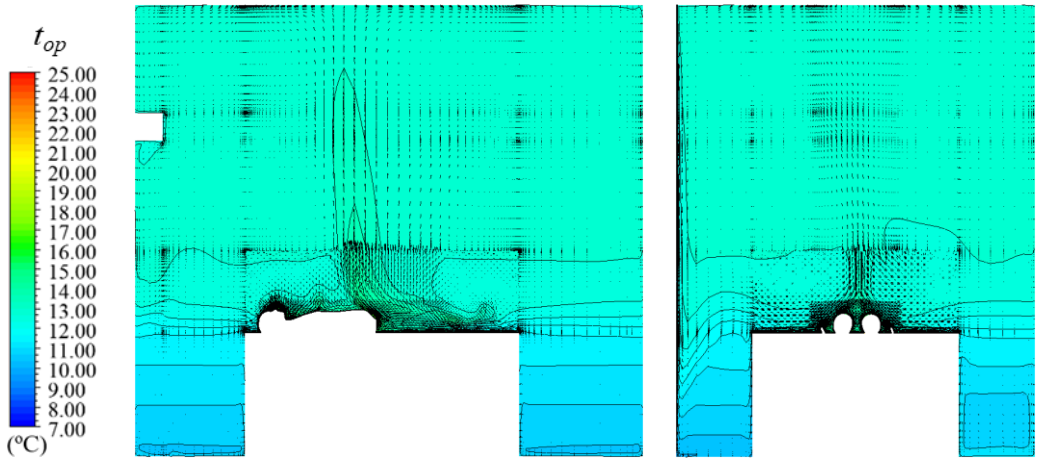

(a) Case 6.2, H-Section, M1, Q2, t_{bed} = 43 ºC, *WPD* = 10.27 %

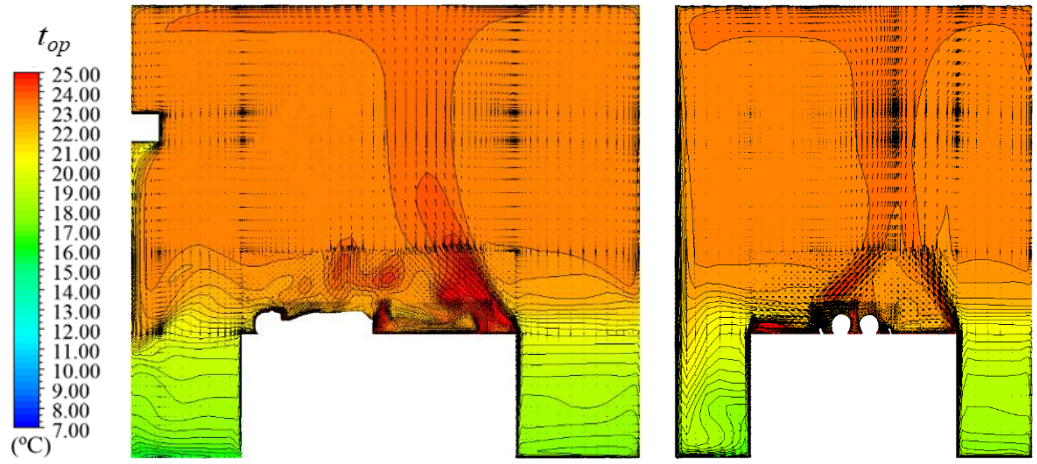

(b) Case 6.3, H+V-Section, M1, Q2, t_{bed} = 43 ºC, *WPD* = 28.29 %

Fig. 6.7 Simulated indoor operative temperature fields and air velocity vectors in the study cases in Group 6.1

6.3.4 Effects of t_{bed} on the sleeping thermal environment (Group 6.2)

Fig. 6.8 shows the variations of the simulated volume-averaged operative temperatures in Domain 1 ($t_{op,d1}$) and Domain 2 ($t_{op,d2}$), and surface temperature of the mattress (t_{mat}), at different t_{bed} values when only using H-Section, respectively. As seen, with an increase in t_{bed}, there were obvious rises in $t_{op,d1}$, $t_{op,d2}$ and t_{mat}, and the differences between $t_{op,d1}$ and $t_{op,d2}$ were gradually enlarged. From Fig. 6.9 and Fig. 6.10, a PTS_{CB} value of -4.23 and a *WPD* value of 100 % in Case 6.4 could be observed, when no bed-based heating was provided, suggesting a cold sleeping thermal environment.

Moreover, the values of PTS_{CB} were higher than those of PTS_H in all cases in Group 6.2, suggesting a warmer thermal sensation for the other body parts covered by quilt than the head region. As seen in Fig. 6.9 and Fig. 6.10, the lowest *WPD* value in Group 6.2 study cases was in Case 6.9 at 6.19 %, when the PTS_{CB} value was 0.81 and PTS_H value was -1.08. Therefore, although the thermal sensation in the head region was cold, an overall thermal comfort can be achieved due to a warmer micro-environment inside the quilt around the other body parts of a sleeping person.

On the other hand, as shown in Fig. 6.10, increasing t_{bed} values could obviously decrease the calculated *WPD* values. However, further increasing t_{bed} from 50 ^{o}C to 55 ^{o}C would actually result in an increase in calculated *WPD* from 6.19 - 15.88 %, suggesting that a higher-than-necessary t_{bed} would reduce the comfort level for a sleeping person. Hence, in order to both maintain an acceptable sleeping thermal environment and achieve the best possible operating efficiency of the B-ASHP system simultaneously, the value of t_{bed} should be carefully selected, and the numerical study results from this study group suggested that t_{bed} value between 44 ^{o}C and 50 ^{o}C (Cases

6.7 - 6.9) may be appropriate, where *WPD* values were all below 10 %. Therefore, the lowest t_{bed} of 44 °C was selected in the study cases in Groups 6.3 and 6.4.

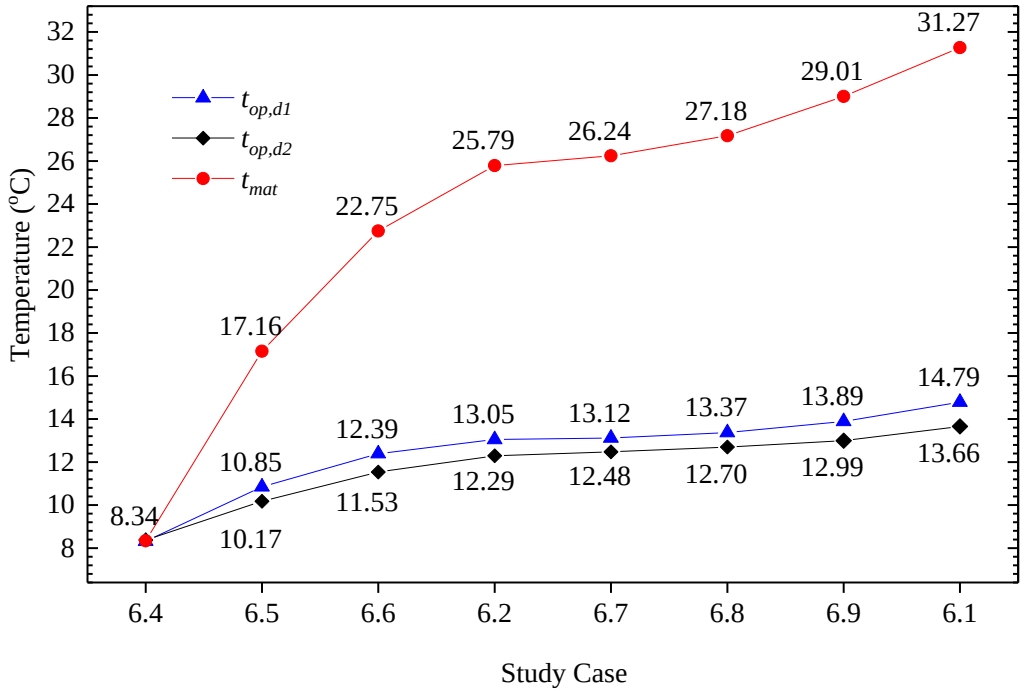

Fig. 6.8 The simulated t_{op} values and mattress surface temperatures at different t_{bed} values in the study cases in Group 6.2

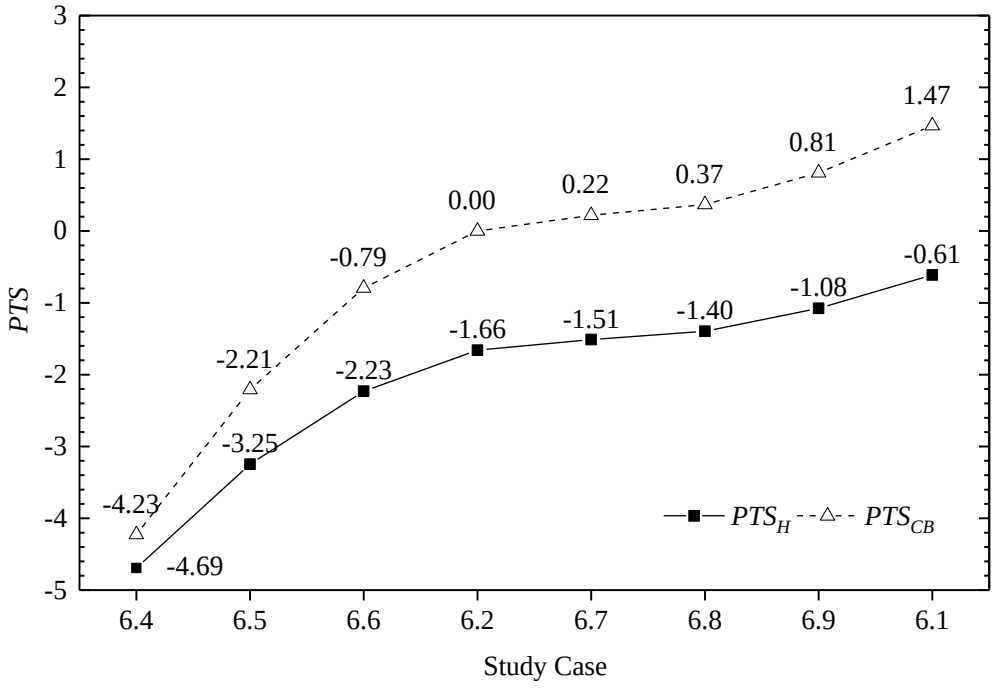

Fig. 6.9 The calculated PTS_H and PTS_{CB} values in the study cases in Group 6.2

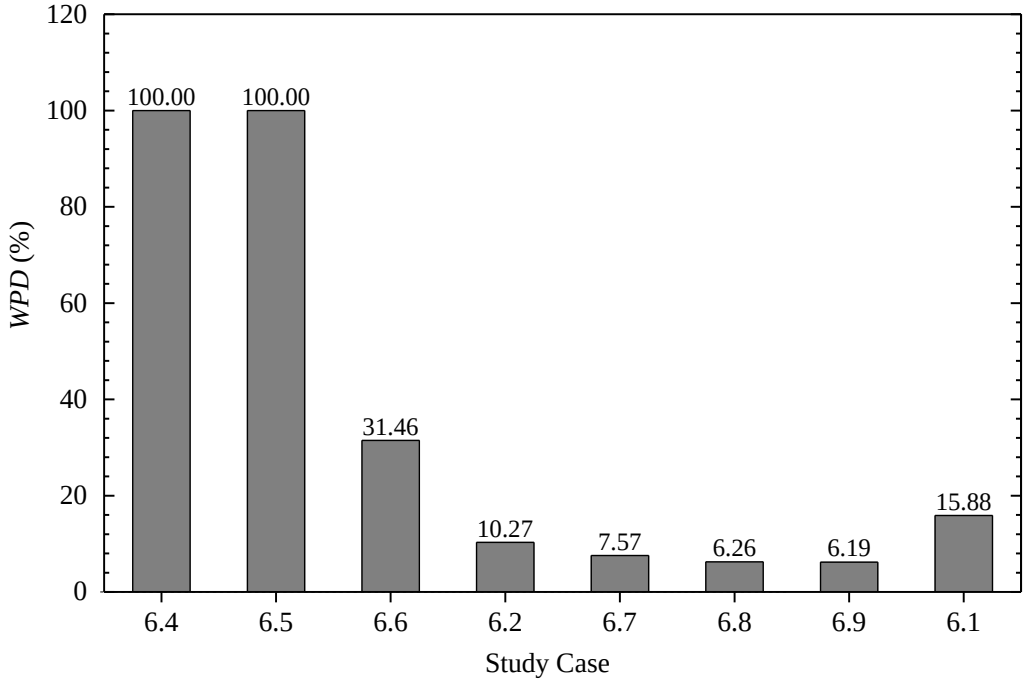

Fig. 6.10 The calculated *WPD* values in the experimental indoor space in study cases in Group 6.2

6.3.5 Effects of the thermal resistance of mattresses on the sleeping thermal environment (Group 6.3)

Fig. 6.11 shows the simulated $t_{op,d1}$ values at different R_{mat} values in Group 6.3 study cases. As seen, at a constant t_{bed} of 44 ^{o}C, $t_{op,d1}$ values were decreased with an increased R_{mat} value (Cases 6.8, 6.11, 6.12, 6.13). Fig. 6.12 shows that with an increased R_{mat}, *PTS* values were decreased, suggesting a cooler sleeping environment as less heat was provided by the bed-based heating terminal. Moreover, as seen in Fig. 6.13, the lowest *WPD* value in Group 6.3 study cases was in Case 6.8 at 7.57 %. Further increasing R_{mat} value from 0.1519 W/m$^2 \cdot ^{o}$C for M1 in Case 6.8, to 0.3038 W/m$^2 \cdot ^{o}$C for M2 in Case 6.12 and finally to 0.9079 W/m$^2 \cdot ^{o}$C for M3 in Case 6.13, would result in higher *WPD* values at 15.39 % (Case 6.12) and 41.18 % (Case 6.13), respectively. Therefore, although using a higher R_{mat} could prevent a sleeping person from becoming over-heated, an excessively higher R_{mat} would reduce the heat transfer from the bed-based heating terminal and lead to a cold sleeping environment.

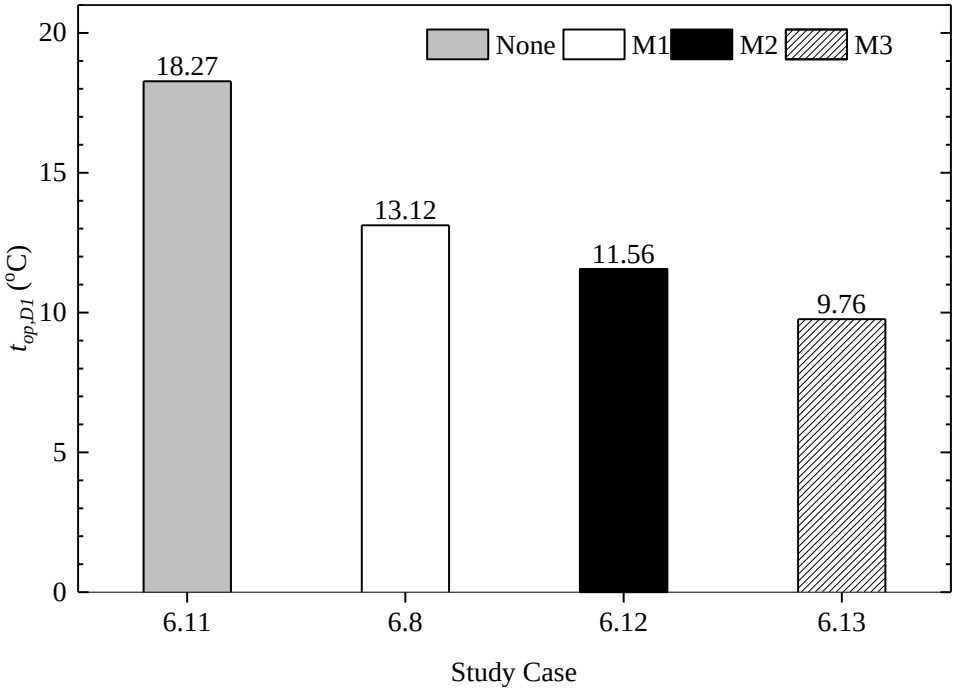

Fig. 6.11 The simulated t_{op} values in the study cases in Group 6.3

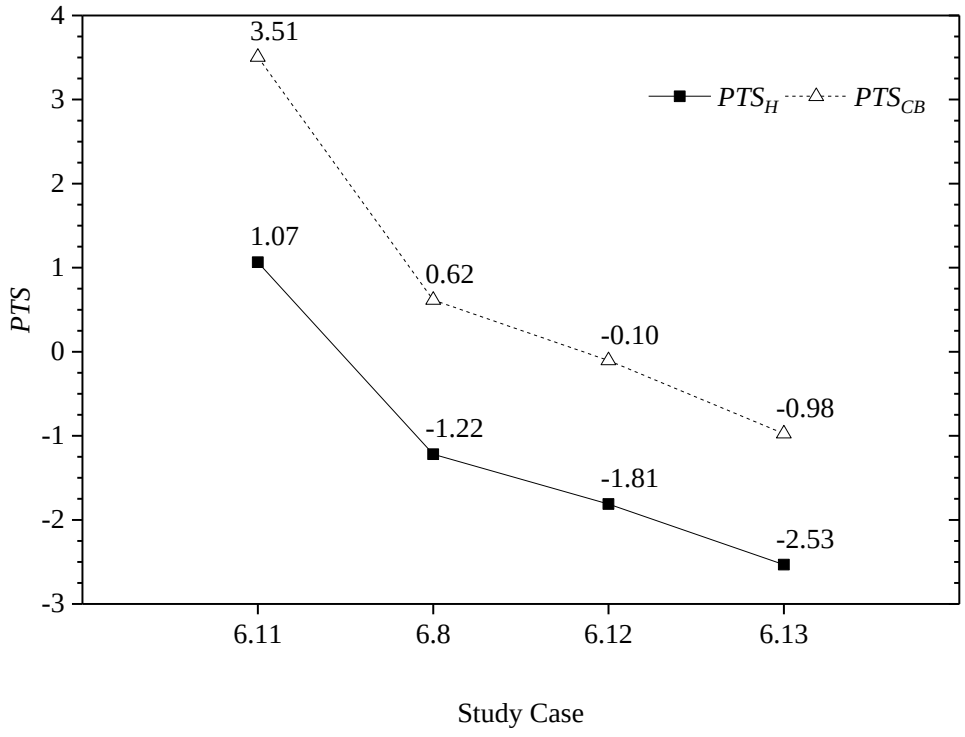

Fig. 6.12 The calculated PTS_H and PTS_{CB} values in the study cases in Group 6.3

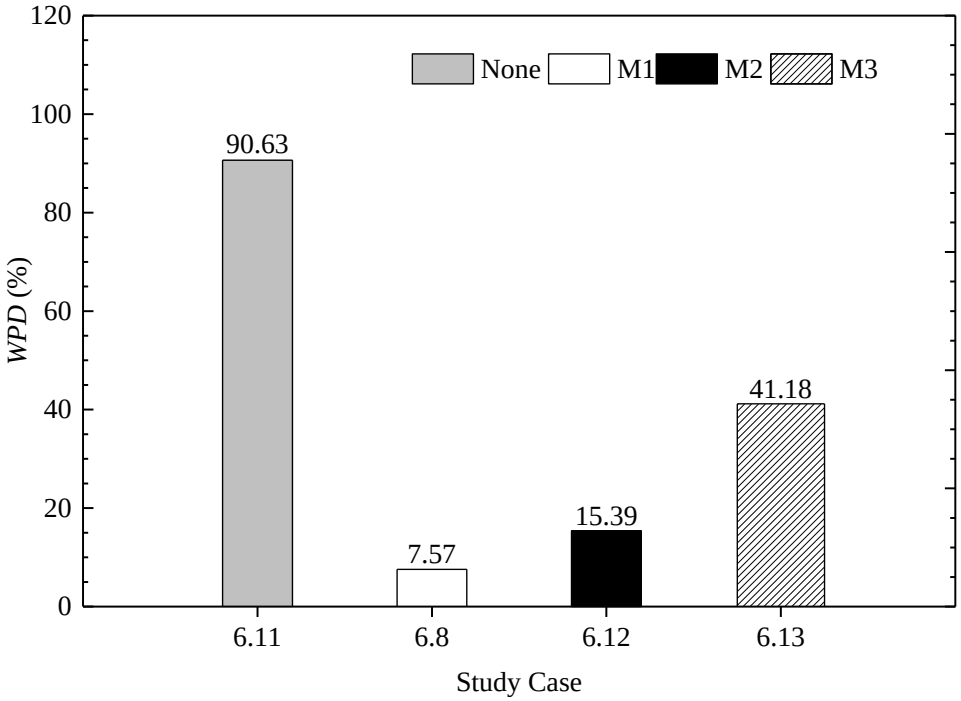

Fig. 6.13 The calculated *WPD* values in the study cases in Group 6.3

6.3.6 Effects of the thermal resistance of quilt on the sleeping thermal environment (Group 6.4)

Fig. 6.14 shows the simulated t_{op} values in Domain 1 at different R_q values in the four study cases in Group 6.4. As seen, at a constant t_{bed} of 44 ^{o}C and using M1 at an R_{mat} of 0.1519 W/m$^2 \cdot ^{o}$C, an increase in R_q value would lead to a moderate decrease in $t_{op,d1}$ as more heat was kept inside a quilt. Furthermore, Fig. 6.15 shows that as R_q was increased, *PTS* values were also increased, suggesting a warmer sleeping thermal environment.

On the other hand, a higher R_q of quilt could increase the difference between PTS_H value and PTS_{CB} value, suggesting a larger thermal sensation difference between the body parts covered by quilt and the head region. As seen in Fig. 6.15, the differences

between PTS_H and PTS_{CB} ranged from 0.21 to 1.99 as R_q was increased from 0 to 0.75 W/m$^2 \cdot$ ^{o}C. Moreover, as seen in Fig. 6.16, the lowest *WPD* value in Group 6.4 was in Case 6.8 at 7.57 %. However, further increasing the value of R_q from 0.4774 W/m$^2 \cdot$ ^{o}C for Q2 in Case 6.8 to 0.75 W/m$^2 \cdot$ ^{o}C for Q3 in Case 6.16 would lead to a slightly higher *WPD* at 8.24 %. Therefore, although using a higher R_q could improve the thermal sensation of a sleeping person, an excessively higher R_q would not help further improve the sleeping thermal comfort level.

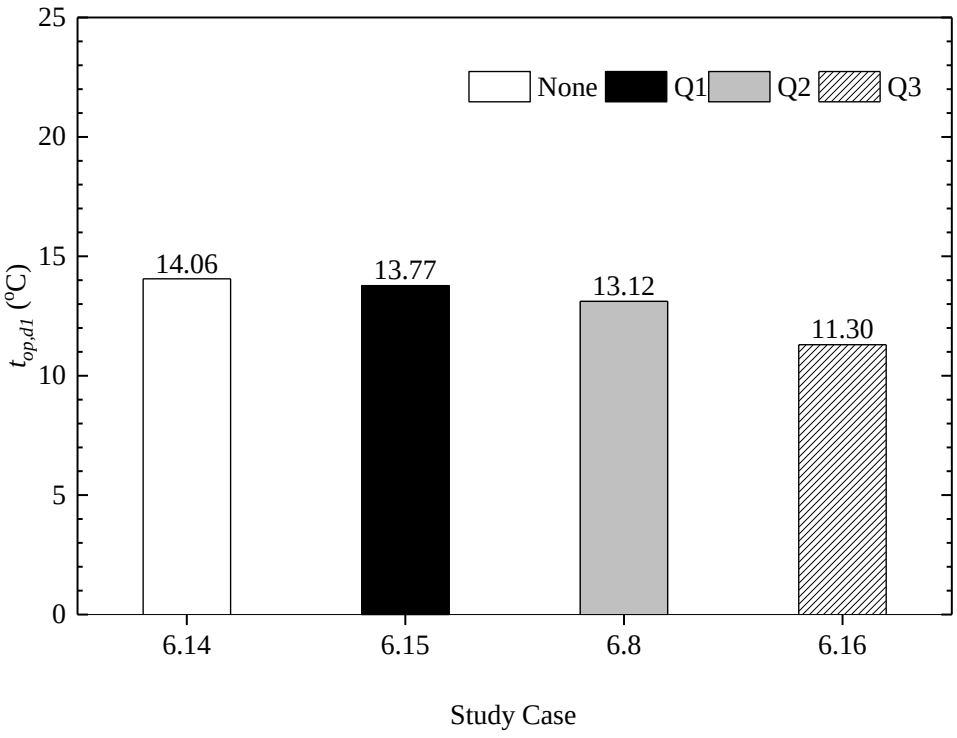

Fig. 6.14 The simulated t_{op} values in the study cases in Group 6.4

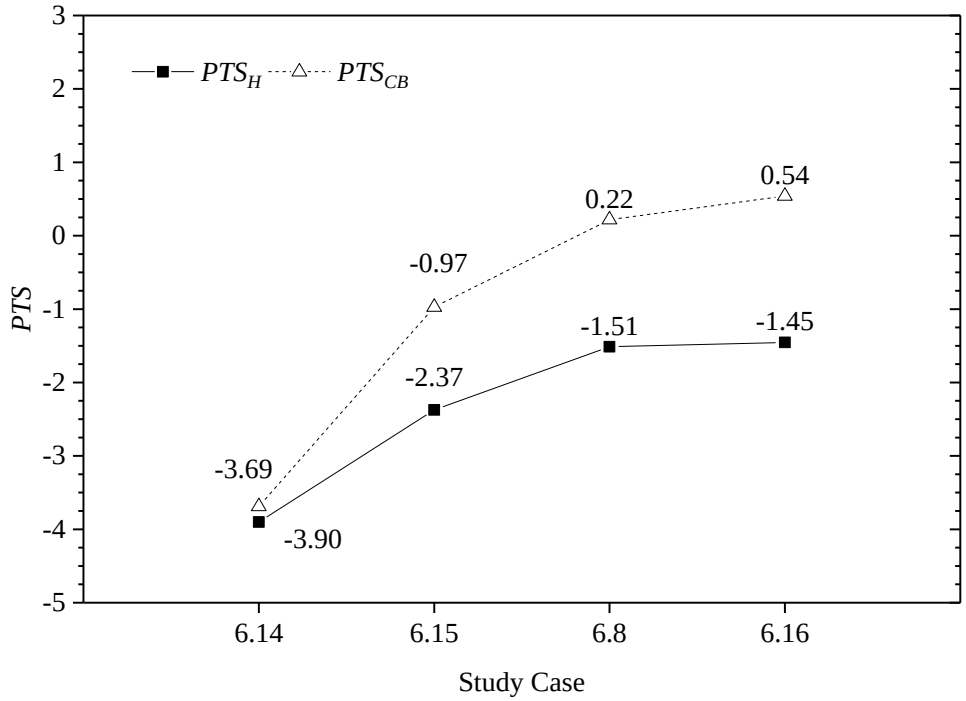

Fig. 6.15 The calculated PTS_H and PTS_{CB} values in the study cases in Group 6.4

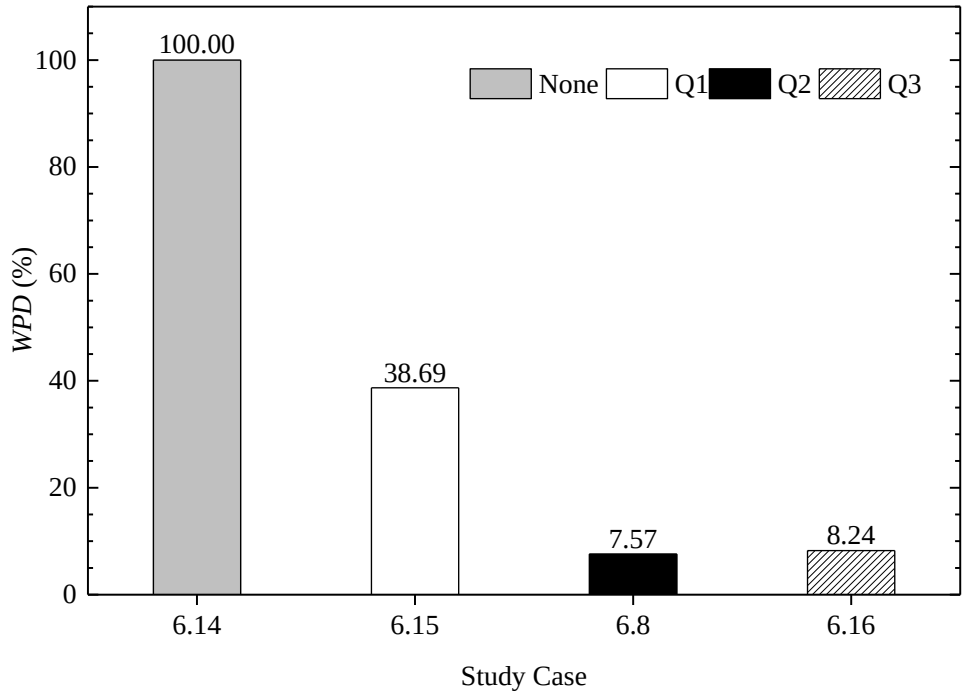

Fig. 6.16 The calculated *WPD* values in the study cases in the experimental indoor space in Group 6.4

6.4 Conclusions

As a follow-up to the experimental and numerical studies reported in Chapters 4 and 5, respectively, a further numerical study on the impacts of four factors, i.e., operating mode of the bed-based heating terminal, bed surface temperature (t_{bed}), and thermal resistance of mattress (R_{mat}) and that of quilt (R_q) on the thermal comfort for a sleeping person when using the B-ASHP system is reported in this Chapter. A revised CFD method based on a digital thermal manikin was firstly established and experimentally validated. Numerical studies were carried out and the following conclusions may be drawn:

1. The numerical results from Group 6.1 study cases suggested that, the use of H-Section only was adequate to maintain a suitable sleeping thermal environment. However, using H+V-Section of the B-ASHP system could provide an acceptable sleeping thermal comfort level and minimize the temperature difference between the micro-environment inside a quilt and its outer environment, at the expense of consuming more energy.

2. It was demonstrated by the numerical results from Group 6.2 study cases that, to both maintain an acceptable indoor sleeping thermal environment and achieve the best possible operating efficiency when using H-Section of the B-ASHP system, t_{bed} should be carefully selected. The numerical study results suggested that the suitable t_{bed} ranged from 44 ^{o}C - 50 ^{o}C. Therefore, it was recommended to use 44 ^{o}C to meet the required thermal comfort requirement for a sleeping person and at the same time achieve the highest possible operating efficiency of the B-ASHP system.

3. It was demonstrated by the numerical results from Group 6.3 study cases that, the presence of a mattress would reduce the heat transfer from the bed-based heating terminal to a sleeping person and indoor space. Although a mattress was actually necessary, a mattress with a higher R_{mat} value would not only reduce the output heating capacity and lower the operating efficiency of the B-ASHP system, but also lead to a cold sleeping environment.

4. Group 6.4 study cases indicated that, using quilts of appropriate R_q value would help prevent the heat loss from a sleeping person, thereby maintaining a warmer sleeping thermal environment. However, a higher-than-necessary R_q would rather decrease the thermal comfort of a sleeping person.

Chapter 7 Conclusions and future work

7.1 Conclusions

A research project to develop an experimental B-ASHP system by experimentally and numerically studying its operating characteristics, the indoor thermal environment and sleeping thermal comfort when using the experimental B-ASHP system has been carried out and the project outcomes are presented in this Thesis. The conclusions of the Thesis are as follows:

1. By combining the merits from both a conventional ASHP system and a traditional Chinese Kang-based heating system, an experimental B-ASHP system was proposed. The operating performances of the experimental B-ASHP system were experimentally evaluated and the study are reported in Chapter 4. Four test cases were organized, for both dynamic and steady state performance evaluation and comparisons. The study results showed that, first of all, the use of the experimental B-ASHP system can lead to a quicker increase in the t_a in the OZ and t_{bed}, than the use of traditional Kang heating systems, and that a B-ASHP system was also responsive to the changes in space heating load. Secondly, the experimental B-ASHP system can be satisfactorily operated at both nighttime and daytime modes. However, the test results also suggested that only varying the surface area of the bed-based heating terminal for heat transfer may not be an effective way to varying output heating capacity of a B-ASHP system, but varying compressor system can be more effective. Thirdly, compared to using a conventional convection-based heating terminal, the use of the bed-based heating terminal in

the B-ASHP system can lead to a more uniformed vertical indoor air temperature gradient, thus a better occupants' thermal comfort. Fourthly, the use of the B-ASHP system can lead to a more uniformed t_{bed}, than the use of Kang-based heating systems.

2. Chapter 5 reports a numerical study on the effects of varying four design/operating parameters, i.e., location, dimension, t_{bed} and surface emissivity of the bed-based heating terminal in a B-ASHP system, on the indoor thermal environment and the operating efficiency of the B-ASHP system. A CFD method was firstly established and experimentally validated using the experimental data obtained in the experimental study reported in Chapter 4. The numerical study results demonstrated that, firstly, be placing the bed-based heating terminal in the center of the experimental indoor space, a larger output heating capacity, a more uniformed indoor thermal environment and a better air velocity distribution could be achieved, with however different installation space requirements. Secondly, to increase the width and height of the bed-based heating terminal would lead to a larger output heating capacity with a larger surface area, thus a better operating efficiency. However, a larger bed would occupy more indoor space and be more costly. Thirdly, to both maintain an acceptable indoor thermal environment and achieve the best possible operating efficiency of the B-ASHP system, the t_{bed} of its bed-based heating terminal may be set at around 35 ^{o}C. The changes in the surface emissivity did not significantly impact much on indoor thermal environment at a fixed t_{bed}, however, the variation trend would suggest that when a lower t_{bed} was used, a higher surface emissivity would be preferred.

3. As a follow-up to the experimental and numerical studies reported in Chapters 4 and 5, respectively, a further numerical study on the impacts of four factors, i.e., operating mode of the bed-based heating terminal, bed surface temperature (t_{bed}), and thermal resistance of mattress (R_{mat}) and that of quilt (R_q) on the thermal comfort for a sleeping person when using the B-ASHP system is reported in Chapter 6. A revised CFD method based on a digital thermal manikin was firstly established and experimentally validated. Numerical studies were carried out and the following conclusions may be drawn: Firstly, the use of H-Section only was adequate to maintain a suitable sleeping thermal environment. However, using H+V-Section of the B-ASHP system could provide an acceptable sleeping thermal comfort level and minimize the temperature difference between the micro-environment inside a quilt and its outer environment, at the expense of consuming more energy. Secondly, to both maintain an acceptable indoor sleeping thermal environment and achieve the best possible operating efficiency when using H-Section of the B-ASHP system, t_{bed} should be carefully selected. The numerical study results suggested that the suitable t_{bed} ranged from 44 ^{o}C - 50 ^{o}C. Therefore, it was recommended to use 44 ^{o}C to meet the required thermal comfort requirement for a sleeping person and at the same time achieve the highest possible operating efficiency of the B-ASHP system. Thirdly, the presence of a mattress would reduce the heat transfer from the bed-based heating terminal to a sleeping person and indoor space. Although a mattress was actually necessary, a mattress with a higher R_{mat} value would not only reduce the output heating capacity and lower the operating efficiency of the B-ASHP system, but also lead to a cold sleeping environment. Finally, using quilts of appropriate R_q value would help prevent the heat loss from a sleeping person, thereby

maintaining a warmer sleeping thermal environment. However, a higher-than-necessary R_q would rather decrease the thermal comfort of a sleeping person.

4. The innovations of the research project are: Firstly, the use of B-ASHP system promotes the "coal to electricity" national strategy for clean space heating. Secondly, it's a human-oriented technology, which provides a comfort, harmony, sustainable indoor environment for occupants' living. Thirdly, it's a solution to the goal of a "low-carbon" society, which significantly reduces the energy consumption for residential heating and provides a faster way for reaching the peak of carbon emission.

7.2 Proposed future work

Following on the successful completion of the research project reported in this Thesis, a number of possible future studies are proposed:

1. In the experimental study reported in Chapter 4, although the current experimental B-ASHP system can be satisfactorily operated, there were still a number of issues requiring further considerations for its efficient and safe operation, such as the selection of a suitable refrigerant, optimizations of refrigerant tube layouts, and the use of a variable speed compressor for improved capacity control.

2. The bed-based heating terminal played a virtual role in the successful development of a B-ASHP system. In the current experimental study reported in Chapter 4, the design of the bed-based heating terminal of the experimental B-ASHP system was preliminary, with respect to its dimension, heat transfer surface

area, etc. Future optimization studies should therefore be carried out, with the considerations on the practical use of such a bed-based heating terminal in a bedroom.

3. In the numerical studies reported in Chapter 5 and Chapter 6, respectively, the outdoor air temperature was fixed at 7 ^{o}C. Since the outdoor air temperature significantly impacted on the operating efficiency of a B-ASHP system and indoor thermal environment, future experimental and numerical studies on investigating the operating characteristics of a B-ASHP system and indoor thermal environment control at different outdoor air temperatures shall be organized.

Appendix A-Photos of the experimental setup for the prototype B-ASHP system

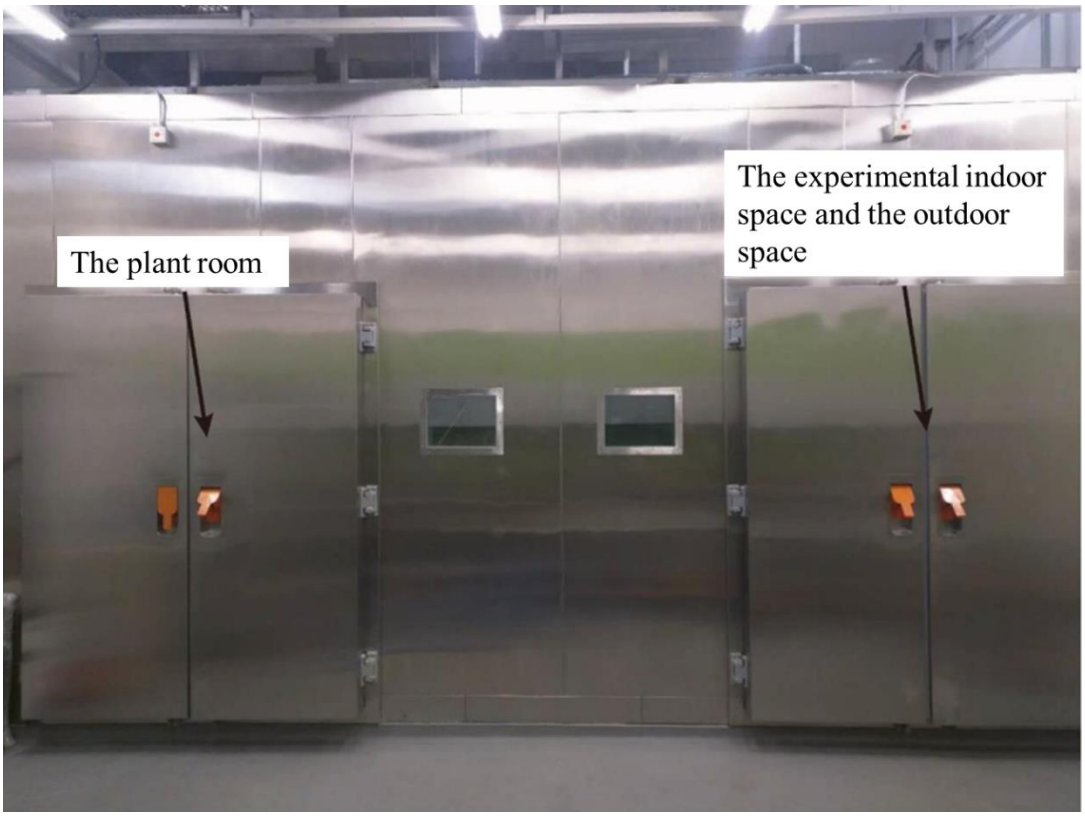

Photo 1 The environmental chamber at ZB 208, The Hong Kong Polytechnic University (Du 2018)

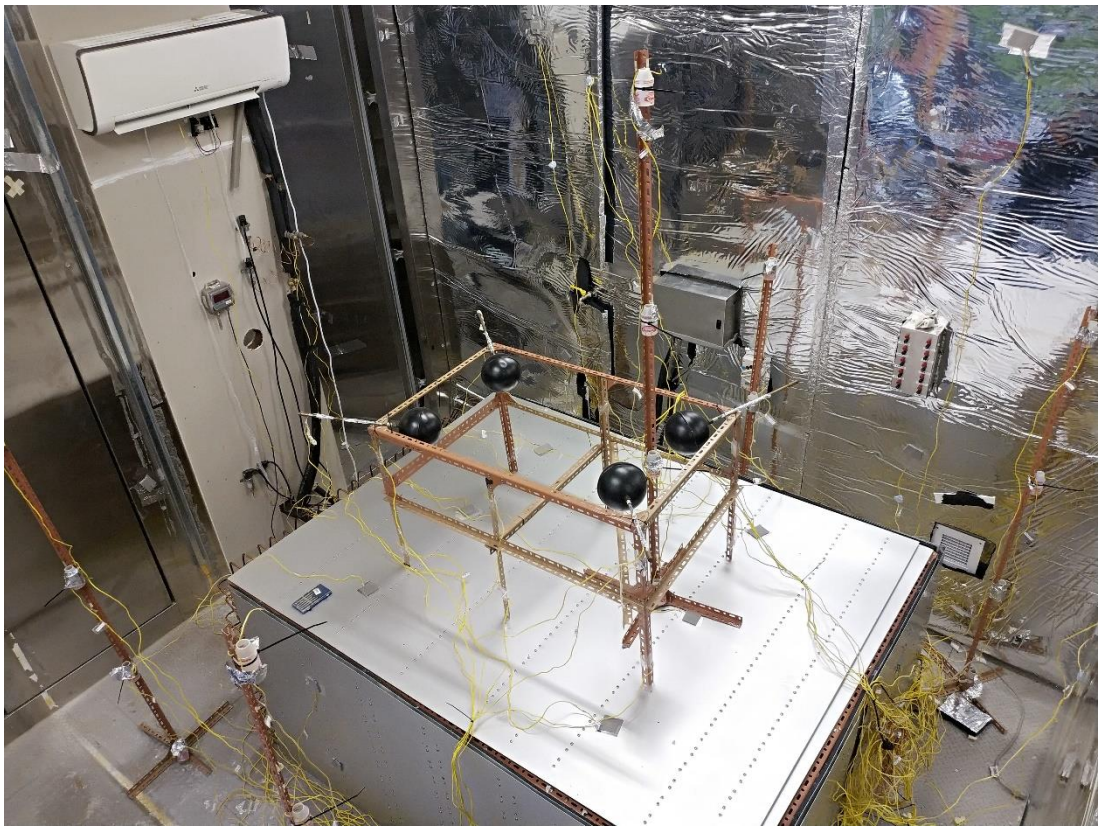

Photo 2 The experimental indoor space

Photo 3 Outdoor coil of the B-ASHP system

Photo 4 Convection-based heating terminal

Photo 5 Bed-based heating terminal and the DTM

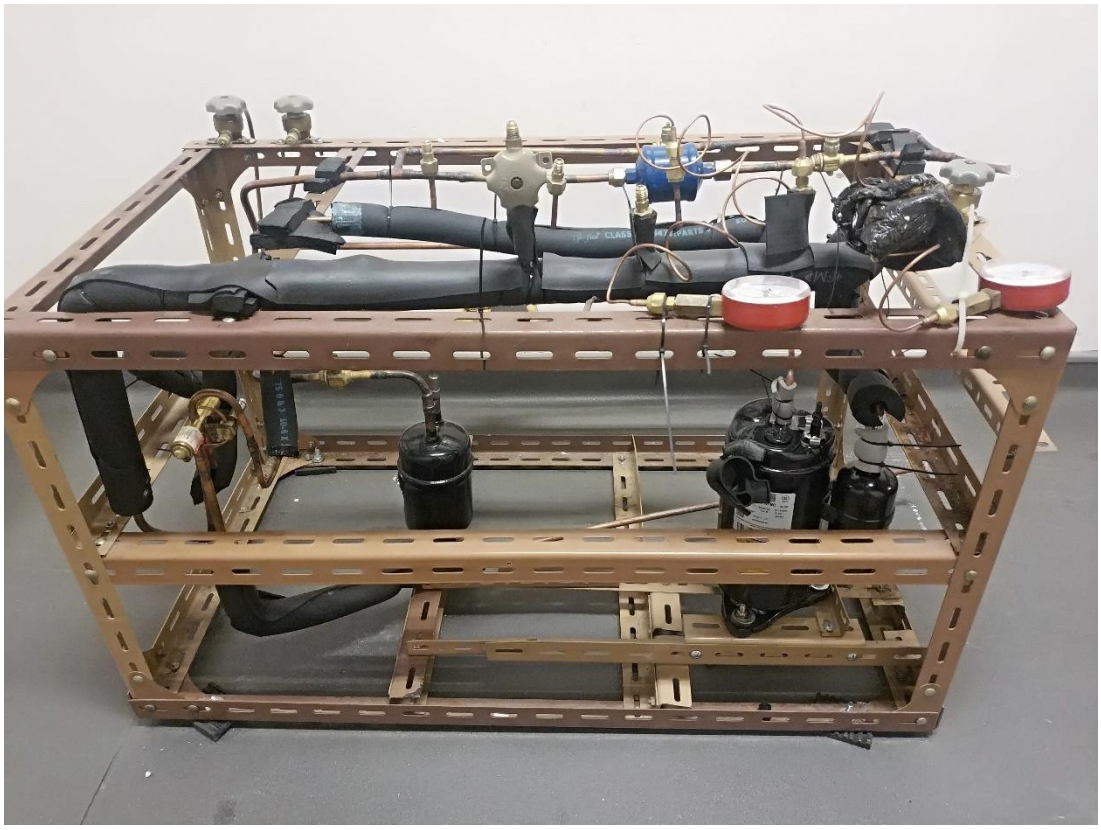

Photo 6 The Compressor and EEV of the B-ASHP system

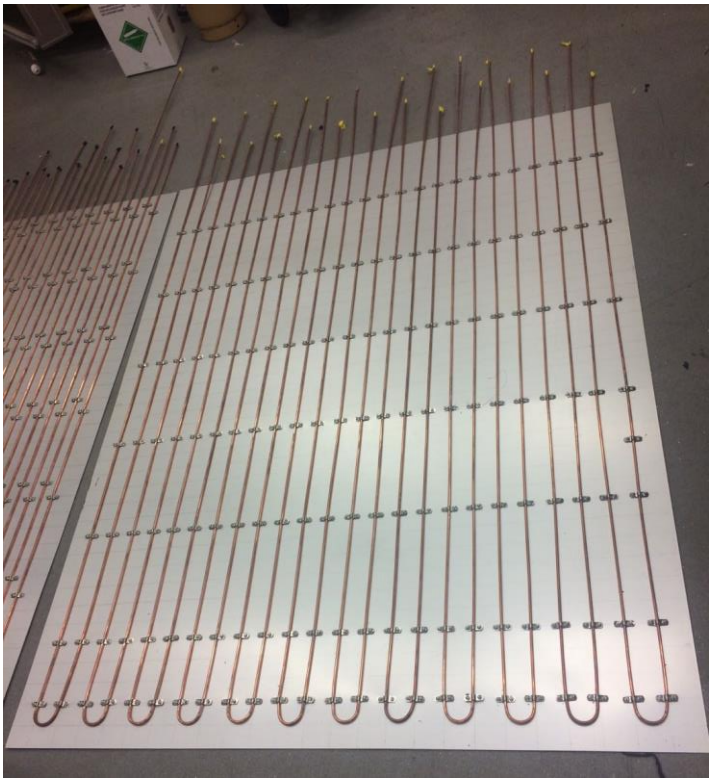

(a) H-Section of the bed-based heating terminal

(b) V-Section of the bed-based heating terminal

Photo 7 Details of the bed-based heating terminal

References

[1] AHRI 2021

AHRI.

Central Air Conditioners and Air-Source Heat Pumps. The Air-Conditioning, Heating and Refrigeration Institute (AHRI), 2021, See also: https://www.ahrinet.org/resources/statistics/historical-data/central-airconditioners-and-air-source-heat-pumps.

[2] Åkerstedt and Nilsson 2003

Åkerstedt, T. and Nilsson, P.

Sleep as restitution: an introduction. *Journal of internal medicine*, 2003, Vol. 254, No. 1, pp. 6-12.

[3] Ankit Gupta 2020

Ankit Gupta, A.

U.S. Residential Heat Pump Market size is expected to surpass annual installation of 2.8 Million Units by 2026. *Global Market Insights Inc*, 2020.

[4] ANSYS Fluent 2010

ANSYS.

ANSYS Fluent, 13.0 User's Guide, Ansys Inc, 2010.

[5] ANSYS ICEM CFD 2010

ANSYS.

ANSYS ICEM CFD. ANSYS Help Manual, Ansys Inc, 2010.

[6] Arun and Tulapurkara 2005

Arun, M. and Tulapurkara, E.

Computation of turbulent flow inside an enclosure with central partition. *Progress in Computational Fluid Dynamics, an International Journal*, 2005, Vol. 5, No. 8, pp. 455-465.

[7] ASHRAE 2017

ASHRAE.

ASHRAE Handbook of fundamentals, 2017.

[8] ASHRAE Standard 55 2017

ASHRAE.

Thermal environmental conditions for human occupancy, *ANSI/ASHRAE Standard 55-2017*, 2017.

[9] Bansal and Shail 1998

Bansal, N. and Shail.

Characteristic parameters of a hypocaust construction. *Building and Environment*, 1998, Vol. 34, No. 3, pp. 305-318.

[10] Basner et al. 2011

Basner, M., Müller, U. and Elmenhorst, E.

Single and combined effects of air, road, and rail traffic noise on sleep and recuperation. *Sleep*, 2011, Vol. 34, No. 1, pp. 11-23.

[11] Benington and Frank 2003

Benington, J. and Frank, M.

Cellular and molecular connections between sleep and synaptic plasticity. *Progress in neurobiology*, 2003, Vol. 69, No. 2, pp. 71-101.

[12] Bischof et al. 1993

Bischof, W., Madsen, T., Clausen, J., Madsen, P. and Wildschi, G.

Sleep and the temperature field of the bed. *Journal of thermal biology*, 1993, Vol. 18, No. 5-6, pp. 393-398.

[13] Brebbia and Altshuler 1965

Brebbia, D. and Altshuler, K.

Oxygen consumption rate and electroencephalographic stage of sleep. Science, 1965, Vol. 150, No. 3703, pp. 1621-1623.

[14] Brohus and Nielsen 1995

Brohus, H. and Nielsen, P.

Personal exposure to contaminant sources in a uniform velocity field. *Proceedings of Healthy Buildings*, 1995.

[15] Buguet et al. 1979

Buguet, A., Livingstone, S. and Reed, L.

Skin temperature changes in paradoxical sleep in man in the cold. *Aviation, space, and environmental medicine,* 1979, Vol. 50, No. 6, pp. 567-570.

[16] Candas et al. 1982

Candas, V., Libert, J. and Muzet, A.

Heating and cooling stimulations during SWS and REM sleep in man. *Journal of Thermal Biology,* 1982, Vol. 7, No. 3, pp. 155-158.

[17] Cao et al. 2011

Cao, G., Jokisalo, J., Feng, G., Lin, Duanmu., Vuolle, M. and Kurnitski, J.

Simulation of the heating performance of the Kang system in one Chinese detached house using biomass. *Energy and Buildings*, 2011, Vol. 43, No. 1, pp. 189-199.

[18] Chen and Srebric 2002

Chen, Q. and Srebric, J.

A procedure for verification, validation, and reporting of indoor environment CFD analyses. *HVAC&R Research*, 2002, Vol. 8, No. 2, pp. 201-216.

[19] Chen and Xu 1998

Chen, Q. and Xu, W.

A zero-equation turbulence model for indoor airflow simulation. *Energy and Buildings*, 1998, Vol. 28, No. 2, pp. 137-144.

[20] Chen 2018

Chen, W.

Development of a novel direct expansion based standalone enhanced dehumidification air conditioning system for improved year-round indoor humidity control. *The Hong Kong Polytechnic University*, 2018.

[21] Chen et al. 2011

Chen, X., Zhou, Y. and Yu, J.

A theoretical study of an innovative ejector enhanced vapor compression heat pump cycle for water heating application. *Energy and buildings*, 2011, Vol. 43, No. 12, pp. 3331-3336.

[22] Cuellar et al. 2006

Cuellar, N., Ratcliffe, S. and Chien, D.

Effects of depression on sleep quality, fatigue, and sleepiness in persons with restless legs syndrome. *Journal of the American Psychiatric Nurses Association*, 2006, Vol. 12, No. 5, pp. 262-271.

[23] Davidson et al. 2003

Davidson, L., Nielsen, P. and Sveningsson, A.

Modification of the v2f model for computing the flow in a 3D wall jet. *Modifications of the model for computing the flow in a 3D wall jet*, 2003, Vol. 4, pp. 577-584.

[24] De Dear and Brager 2002

De Dear, R. and Brager, G.

Thermal comfort in naturally ventilated buildings: revisions to ASHRAE Standard 55. *Energy and buildings*, 2002, Vol. 34, No. 6, pp. 549-561.

[25] DEEP 2018

DEEP.

2018 Comprehensive Energy Strategy. Department of Energy and Environmental Protection (DEEP), State of Connecticut, 2018, See also: https://portal.ct.gov/-/media/DEEP/energy/CES/2018ComprehensiveEnergyStrategypdf.pdf

[26] Dewasmes et al. 2000

Dewasmes, G., Telliez, F. and Muzet, A.

Effects of a nocturnal environment perceived as warm on subsequent daytime sleep in humans. *Sleep*, 2000, Vol. 23, No. 3, pp. 409-413.

[27] Di Nisi et al. 1989

Di Nisi, J., Ehrhart, J., Galeou, M. and Libert, J.

Influence of repeated passive body heating on subsequent night sleep in humans. *European journal of applied physiology and occupational physiology*, 1989, Vol. 59, No. 1-2, pp. 138-145.

[28] Dong et al. 2012

Dong, J., Deng, S., Jiang, Y., Xia, L. and Yao, Y.

An experimental study on defrosting heat supplies and energy consumptions during a reverse cycle defrost operation for an air source heat pump. *Applied Thermal Engineering*, 2012, Vol. 37, pp. 380-387.

[29] Du 2018

Du, J.

An experimental and numerical study on improving thermal comfort and energy saving measures in a sleeping environment, *The Hong Kong Polytechnic University*, 2018.

[30] Du et al. 2017

Du, J., Chan, M., Pan, D. and Deng, S.

A numerical study on the effects of design/operating parameters of the radiant panel in a radiation-based task air conditioning system on indoor thermal comfort and energy saving for a sleeping environment. *Energy and Buildings*, 2017, Vol. 151, pp. 250-262.

[31] EHPA 2018a

EHPA.

European heat pump market and statistics report 2018 executive summary. *European Heat Pump Association*, 2018a.

[32] EHPA 2018b

EHPA.

European Heat pump sales overview. *European Heat Pump Association*, 2018b, See also: http://www.stats.ehpa.org/ hp_sales/story_sales.

[33] Engle-Friedman et al. 2003

Engle-Friedman, M., Riela, S., Golan, R., Ventuneac, A. M., Davis, C. M., Jefferson, A. D. and Major, D.

The effect of sleep loss on next day effort. *Journal of Sleep Research*, 2003, Vol. 12, No. 2, pp. 113-124.

[34] European Parliament 2011

European Parliament.

Energy Roadmap 2050. *Communication from the Commission to the European Parliament*, 2011.

[35] Fanger 1970

Fanger, P.

Thermal comfort. *Analysis and applications in environmental engineering*, 1970.

[36] Feng et al. 2016

Feng, G., Wang, Q., Li, G. and Xu, X.

Study on solar Kang heating system for cold areas. *Procedia Engineering*, 2016, Vol. 146, pp. 536-540.

[37] Gagge 1973

Gagge, A.

A two node model of human temperature regulation in FORTRAN. *Bioastronautics data book*, 1973, Vol. 2, pp. 142-148.

[38] Gagge et al. 1986

Gagge, A., Fobelets, A. and Berglund, L.

A standard predictive index of human response to the thermal environment. *ASHRAE Transactions*, 1986, Vol. 92.

[39] Gao and Niu 2004

Gao, N. and Niu, J.

CFD study on micro-environment around human body and personalized ventilation. *Building and Environment*, 2004, Vol. 39, No. 7, pp. 795-805.

[40] Gao and Niu 2005

Gao, N. and Niu, J.

CFD study of the thermal environment around a human body: A review. *Indoor and built environment*, 2005, Vol. 14, No. 1, pp. 5-16.

[41] Gao et al. 2017

Gao, X., Liu, J., Hu, R., Akashi, Y. and Sumiyoshi, D.

A simplified model for dynamic analysis of the indoor thermal environment of rooms with a Chinese kang. *Building and Environment*, 2017, Vol. 111, pp. 265-278.

[42] Gatski and Speziale 1993

Gatski, T. and Speziale, C.

On explicit algebraic stress models for complex turbulent flows. *Journal of fluid Mechanics*, 1993, Vol. 254, pp. 59-78.

[43] GB 50736-2012 2012

GB.

Design code for heating ventilation and air conditioning of civil buildings. *GB 50736-2012*, 2012 (in Chinese).

[44] GB/T 7725-2004 2004

GB/T.

Room air conditioners. GB/T 7725-2004, 2004 (in Chinese).

[45] Germano et al. 1991

Germano, M., Piomelli, U., Moin, P. and Cabot, W.

A dynamic subgrid-scale eddy viscosity model. *Physics of Fluids A: Fluid Dynamics (1989-1993)*, 1991, Vol. 3, No. 7, pp. 1760-1765.

[46] Gibson and Launder 1978

Gibson, M. and Launder, B.

Ground effects on pressure fluctuations in the atmospheric boundary layer. *Journal of Fluid Mechanics*, 1978, Vol. 86, No. 03, pp. 491-511.

[47] Gooley et al. 2011

Gooley, J., Chamberlain, K., Smith, K., Khalsa, S., Rajaratnam, S., Van Reen, E., Zeitzer, J., Czeisler, C. and Lockley, S.

Exposure to room light before bedtime suppresses melatonin onset and shortens melatonin duration in humans. T*he Journal of Clinical Endocrinology & Metabolism*, 2011, Vol. 96, No. 3, pp. E463-E472.

[48] Guo 2002

Guo, Q.

The Chinese Domestic Architectural Heating System [Kang]: Origins, Applications and Techniques. *Architectural History*, 2002, Vol. 45, pp. 32-48.

[49] Hakkaki-Fard et al. 2014

Hakkaki-Fard, A., Aidoun, Z. and Ouzzane, M.

Applying refrigerant mixtures with thermal glide in cold climate air-source heat pumps. *Applied thermal engineering*, 2014, Vol. 62, No. 2, pp. 714-722.

[50] Haskell et al. 1981

Haskell, E., Palca, J., Walker, J., Berger, R. and Heller, H.

Metabolism and thermoregulation during stages of sleep in humans exposed to heat and cold. *Journal of Applied Physiology*, 1981, Vol. 51, No. 4, pp. 948-954.

[51] Hayashi et al. 2002

Hayashi, T., Ishizu, Y., Kato, S. and Murakami, S.

CFD analysis on characteristics of contaminated indoor air ventilation and its application in the evaluation of the effects of contaminant inhalation by a human occupant. *Building and Environment*, 2002, Vol. 37, No. 3, pp. 219-230.

[52] He et al. 2013

He, W., Jiang, Q. Y., Ji, J. and Wei, W.

A study on thermal performance, thermal comfort in sleeping environment and solar energy contribution of solar Chinese Kang. *Energy and Buildings*, 2013, Vol. 58, pp. 66-75.

[53] Henane et al. 1977

Henane, R., Buguet, A., Roussel, B. and Bittel, J.

Variations in evaporation and body temperatures during sleep in man. *Journal of Applied Physiology*, 1977, Vol. 42, No. 1, pp. 50-55.

[54] Hewitt et al. 2011

Hewitt, N. J., Huang, M., Anderson, M. and Quinn, M.

Advanced air source heat pumps for UK and European domestic buildings. *Applied Thermal Engineering*, 2011, Vol. 31, No. 17, pp. 3713-3719.

[55] Hobson 1995

Hobson, J.

Sleep, *Henry Holt and Company*, 1995.

[56] Holmér 2004

Holmér, I.

Thermal manikin history and applications. *European Journal of Applied Physiology*, 2004, Vol. 92, No. 6, pp. 614-618.

[57] Horton et al. 2014

Horton, W., Groll, E. and Braun, J.

Development of a high performance cold climate heat pump, 2014, Purdue University.

[58] Imanari et al. 1999

Imanari, T., Omori, T. and Bogaki, K.

Thermal comfort and energy consumption of the radiant ceiling panel system.: Comparison with the conventional all-air system. *Energy and Buildings*, 1999, Vol. 30, No. 2, pp. 167-175.

[59] International Standard ISO 5151 2017

International Standard.

Non-ducted air conditioners and heat pumps ergonomics of the thermal environment - Testing and rating for performance, 2017.

[60] International Standard ISO 7730 2015

International Standard.

Ergonomics of the thermal environment-analytical determination and interpretation of thermal comfort using calculation of the PMV and PPD indices and local thermal comfort criteria 2015, 2015.

[61] Jones and Launder 1973

Jones, W. and Launder, B.

The calculation of low-Reynolds-number phenomena with a two-equation model of turbulence. *International Journal of Heat and Mass Transfer*, 1973, Vol. 16, No. 6, pp. 1119-1130.

[62] Karacan et al. 1978

Karacan, I., Thornby, J., Anch, A., Williams, R. and Perkins, H.

Effects of high ambient temperature on sleep in young men. *Aviation, space, and environmental medicine*, 1978, Vol. 49, No. 7, pp. 855-860.

[63] Karmann et al. 2017

Karmann, C., Schiavon, S. and Bauman, F.

Thermal comfort in buildings using radiant vs. all-air systems: A critical literature review. *Building and Environment*, 2017, Vol. 111, pp. 123-131.

[64] Kaufman et al. 2019

Kaufman, N., Sandalow, D., Di Schio, C. R. and Higdon, J.

Decarbonizing space heating with air source heat pumps. *Center on Global Energy Policy*, 2019

[65] Kemal Sayar et al. 2002

Kemal Sayar, M., Meltem Arikan, M. and Tulin Yontem, M.

Sleep quality in chronic pain patients. *The Canadian Journal of Psychiatry*, 2002, Vol. 47, pp. 844-848.

[66] Kendel and Schmidt-Kessen 1973

Kendel, K. and Schmidt-Kessen, W.

The influence of room temperature on night-sleep in man (polygraphic night-sleep recordings in the climatic chamber). *Sleep*, 1973.

[67] Kim et al. 2010

Kim, M., Chun, C. and Han, J.

A study on bedroom environment and sleep quality in Korea. *Indoor and Built Environment*, 2010, Vol. 19, No. 1, pp. 123-128.

[68] Kim and Kim 2005

Kim, S. and Kim, H.

Comparison of formaldehyde emission from building finishing materials at various temperatures in under heating system; ONDOL. *Indoor Air*, 2005, Vol. 15, No. 5, pp. 317-325.

[69] Kreider et al. 1958

Kreider, M., Buskirk, E. and Bass, D.

Oxygen consumption and body temperatures during the night. *Journal of Applied Physiology*, 1958, Vol. 12, No. 3, pp. 361-366.

[70] Kuznik et al. 2007

Kuznik, F., Rusaouën, G. and Brau, J.

Experimental and numerical study of a full scale ventilated enclosure: Comparison of four two equations closure turbulence models. *Building and Environment*, 2007, Vol. 42, No. 3, pp. 1043-1053.

[71] Lam and Bremhorst 1981

Lam, C. and Bremhorst, K.

A modified form of the k-ε model for predicting wall turbulence. *Journal of Fluids Engineering*, 1981, Vol. 103, No. 3, pp. 456-460.

[72] Lan et al. 2017

Lan, L., Tsuzuki, K., Liu, Y. and Lian, Z.

Thermal environment and sleep quality: A review. *Energy and Buildings*, 2017, Vol. 149, pp. 101-113.

[73] Launder and Sharma 1974

Launder, B. and Sharma, B.

Application of the energy-dissipation model of turbulence to the calculation of flow near a spinning disc. *Letters in heat and mass transfer*, 1974, Vol. 1, No. 2, pp. 131-137.

[74] Launder and Spalding 1974

Launder, B. and Spalding, D.

The numerical computation of turbulent flows. *Computer Methods in Applied Mechanics and Engineering*, 1974, Vol. 3, No. 2, pp. 269-289.

[75] Laurence et al. 2005

Laurence, D., Uribe, J. and Utyuzhnikov, S.

A robust formulation of the v2-f model. *Flow, Turbulence and Combustion*, 2005, Vol. 73, No. 3-4, pp. 169-185.

[76] Lavie1998

Lavie, P.

The enchanted world of sleep, *Yale University Press*, 1998.

[77] Li et al. 2016

Li, A., Gao, X. and Yang, L.

Field measurements, assessments and improvement of Kang: Case study in rural northwest China. *Energy and Buildings*, 2016, Vol. 111, pp. 497-506.

[78] Li 2018

Li, C.

Analysis of air source heat pump industry. Chinese Journal of Refrigeration Technology, 2018, No. 38, pp. 78-84 (in Chinese).

[79] Li et al. 2015

Li, R., Yoshidomi, T., Ooka, R. and Olesen, B.

Field evaluation of performance of radiant heating/cooling ceiling panel system. *Energy and Buildings*, 2015, Vol. 86, pp. 58-65.

[80] Li et al. 2018

Li, T., Liu, Y., Chen, Y., Wang, D. and Wang, Y.

Experimental study of the thermal performance of combined floor and Kang heating terminal based on differentiated thermal demands. *Energy and Buildings*, 2018, Vol. 171, pp. 196-208.

[81] Li et al. 2009

Li, Y., Zhuang, Z. and Liu, J.

Chinese kangs and building energy consumption. *Science Bulletin*, 2009, Vol. 54, No. 6, pp. 992-1002.

[82] Liang et al. 2020

Liang, S., Wang, W., Sun, Y., Lin, Y., Luo, Q. and Deng, S.

Field investigations on frosting suppression for variable-capacity ASHPs through optimizing their operations and configurations. *Energy and Buildings*, 2020, Vol. 224, pp. 110266.

[83] Lilly 1992

Lilly, D.

A proposed modification of the Germano subgrid-scale closure method. *Physics of Fluids A: Fluid Dynamics (1989-1993)*, 1992, Vol. 4, No. 3, pp. 633-635.

[84] Lin et al. 2016

Lin, B., Wang, Z., Sun, H., Zhu, Y. and Ouyang, Q.

Evaluation and comparison of thermal comfort of convective and radiant heating terminals in office buildings. *Building and Environment*, 2016, Vol. 106, pp. 91-102.

[85] Lin and Deng 2008

Lin, Z. and Deng, S.

A study on the thermal comfort in sleeping environments in the subtropics-developing a thermal comfort model for sleeping environments. *Building and Environment*, 2008, Vol. 43, No. 1, pp. 70-81.

[86] Liu et al. 2016

Liu, Y., Song, C., Zhou, X., Liu, J. and Wang, Y.

Thermal requirements of the sleeping human body in bed warming conditions. *Energy and Buildings*, 2016, Vol. 130, pp. 709-720.

[87] Macpherson 1973

Macpherson, R.

Thermal stress and thermal comfort. *Ergonomics*, 1973, Vol. 16, No. 5, pp. 611-622.

[88] Mao 2015

Mao, N.

A study on thermal environmental control, indoor air quality and energy efficiency using task/ambient air conditioning (TAC) systems in sleeping environments in the subtropics. *The Hong Kong Polytechnic University*, 2015.

[89] Mao et al. 2014a

Mao, N., Pan, D., Chan, M. and Deng, S.

Experimental and numerical studies on the performance evaluation of a bed-based task/ambient air conditioning (TAC) system. *Applied energy*, 2014a, Vol. 136, pp. 956-967.

[90] Mao et al. 2014b

Mao, N., Pan, D., Chan, M. and Deng, S.

Performance evaluation of an air conditioning system with different heights of supply outlet applied to a sleeping environment. *Energy and buildings*, 2014b. Vol. 77, pp. 281-291.

[91] Mao et al. 2018

Mao, N., Hao, J., Cui, B., Li, Y., Song, M., Xu, Y. and Deng, S.

Energy performance of a bedroom task/ambient air conditioning (TAC) system applied in different climate zones of China. *Energy*, 2018, Vol. 159, pp. 724-736.

[92] Menter 1994

Menter, F.

Two-equation eddy-viscosity turbulence models for engineering applications. *AIAA journal*, 1994, Vol. 32, No. 8, pp. 1598-1605.

[93] Murakami 1997

Murakami, S.

Flow and temperature fields around human body with various room air distribution, CFD study on computational thermal manikin (Part 1). *ASHRAE transactions*, 1997, Vol. 103.

[94] Murakami et al. 1995

Murakami, S., Kato, S. and Zeng, J.

Development of a computational thermal manikin-CFD analysis of thermal environment around human body. *Tsinghua-HVAC*, 1995, Vol. 95, pp. 2349-354.

[95] Murakami et al. 2000

Murakami, S., Kato, S. and Zeng, J.

Combined simulation of airflow, radiation and moisture transport for heat release from a human body. *Building and Environment*, 2000, Vol. 35, No. 6, pp. 489-500.

[96] Muzet 2007

Muzet, A.

Environmental noise, sleep and health. *Sleep medicine reviews*, 2007, Vol. 11, No. 2, pp. 135-142.

[97] Myhren and Holmberg 2008

Myhren, J. and Holmberg, S.

Flow patterns and thermal comfort in a room with panel, floor and wall heating. *Energy and Buildings*, 2008, Vol. 40, No. 4, pp. 524-536.

[98] Nagano et al. 2005

Nagano, K., Takaki, A., Hirakawa, M. and Tochihara, Y.

Effects of ambient temperature steps on thermal comfort requirements. *International journal of biometeorology*, 2005, Vol. 50, No. 1, pp. 33-39.

[99] Nakano et al. 2002

Nakano, J., Tanabe, S. and Kimura, K.

Differences in perception of indoor environment between Japanese and non-Japanese workers. *Energy and Buildings*, 2002, Vol. 34, No. 6, pp. 615-621.

[100] Niu and Van der Kooi 1992

Niu, J. and Van der Kooi, J.

Grid-optimization for k-ε turbulence model simulation of natural convection in rooms. *Proceedings ROOMVENT-92: Air Distribution in Rooms-Third International Conference*, 1992.

[101] Nowak and Westring 2015

Nowak, T. and Westring, P.

European heat pump market and statistics report 2015. The European Heat Pump Association, 2015.

[102] Okamoto-Mizuno et al. 1999

Okamoto-Mizuno, K., Mizuno, K., Michie, S., Maeda, A. and lizuka, S.

Effects of humid heat exposure on human sleep stages and body temperature. *Sleep*, 1999, Vol. 22, No. 6, pp. 767-773.

[103] Olesen 2002

Olesen, B.

Radiant floor heating in theory and practice. *ASHRAE journal*, 2002, Vol. 44, No. 7, pp. 19.

[104] Olesen et al. 1980

Olesen, B., Mortensen, E., Thorshauge, J. and Berg-Munch, B.

Thermal comfort in a room heated by different methods. *ASHRAE transactions*, 1980, Vol. 86, No. 1, pp. 34-48.

[105] Orszag 1970

Orszag, S.

Analytical theories of turbulence. *Journal of Fluid Mechanics*, 1970, Vol. 41, No. 2, pp. 363-386.

[106] P.T. Teknik 2008

P.T. Teknik.

Manikin User's Guide, *P.T. Teknik Inc*, 2008.

[107] Pan et al. 2011

Pan, D., Chan, M., Deng, S., Xia, L. and Xu, X.

Numerical studies on the microclimate around a sleeping person and the related thermal neutrality issues. *Ergonomics*, 2011, Vol. 54, No. 11, pp. 1088-1100.

[108] Pan et al. 2012

Pan, D., Chan, M., Deng, S. and Qu, M.

A four-node thermoregulation model for predicting the thermal physiological responses of a sleeping person. *Building and Environment*, 2012, Vol. 52, pp. 88-97.

[109] Qiu et al. 2018

Qiu, H., Yan, J., Lei, Z. and Sun, D.

Rising wages and energy consumption transition in rural China. *Energy Policy*, 2018, Vol. 119, pp. 545-553.

[110] Qu et al. 2010

Qu, M., Deng, S. and Jiang, Y.

An experimental study on the defrosting performance of a PCM-based reverse-cycle defrosting method for air source heat pumps. *International Journal of Air-Conditioning and Refrigeration*, 2010, Vol. 18, No. 04, pp. 327-337.

[111] Ramaraj et al. 2014

Ramaraj, S., Yang, B., Braun, J. E., Groll, E. A. and Horton, W. T.

Experimental analysis of oil flooded R410A scroll compressor. *International journal of refrigeration*, 2014, Vol. 46, pp. 185-195.

[112] Schiller 1990

Schiller, G.

A comparison of measured and predicted comfort in office buildings. *ASHRAE transactions*, 1990, Vol. 96, No. 1, pp. 609-622.

[113] Seyam et al. 2014

Seyam, S., Huzayyin, A., El-Batsh, H. and Nada, S.

Experimental and numerical investigation of the radiant panel heating system using scale room model. *Energy and Buildings*, 2014, Vol. 82, pp. 130-141.

[114] Shan et al. 2015

Shan, M., Wang, P., Li, J., Yue, G. and Yang, X.

Energy and environment in Chinese rural buildings: Situations, challenges, and intervention strategies. *Building and Environment*, 2015, Vol. 91, pp. 271-282.

[115] Shen et al. 2019

Shen, C., Lei, Z., Lv, G., Ni, L. and Deng, S.

Experimental performance evaluation of a novel anti-fouling wastewater source heat pump system with a wastewater tower. *Applied energy*, 2019, Vol. 236, pp. 690-699.

[116] Shih 1995

Shih, T.

A New-Eddy-Viscosity Model for High Reynolds Number Turbulent Flows-Model Development and Validation. *Computers Fluids*, 1995, No. 24, pp. 3.

[117] Silva and Coelho 2002

Silva, M. and Coelho, J.

Convection coefficients for the human body parts-Determined with a thermal mannequin. *Proceedings of the 8th International Conference on air distribution in rooms*, 2002.

[118] Sleep in America poll 2014

Sleep in America poll.

Sleep in America poll 2014. *Sleep in America poll: Sleep in the modern family*, 2014.

[119] Smagorinsky 1963

Smagorinsky, J.

General circulation experiments with the primitive equations: I. the basic experiment. *Monthly weather review*, 1963, Vol. 91, No. 3, pp. 99-164.

[120] Song et al. 2018a

Song, C., Liu, Y. and Liu, J.

The sleeping thermal comfort model based on local thermal requirements in winter. *Energy and Buildings*, 2018a, Vol. 173, pp. 163-175.

[121] Song et al. 2018b

Song, M., Deng, S., Dang, C., Mao, N. and Wang, Z.

Review on improvement for air source heat pump units during frosting and defrosting. *Applied energy*, 2018b, Vol. 211, pp. 1150-1170.

[122] Sørensen and Voigt 2003

Sørensen, D. and Voigt, L.

Modelling flow and heat transfer around a seated human body by computational fluid dynamics. *Building and Environment*, 2003, Vol. 38, No. 6, pp. 753-762.

[123] Stamou and Katsiris 2006

Stamou, A. and Katsiris, I.

Verification of a CFD model for indoor airflow and heat transfer. *Building and Environment*, 2006, Vol. 41, No. 9, pp. 1171-1181.

[124] Sterman 1974

Sterman, M.

Sleep. Limbic and Autonomic Nervous Systems Research. *Springer*, 1974.

[125] Stern 2017

Stern, F.

Low-emissions buildings and sources of heat energy. *California Legislative Information*, 2017.

[126] Stickgold et al. 2001

Stickgold, R., Hobson, J. A., Fosse, R. and Fosse, M.

Sleep, learning, and dreams: off-line memory reprocessing. *Science*, 2001, Vol. 294, No. 5544, pp. 1052-1057.

[127] Su et al. 2018

Su, C., Madani, H. and Palm, B.

Heating solutions for residential buildings in China: Current status and future outlook. *Energy Conversion and Management*, 2018, Vol. 177, pp. 493-510.

[128] Teofilo 2011

Teofilo, L.

Sleep medicine essentials. *John Wiley & Sons*, 2011.

[129] Tsuzuki et al. 2008

Tsuzuki, K., Okamoto-Mizuno, K., Mizuno, K. and Iwaki, T.

Effects of airflow on body temperatures and sleep stages in a warm humid climate. *International journal of biometeorology*, 2008, Vol. 52, No. 4, pp. 261-270.

[130] USDOE 2021

USDOE.

Air-Source heat pumps. *USDOE*, See also: https://www.energy.gov/ energysaver/heat-and-cool/ heat-pump-systems/ air-source-heat-pumps

[131] Van Someren 2006

Van Someren, E.

Mechanisms and functions of coupling between sleep and temperature rhythms. *Progress in brain research*, 2006, Vol. 153, pp. 309-324.

[132] Victor Y. and Orszag 1986

Victor Y. and Orszag, S.

Renormalization group analysis of turbulence. I. Basic theory. *Journal of scientific computing*, 1986, Vol. 1, No. 1, pp. 3-51.

[133] Voigt et al. 2001

Voigt, L., Nørker, J. and Melikov, A.

Navier-Stokes simulations of airflow in rooms and around a human body. *Technical University of Denmark*. 2001.

[134] Wang et al. 2017a

Wang, D., Chen, P., Liu, Y., Wu, C. and Liu, J.

Heat transfer characteristics of a novel sleeping bed with an integrated hot water heating system. *Applied Thermal Engineering*, 2017a, Vol. 113, pp. 79-86.

[135] Wang et al. 2017b

Wang, D., Wu, C., Liu, Y., Chen, P. and Liu, J.

Experimental study on the thermal performance of an enhanced-convection overhead radiant floor heating system. *Energy and Buildings*, 2017b, Vol. 135, pp. 233-243.

[136] Wang et al. 2014

Wang, P., Shan, M., Xiong, D. and Yang, X.

A new Chinese Kang with forced convection: System design and thermal performance measurements. *Energy and Buildings*, 2014, Vol. 85, pp. 410-415.

[137] Wang and Liu 2000

Wang, Y. and Liu, J.

Thermal comfort properties for air conditioned space in winter. *HV & AC*, 2000, Vol. 3, pp. 3 (in Chinese).

[138] Wei et al. 2015

Wei, W., Ji, J., Chow, T., He, W., Chen, H., Guo, C. and Yu, H.

Experimental study of a combined system of solar Kang and solar air collector. *Energy Conversion and Management*, 2015, Vol. 103, pp. 752-761.

[139] WHO 2009

WHO.

Night noise guidelines for Europe. *World Health Organization-Regional Office for Europe*, 2009.

[140] Wilcox 1994

Wilcox, D.

Simulation of transition with a two-equation turbulence model. *AIAA journal*, 1994, Vol. 32, No. 2, pp. 247-255.

[141] Wolpert 1969

Wolpert, E.

A Manual of Standardized Terminology, Techniques and Scoring System for Sleep Stages of Human Subjects. *Archives of General Psychiatry*, 1969, Vol. 20, No. 2, pp. 246-247.

[142] Xia et al. 2017

Xia, Y., Deng, S. and Chan, M.

Inherent operational characteristics and operational stability of a variable speed direct expansion air conditioning system. *Applied Thermal Engineering*, 2017, Vol. 113, pp. 268-277.

[143] Xiao et al. 2020

Xiao, B., He, L., Zhang, S., Kong, T., Hu, B. and Wang, R. Z.

Comparison and analysis on air-to-air and air-to-water heat pump heating systems. *Renewable Energy*, 2020, Vol. 146, pp. 1888-1896.

[144] Xiong et al. 2016a

Xiong, J., Lian, Z. and Zhang, H.

Effects of exposure to winter temperature step-changes on human subjective perceptions. *Building and Environment*, 2016a, Vol. 107, pp. 226-234.

[145] Xiong et al. 2016b

Xiong, J., Lian, Z., Zhou, X., You, J. and Lin, Y.

Potential indicators for the effect of temperature steps on human health and thermal comfort. *Energy and Buildings*, 2016b, Vol. 113, pp. 87-98.

[146] Xiong et al. 2017a

Xiong, J., Lian, Z. and Zhang, H.

Physiological response to typical temperature step-changes in winter of China. *Energy and Buildings*, 2017a, Vol. 138, pp. 687-694.

[147] Xiong et al. 2017b

Xiong, J., Lian, Z., Zhang, H. and Yoshino, H.

Correlation between health discomforts and temperature steps in winter of China. *Building and Environment*, 2017b, Vol. 114, pp. 387-396.

[148] Yan et al. 2016

Yan, G., Jia, Q. and Bai, T.

Experimental investigation on vapor injection heat pump with a newly designed twin rotary variable speed compressor for cold regions. *International Journal of Refrigeration*, 2016, Vol. 62, pp. 232-241.

[149] Yan et al. 2018

Yan, H., Xia, Y., Xu, X. and Deng, S.

Inherent operational characteristics aided fuzzy logic controller for a variable speed direct expansion air conditioning system for simultaneous indoor air temperature and humidity control. *Energy and Buildings*, 2018, Vol. 158, pp. 558-568.

[150] Yang et al. 2002

Yang, J., Kato, S., Hayashi, T. and Murakami, S.

Measurement of local convective heat transfer coefficients of the human body in outdoor and indoor environments. *Proceedings of ROOMVENT 2002*, 2002.

[151] Yang et al. 2020

Yang, L., Yan, H., Deng, S. and Li, W.

An experimental investigation on the operational characteristics of a novel direct expansion based air conditioning system with a two-sectioned cooling coil. *International Journal of Refrigeration*, 2020, Vol. 118, pp. 131-138.

[152] Yang and Jiang 2008

Yang, X. and Jiang, Y.

Energy and environment in Chinese rural housing: road to sustainability. *The First International Conference on Building Energy and Environment*, 2008.

[153] Yeo et al. 2003

Yeo, M., Yang, I. and Kim, K.

Historical changes and recent energy saving potential of residential heating in Korea. *Energy and Buildings*, 2003, Vol. 35, No. 7, pp. 715-727.

[154] Yu et al. 2020

Yu, K., Tan, Y., Zhang, T., Zhang, J. and Wang, X.

The traditional Chinese kang and its improvement: A review. *Energy and Buildings*, 2020, pp. 110051.

[155] Zhai et al. 2015

Zhai, Z., Yates, A., Lin, D. and Wang, Z.

An evaluation and model of the Chinese Kang system to improve indoor thermal comfort in northeast rural China - Part-1: Model development. *Renewable Energy*, 2015, Vol. 84, pp. 3-11.

[156] Zhang et al. 2000

Zhang, J., Smith, K., Ma, Y., Ye, S., Jiang, F., Qi, W., Liu, P., Khalil, M., Rasmussen, R. and Thorneloe, S.

Greenhouse gases and other airborne pollutants from household stoves in China: a database for emission factors. *Atmospheric Environment*, 2000, Vol. 34, No. 26, pp. 4537-4549.

[157] Zhang et al. 2018a

Zhang, L., Jiang, Y., Dong, J. and Yao, Y.

Advances in vapor compression air source heat pump system in cold regions: A review. *Renewable and Sustainable Energy Reviews*, 2018a, Vol. 81, pp. 353-365.

[158] Zhang et al. 2017

Zhang, Q., Zhang, L., Nie, J. and Li, Y.

Techno-economic analysis of air source heat pump applied for space heating in northern China. *Applied Energy*, 2017, Vol. 207, pp. 533-542.

[159] Zhang and Chen 2000

Zhang, W. and Chen, Q.

Large eddy simulation of indoor airflow with a filtered dynamic subgrid scale model. *International Journal of Heat and Mass Transfer*, 2000, Vol. 43, No. 17, pp. 3219-3231.

[160] Zhang and Chen 2005

Zhang, W. and Chen, Q.

Large eddy simulation of the buoyancy flow driven by a corner heat source in a compartment. *Proceedings of Indoor Air 2005*, 2005, Vol. 1, No. 2, pp. 1294-99.

[161] Zhang and Chen 2016

Zhang, X. and Chen, B.

The coupling heat transfer of hot water heating system based on thermal utilization of a burning cave in a rural house of northern China. *Energy and Buildings*, 2016, Vol. 111, pp. 401-407.

[162] Zhang et al. 2018b

Zhang, X., Strbac, G., Teng, F. and Djapic, P.

Economic assessment of alternative heat decarbonisation strategies through coordinated operation with electricity system-UK case study. *Applied energy*, 2018b, Vol. 222, pp. 79-91.

[163] Zhao et al. 2017

Zhao, D., Ji, J., Yu, H., Wei, W. and Zheng, H.

Numerical and experimental study of a combined solar Chinese kang and solar air heating system based on Qinghai demonstration building. *Energy and Buildings*, 2017, Vol. 143, pp. 61-70.

[164] Zhao et al. 2019

Zhao, D., Ji, J., Yu, H. and Zhao, X.

A study on thermal characteristic and sleeping comfort of a hybrid solar heating system applied in cold rural areas. *Energy and Buildings*, 2019, Vol. 182, pp. 242-250.

[165] Zhao et al. 2014

Zhao, L., Zheng, N. and Deng, S.

A thermodynamic analysis of an auto-cascade heat pump cycle for heating application in cold regions. *Energy and buildings*, 2014, Vol. 82, pp. 621-631.

[166] Zhou and He 2015

Zhou, G. and He, J.

Thermal performance of a radiant floor heating system with different heat storage materials and heating pipes. *Applied Energy*, 2015, Vol. 138, pp. 648-660.

[167] Zhu and Yu 2015

Zhu, L. and Yu, J.

Theoretical study of a thermoelectric-assisted vapor compression cycle for air-source heat pump applications. *International Journal of Refrigeration*, 2015, Vol. 51, pp. 33-40.

[168] Zhuang et al. 2009a

Zhuang, Z., Li, Y. and Chen, B.

Thermal storage performance analysis on Chinese kangs. *Energy and Buildings*, 2009a, Vol. 41, No. 4, pp. 452-459.

[169] Zhuang et al. 2009b

Zhuang, Z., Li, Y., Chen, B. and Guo, J.

Chinese kang as a domestic heating system in rural northern China-A review. *Energy and Buildings*, 2009b, Vol. 41, No. 1, pp. 111-119.

[170] Zhuang et al. 2015

Zhuang, Z., Li, Y., Lin, D., Chen, B. and Qian, H.

Experimental assessment on heat transfer and smoke flow characteristics of a typical elevated Chinese kang. *International journal of green energy*, 2015, Vol. 12, No. 11, pp. 1178-1188.